Late Quaternary variability of hydrography and weathering inputs on the SW Iberian shelf from clay minerals and the radiogenic isotopes of neodymium, strontium and lead

Dissertation
zur Erlangung des Doktorgrades

Dr. rer. nat.

der Mathematisch-Naturwissenschaftlichen Fakultät
der Christian-Albrechts-Universität
zu Kiel

vorgelegt von

Roland Stumpf

Kiel, 2011

Referent:	Prof. Dr. Martin Frank
Koreferent:	Prof. Dr. Dirk Nürnberg
Tag der Disputation:	24. Mai 2011
zum Druck genehmigt:	24. Mai 2011

gez., der Dekan

Erklärung

Hiermit versichere ich an Eides statt, dass ich diese Dissertation selbständig und nur mit Hilfe der angegebenen Quellen und Hilfsmittel erstellt habe. Weiterhin versichere ich, dass der Inhalt dieser Arbeit weder in dieser, noch in veränderter Form, einer weiteren Prüfungsbehörde vorliegt. Die Arbeit wurde unter Einhaltung der Regeln guter wissenschaftlicher Praxis der Deutschen Forschungsgemeinschaft verfasst.

Kiel, den 02.05.2011

(Roland Stumpf, Dipl.-Geol.)

Contents

Abstract

The radiogenic isotope systems of neodymium (Nd), strontium (Sr) and lead (Pb) have been used in numerous studies throughout the last decades to investigate water mass circulations of the past and present oceans, and to trace changing contributions of detrital material from different source areas. Clay mineral assemblages and clay mineral ratios from the fine fraction of marine sediments have also been used to characterize endmember sources.

This thesis focuses on a reconstruction of the late Quaternary hydrographic variability of the flow path of the Mediterranean Outflow Water (MOW) and the changing weathering contributions of the detrital clay-size fraction to the SW Iberian shelf.

Mediterranean Outflow Water is characterized by higher temperatures and salinities than other ambient water masses. MOW spreads at water depths between 500 and 1500 m from the Strait of Gibraltar into the eastern North Atlantic and has been a source of salinity for the Atlantic Meridional Overturning Circulation in the North Atlantic. In order to evaluate the hydrographic changes of MOW since the Last Glacial Maximum (LGM) high-resolution Nd and Pb isotope records of past ambient seawater obtained from authigenic ferromanganese oxyhydroxide coatings of bulk marine sediments from three gravity cores in the Gulf of Cadiz (577 m water depth) and along the Portuguese margin (1 745 m and 1 974 m water depth) were produced. The surface and downcore Nd isotope data from all water depths exhibit only a very small variability close to the present day composition of MOW but do not reflect the present day Nd isotopic stratification of the water column as determined from a nearby open ocean hydrographic station. In contrast, the Pb isotope records show significant and systematic variations, which provide evidence for a significantly different pattern of the MOW pathways between 20 000 and 12 000 years ago compared with the subsequent period of time.

The assemblages of marine sediments on the SW Iberian shelf consist of the various regional particulate sources that comprise North African dust, river transported particles from the Iberian Peninsula and suspended particulate matter (SPM) carried by Mediterranean Outflow Water. It is noted that the relatively rapid, decadal scale Mediterranean overturning circulation permits mixing of suspended particles from the entire Mediterranean Sea.

In order to reconstruct climate and circulation driven changes in the supply of sediments from these sources over the past ~23 000 years, radiogenic Nd, Sr and Pb isotope records from the clay-size sediment fraction of the three core locations in the Gulf of Cadiz and along the Portuguese margin were produced. These records were supplemented by time series analyses of clay mineral abundances and clay mineral ratios from the same set of samples. Contrary to expectations, the transition from the LGM to the Holocene was not marked by very strong environmental changes but Heinrich stadial 1 and the African Humid Period (AHP; ~5500-12000 B.P.) are reflected by significantly different isotopic records. Interestingly, the mineralogical time series vary significantly out-of-phase to the isotope records. This suggests that due to the sensitivity of clay formation to climate conditions, the clay mineral assemblages allow insights to the prevailing chemical weathering regime through time in addition to information about detrital source areas.

Kurzfassung

Die radiogenen Isotopensysteme von Neodym (Nd), Strontium (Sr) und Blei (Pb) wurden erfolgreich in zahlreichen Studien dazu verwendet, um sowohl gegenwärtige als auch vergangene Ozeanzirkulationen zu untersuchen und um detritisches Material bestimmten Ausgangsgesteinen zuzuordnen. Eine weitere Möglichkeit zur Charakterisierung von Liefergebieten bietet die Analyse der Tonmineralzusammensetzung und der Tonmineralverhältnisse in der Feinfraktion mariner Sedimente.

Ziel dieser Doktorarbeit ist eine Rekonstruktion des spätquartären Fließweges des Mittelmeerausstromwassers sowie Änderungen in den Verwitterungseinträgen entlang diese Fließweges am Kontinentalhang im SW der Iberischen Halbinsel.

Das Mittelmeerausstromwasser ist wärmer und salzreicher als die es umgebenden atlantischen Wassermassen. Es breitet sich, ausgehend von der Strasse von Gibraltar, in Tiefen zwischen 500 und 1500 m in den östlichen Nordatlantik aus und trägt durch seine erhöhte Salinität wahrscheinlich nachhaltig zur Nordatlantischen Tiefenwasserbildung bei. Mögliche Änderungen des Fließweges des Mittelmeeraustroms seit dem Letzten Glazialen Maximum (LGM) wurden mittels hochauflösender Zeitserien der Nd und Pb Meerwasserisotopie, welche aus den hydrogenetischen Eisen-Mangan-Hydroxiden auf den Oberflächen von marinen Sedimenten extrahiert werden können, untersucht. Die analysierten Sedimente stammen von drei Kernlokationen im Golf von Cadiz (577 m Wassertiefe) und entlang des Portugiesischen Kontinentalhanges (1745 m bzw. 1974 m Wassertiefe). Die Nd Isotopie der Oberflächensedimente als auch die Nd Zeitserien von allen drei Lokationen zeigen kaum Veränderungen und entsprechen in etwa der Nd Isotopie des heutigen Mittelmeerausstromwassers. Die Fe-Mn-Hydroxide der Oberflächensedimente, die unterhalb des Austromes gelegen sind, besitzen ebenfalls dessen Nd Isotopie und spiegeln nicht die Isotopie der Wassermasse wieder, mit der sie in Kontakt sind. Die radiogenen Pb Isotope zeigen

dagegen signifikante Variationen seit dem LGM und liefern Hinweise darauf, dass der Fließweg des Mittelmeerausstroms zwischen 20 000 und 12 000 v. Chr. wahrscheinlich massiven Schwankungen unterworfen war.

Die Schelfsedimente im SW der Iberischen Halbinsel sind eine Mischung aus nordafrikanischem Saharastaub, partikulärem Flusseintrag von der Iberischen Halbinsel und partikulärer Suspensionsfracht des Mittelmeeraustromwassers, welche sich aufgrund der relative schnellen zonalen Mittelmeerzirkulation (etwa 10 Jahre) aus Partikeln des gesamten Mittelmeerraumes zusammensetzen kann.

Zur Untersuchung der verschieden Liefergebiete und zeitlicher, klimabedingter Variationen wurde von den Sedimentproben der drei oben beschriebenen Kernlokationen die Tonfraktion abgetrennt, Zeitserien der Nd, Sr und Pb Isotopie erstellt und die Tonmineralzusammensetzung bestimmt. Die Daten zeigen jedoch keine grundlegenden Veränderungen der Liefergebiete seit dem LGM an. Klimaereignisse wie das Heinrich Event 1 und die letzte humide Phase in Nordafrika (AHP; ~5500-12000 v. Chr.) haben die Isotopie der Tonfraktion der Schelfsedimente jedoch deutlich sichtbar beeinflusst. Interessanterweise sind die Schwankungen der radiogenen Zeitserien gegenüber den mineralogischen Zeitserien phasenverschoben. Dies ist wahrscheinlich auf die klimaabhängige Bildung von Tonmineralen zurück zu führen. Die Tonmineralzusammensetzung der Sedimente des SW Iberischen Schelfes erlaubt daher neben der Information über die Liefergebiete des detritischen Materials möglicherweise zusätzliche Einblicke in die Klimageschichte dieser Region.

Acknowledgments

First of all I would like to thank my supervisor. Martin, although you are a very busy man, you are always available for your students. I seriously consider myself a very lucky and privileged student to have you as my thesis advisor – Thank you very much!

Claudia and Brian - two important friends I met on my very first day at IFM-GEOMAR. Brian, everything I know about column chemistry and mass-specs bases upon your patient instructions. Claudia, you made my life in Kiel much more comfortable than I ever had expected. Thanks to both of you!

Special thanks go to Paddy, Moritz and, in particular, to Torben: You guys have been reliable buddies in the office, on conferences, during cruises and even in your spare time!

I would like to express my gratitude to Jutta, Ana, Jan and Folkmar! You have always taken your time when immediate problems occurred during my research.

Further, I honestly need to thank numerous colleagues and friends, who effectively distracted me from my thesis work whenever necessary: Clauschi, Steffi, Kristin, Irina, Anne, Basak, Cecille, Ed, Nabil, Hauke, Jan, Lasse, 'little' Torben and many others. Special thanks got to Jacek, whose unlimited knowledge about sports and inimitable way of storytelling promoted every single coffee break to be an unforgettable event.

Finally, thanks to all relevant people for establishing and running our regular's tables.

Chapter 1

Introduction

1.1. Motivation and objectives

The Mediterranean Outflow Water (MOW) is a distinct water body spreading as a bottom water mass from the sill of Gibraltar along the Iberian margin into the Eastern North Atlantic. Today's distribution of MOW and mixing with other water masses is easily detectable by standard oceanographic in-situ measurements (i.e. temperature, salinity, density). The late Quaternary flow path, extent and intensity of MOW have been investigated by studies using micropaleontological (cf. Schönfeld & Zahn, 2000; Rogerson et al., 2005) and sedimentological (cf. Voelker et al., 2006, 2009) methods, as well as modelling approaches (Rahmstorf, 1998).

The radiogenic isotope systems of neodymium (Nd) and lead (Pb) have been used in numerous studies to investigate ocean circulation and water mass mixing in the past and present oceans (cf. Burton et al., 1997; Abouchami et al., 1999; Piotrowski et al., 2005; Gutjahr et al., 2008, 2009). While the present-day Nd isotope compositions of seawater are obtained directly from water samples (cf. Piepgras & Wasserburg, 1983; Tachikawa et al., 2004), past seawater isotope signatures can be extracted from the authigenic ferromanganese coatings of bulk marine sediments (Bayon et al., 2002; Gutjahr et al., 2007).

Thus, the flow path of past and present Mediterranean Outflow Water is expected to be well preserved in sediments of the SW Iberian shelf. This study aims to reconstruct the hydrographic variability of the flow path of MOW since the Last Glacial Maximum from the first late Quaternary high-resolution Nd and Pb isotope records of past seawater in the Eastern North Atlantic from three gravity cores in the Gulf of Cadiz and from the Portuguese margin.

Furthermore, this study focuses on the detrital clay-size fraction from the same site locations. Radiogenic isotope compositions of Nd, Pb and Sr obtained

from complete dissolution of the clay-size fraction of these sediments, as well as clay mineral abundances and clay mineral ratios have been used to evaluate changing contributions of particles from different ambient source areas and the associated transport processes (cf. Biscaye et al., 1965; Grousset et al., 1988, 1998; Krom et al., 1999; Cole et al., 2009; Hamann et al., 2009; Erel & Torrent, 2010). From a combined investigation of the isotope records and the clay mineralogical records new information on the prevailing weathering regimes over time can be derived due to the sensitivity of clay mineral formation to climate conditions.

In order to reconstruct the late Quaternary history of MOW and climatically driven changes in detrital inputs to the SW Iberian shelf this study has the following objectives:

- *To validate the applicability of Nd isotope compositions obtained from leached ferromanganese coatings as a paleo water mass proxy on the SW Iberian shelf.* For this purpose the data of modern coretop sediments have been calibrated to seawater Nd isotope compositions applying data from corresponding depths of a nearby water column profile.

- *To evaluate the late Quaternary variability of the flow path of MOW.* Downcore records of radiogenic Nd and Pb isotope compositions of paleo seawater leached from bulk marine sediments have been produced. The results are compared to previous studies on records of micropaleontological and sedimentological proxies.

- *To reconstruct changes in the contributions of different endmembers supplying sediments to the SW Iberian shelf since the Last Glacial Maximum.* Investigations of Nd, Pb and Sr isotope compositions, clay mineral abundances and clay mineral ratios of the detrital clay-size fraction have been carried out.

- Due to the sensitivity of clay formation to changing climate conditions, does a comparison of the records of radiogenic isotope compositions and mineralogical compositions of the clay-size fraction allow new insights into the prevailing weathering regime of the SW Iberian margin throughout the late Quaternary?

1.2. The Atlantic Meridional Overturning Circulation

The Atlantic Meridional Overturning Circulation (AMOC) is a key element of the global thermohaline circulation (Fig. 1.1). The AMOC consists of two centres of deep water formation, from which deep waters spread into the Atlantic Ocean. In the Labrador and Nordic Seas, northwards advected saline surface water sinks to greater depth due to heat loss and thus increasing density and forms North Atlantic Deep Water (NADW), which flows into the southern Atlantic Ocean as a western boundary current. In the Weddell Sea and other areas around the Antarctic continent, deep water formation occures through the formation of sea ice

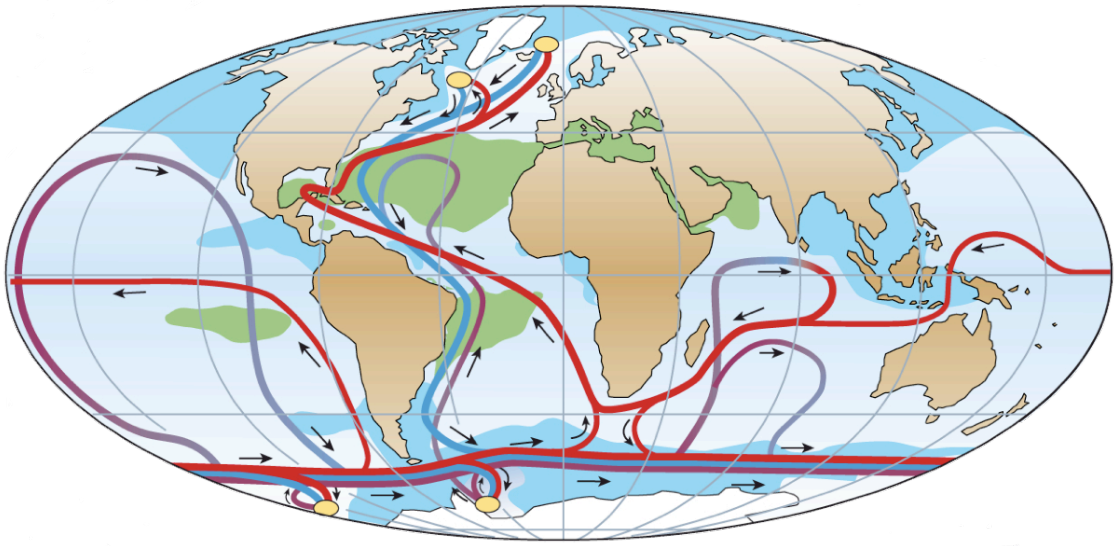

Fig. 1.1. A schematic picture of the global thermohaline circulation. Surface currents are shown in red, deep currents are blue and bottom currents are purple. The yellow circles mark the main locations of deep water formation. The black arrows show the direction of the currents (from Rahmstorf, 2002).

and produces Antarctic Bottom Water (AABW), which flows northward into the North Atlantic basin below NADW, whereby the bottom topography and entrainment into the above water mass leads to mixing of AABW with NADW. Thus, the AMOC controls the heat fluxes of the Atlantic Ocean and exerts a significant control on Earth's climate, in particular on the continents surrounding the Atlantic basin (cf. Kuhlbrodt et al., 2007).

Reconstructions of past ocean circulation have documented significant changes of the AMOC on glacial/interglacial time scales, but also between the stadial and interstadial times of Marine Isotope Stage 3. The circulation described above refers to the circulation mode, which prevailed during interglacials. It has been suggested that North Atlantic Deep Water formation occurred further to the south than today in the subpolar North Atlantic during glacial times. Thus, NADW production was most likely significantly weaker and advection of AABW was extended northwards. In addition, during Heinrich stadials massive iceberg discharge from the Laurentide ice-sheet significantly reduced the density of North Atlantic surface waters. As a consequence, NADW formation was severely interrupted or even completely ceased and the entire Atlantic deep water body was dominated by AABW (cf. Rahmstorf, 2002). It was suggested that the permanent supply of salt from high-salinity Mediterranean Outflow Water into the Eastern North Atlantic has played a key role in sustaining and, in case of a ceased NADW formation during Heinrich stadials, triggering the circulation of the North Atlantic (cf. Rahmstorf, 1998; Bigg et al., 2003).

1.3. The Mediterranean thermohaline circulation

The thermohaline circulation of the Mediterranean Sea is mainly driven by a zonal surface to mid-depth conveyor belt with decadal circulation. It is coupled with a slower meridional overturning connecting the Mediterranean deep and intermediate water bodies with a circulation time of 50-80 yrs (Pinardi & Masetti, 2000). At the Strait of Gibraltar, low-salinity (~36‰) Eastern North Atlantic

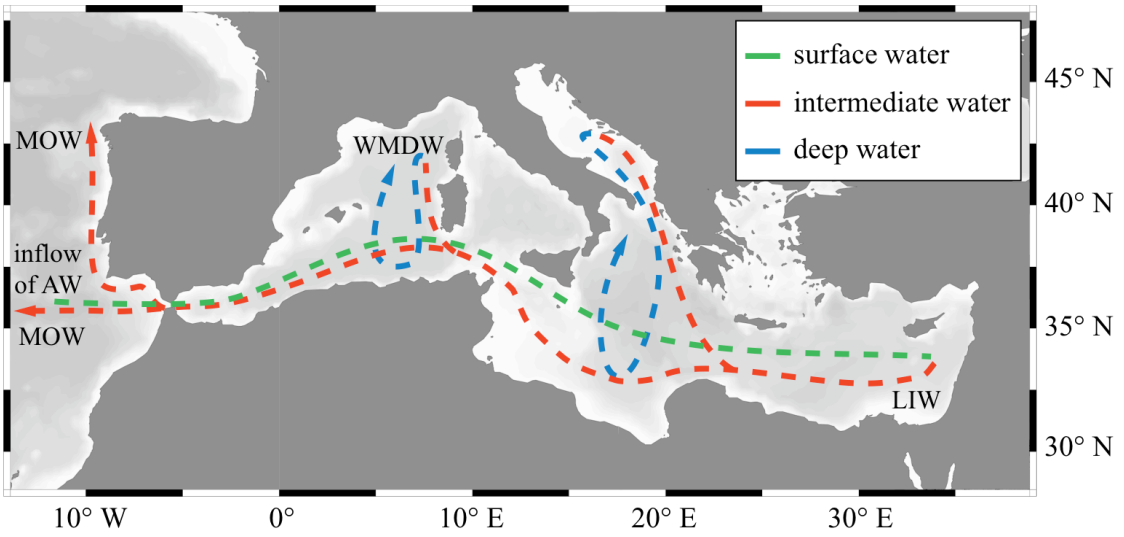

Fig. 1.2. Hydrographic overview of the surface (green), intermediate (red) and deep (blue) branches of the thermohaline circulation in the Mediterranean Sea. AW = Atlantic surface water, LIW = Levantine Intermediate Water, WMDW = Western Mediterranean Deep Water, MOW = Mediterranean Outflow Water (modified from Pinardi & Masetti, 2000).

Central Water (ENACW) enters the western Mediterranean Sea, from where it spreads into the eastern Mediterranean Sea as a surface and sub-surface water mass. Upon reaching the Levantine Sea, constant evaporation increased the density of this water mass, which is subducted and transformed into Levantine Intermediate Water (LIW). The high-salinity (~38‰) LIW recirculates westwards at mid-depth and, with some contributions from Western Mediterranean Deep Water (WMDW), forms Mediterranean Outflow Water (MOW), which spreads in the Eastern North Atlantic (Fig. 1.2; Bryden & Stommel, 1984; Baringer & Price, 1997, 1999; Fusco et al., 2008).

1.3.1 The Mediterranean Outflow Water

The Mediterranean Outflow Water enters the Eastern North Atlantic Ocean as a bottom water mass across the sill of Gibraltar with a volume flow of ~0.8 Sv and is distributed at intermediate water depths between 500 and 1500 m (cf. Schönfeld & Zahn, 2000; Fusco et al., 2008; Sánchez-Román et al., 2009).

Differential mixing with the entrained ENACW and the slope bathymetry in the Gulf of Cadiz lead to a splitting of the plume of MOW into two branches. A lower layer of MOW prevails between 1000 and 1500 m and expands westwards into the central North Atlantic (Zenk, 1975; Thorpe, 1976; Baringer & Price, 1999). An upper layer of MOW is centred between 500 and 800 m and is advected northwards along the Iberian continental slope. The corresponding density surfaces are found as far north as the Norwegian-Greenland Sea (Reid, 1979; Sparrow et al., 2002). This is why it has been argued that MOW preconditions North Atlantic Deep Water (NADW) formation and contributes to the Atlantic Meridional Overturning Circulation (Bigg et al., 2003).

1.3.2. Paleoceanography of MOW

Based on various paleoceanographic proxies (e.g. benthic foraminiferal assemblages, stable carbon and oxygen isotope compositions of benthic foraminifera, grain size data) it was suggested that MOW was denser and prevailed at greater depths than today during the Last Glacial Maximum (Schönfeld & Zahn, 2000; Rogerson et al., 2005; Voelker et al., 2006, 2009). The intensity and composition of MOW was driven by variations of deep-water formation within the Western Mediterranean Sea, which increased during cold climatic periods (Cacho et al., 2000; Sierro et al., 2005; Cacho et al., 2006). High-resolution grain size analyses from the Gulf of Cadiz also provided evidence for enhanced current strength within the deeper layer of MOW during short-term cold events of the last glacial stage, such as Dansgaard/Oeschger Stadials and Heinrich Events (Mulder et al., 2002; Llave et al., 2006; Voelker et al., 2006, 2009). Although the present-day effect of the Mediterranean Outflow Water on the Atlantic Meridional Overturning Circulation is rather small enhanced inputs of MOW during cooler periods supposedly had a stronger and sustaining influence on AMOC and thus northern hemisphere climate (Rahmstorf, 1998).

1.4. Radiogenic isotope systems of Nd, Sr and Pb

Radiogenic isotopes are produced by radioactive decay of a parent isotope (e.g. α-decay of $^{147}Sm \rightarrow {}^{143}Nd$; Tab. 1.1). Due to their different chemical properties, the parent (e.g. Sm) and daughter elements (e.g. Nd) have been fractionated during the Earth's differentiation process resulting in different element ratios (Sm/Nd) for mantle derived and continental crust derived rocks. Thus, radiogenic isotope compositions of rocks are a function of rock type (chemical differentiation) and their age (radioactive decay) leading to significant isotopic variations that can be used to trace geochemical processes on different scales including continental weathering and oceanic water mass mixing.

Through weathering and erosion continental source rocks release and supply particles of distinct isotopic signatures. Hence, the radiogenic isotope systems of Nd, Pb and Sr have successfully been applied to reconstruct source areas of deposited particles that have either been transported by rivers and oceanic water masses (cf. Grousset et al., 1995, 1998; Hemming et al., 1998; Fagel et al., 2002, 2004; Erel & Torrent, 2010) or via the atmosphere (cf. Goldstein et al., 1984; Krom et al., 1999; Grousset & Biscaye, 2005; Cole et al., 2009).

Further, the suspended particulate matter, which is transported as part of the hydrological cycle, is partially dissolved and releases the radiogenic isotope composition of the continental source rocks into weathering solutions and ultimately into the ambient water masses. The radiogenic isotope systems of Nd and Pb have increasingly been applied as water mass tracers for the past and present ocean (e.g. Burton et al., 1997; Abouchami et al., 1999; Frank, 2002; Tachikawa et al., 2004; Piotrowski et al., 2005; Gutjahr et al., 2008; 2009).

Various archives have been found to provide reliable radiogenic isotope compositions of bottom waters, e.g. hydrogenetic ferromanganese crusts, foraminifera and fish teeth (cf. Klevenz et al., 2008; Martin et al., 2010). With prevailing oxic conditions in the pore waters, bottom water isotopic compositions (past and present) are also preserved in early diagenetic, authigenic ferromanganese oxyhydroxide coatings of sediment particles that can be directly

extracted from bulk sediments (Rutberg et al., 2000; Bayon et al., 2002; Gutjahr et al., 2007). It is noted that hydrothermal inputs (in case of Pb) as well as boundary exchange processes at the seawater/continental margin interface are also considered to be important contributors to the seawater budgets of these elements (Frank, 2002; Lacan & Jeandel, 2005; Arsouze et al., 2009).

Tab. 1.1. Radiogenic isotope systems of Nd, Sr and Pb (from Frank, 2002).

Element	Radiogenic Isotope	Parent Isotope	Half-Life
Nd	^{143}Nd	^{147}Sm	106 Gyrs
Sr	^{87}Sr	^{87}Rb	48.8 Gyrs
Pb	^{206}Pb	^{238}U	4.47 Gyrs
	^{207}Pb	^{235}U	704 Myrs
	^{208}Pb	^{232}Th	14 Gyrs

1.4.1. Neodymium isotopes

Radiogenic ^{143}Nd is produced by radioactive α-decay of ^{147}Sm with a half-live of 106 Gyrs. The abundance of ^{143}Nd is commonly normalized to that of the primordial neodymium isotope ^{144}Nd. Sm/Nd ratios are higher in mantle-derived rocks resulting in elevated ^{143}Nd/^{144}Nd ratios in these rock types. Because the differences among the measured ^{143}Nd/^{144}Nd ratios are in general very small, radiogenic Nd isotope compositions are expressed in the ε-notation (equation below).

$$\varepsilon Nd = \left(\frac{\left(^{143}Nd/^{144}Nd\right)_{sample}}{\left(^{143}Nd/^{144}Nd\right)_{CHUR}} - 1 \right) \times 10^4$$

CHUR refers to the chondritic uniform reservoir, which describes the Nd isotope evolution of a uniform reservoir with the same Sm/Nd ratio and age as those of chondritic meteorites, which thus represents the hypothetical isotopic

evolution of the Earth excluding fractionation processes. The present-day $^{143}Nd/^{144}Nd$ ratio of CHUR is 0.512638 (Jacobsen & Wasserburg, 1980).

Dissolved Nd in the oceans originates from riverine and eolian inputs but its isotopic and elemental distributions cannot be explained without significant contributions through boundary exchange. The residence time of Nd in seawater is between 400 and 2000 years (Tachikawa et al., 1999; Arsouze et al., 2009). Because Nd is not fractionated by any biological process or evaporation, it can be used to trace water mass mixing on ocean basin scales. Past bottom water Nd isotope compositions can be extracted from ferromanganese coatings, which precipitate on the surfaces of marine sediments. This approach has successfully been applied to reconstruct bottom water Nd isotope compositions throughout the Quaternary (cf. Rutberg et al., 2000; Piotrowski et al., 2004, 2005; Gutjahr et al., 2008; Pahnke et al., 2008).

1.4.2. Strontium isotopes

The radiogenic strontium isotope ^{87}Sr originates from β^--decay of ^{87}Rb (half-life: 48.8 Gyrs; Tab.1.1). The abundance of ^{87}Sr is commonly normalized to the primordial strontium isotope ^{86}Sr. In general, Rb/Sr ratios are low in the Earth's mantle and high in continental crust, which results in lower $^{87}Sr/^{86}Sr$ ratios in young mantle-derived rocks and higher $^{87}Sr/^{86}Sr$ ratios in old continental rocks.

During weathering, the $^{87}Sr/^{86}Sr$ ratios in continental rocks vary with grain-size. Rubidium substitutes potassium in minerals, which leads to higher $^{87}Sr/^{86}Sr$ ratios in the potassium-rich fine fraction of sediments.

The dissolved Sr in seawater mainly derives from riverine inputs, which can be strongly influenced by the radiogenic Sr isotope signatures of strontium-rich old carbonates within their drainage systems. To a smaller rate, hydrothermal inputs with generally unradiogenic Sr isotope signatures contribute to the oceanic Sr budget. In seawater, Sr is a conservative element with a residence time of several million years. Thus, it is homogenously distributed in seawater with a

uniform present-day $^{87}Sr/^{86}Sr$ value of 0.70916 (Palmer & Edmond, 1989). Due to the long residence time and uniformity of Sr in seawater, paleo radiogenic Sr isotope compositions extracted from ferromanganese coatings of marine bottom sediments cannot be used to trace water masses throughout the latest Quaternary. However, the long-term evolution of radiogenic Sr in the oceans throughout the entire Phanerozoic documents significant variations that can be linked to phases in Earth's history of increased hydrothermal Sr inputs (low $^{87}Sr/^{86}Sr$) or increased inputs from continental weathering (high $^{87}Sr/^{86}Sr$; cf. Veizer et al., 1999).

1.4.3. Lead isotopes

Pb has three stable radiogenic isotopes (^{206}Pb, ^{207}Pb, ^{208}Pb; Tab. 1.1), which are produced by the radioactive decay-series of uranium (U) and thorium (Th) and form the stable endmembers of these decay series. The radiogenic Pb isotopes are either normalized to the primordial isotope ^{204}Pb or are expressed as ratios among each other. Fractionation during differential melting in Earth's evolution has resulted in an enrichment of U and Th in the continental crust compared to the upper mantle. The progressive radioactive decay of the U- and Th-series leads to an accumulation of crystal damages in minerals hosting U and Th. Thus, radiogenic Pb isotopes are more mobile during weathering processes than primordial ^{204}Pb resulting in a fractionation of the Pb isotopes. Due to this incongruent weathering effect, the isotope compositions of dissolved Pb do not necessarily represent the isotope composition of the corresponding source rocks (cf. Frank, 2002).

The dominant source for the dissolved Pb in seawater is riverine input from the continents, but eolian and hydrothermal sources also contribute to the ocean's Pb budget. Because Pb is a highly particle reactive element the residence time of dissolved Pb in seawater is only about 50 years in the Atlantic Ocean and up to 200 years in the deep Pacific Ocean (Schaule and Patterson, 1981; von Blanckenburg and Igel, 1999). Therefore, Pb isotopes are mainly used as tracers for local changes of continental inputs into the ocean and short distance water mass mixing. Due to the anthropogenic input of leaded petrol into the atmosphere, the present-day

dissolved Pb isotope composition of seawater has been altered from its natural values (Schaule and Patterson, 1981; Weiss et al., 2003). Information about the preanthropogenic Pb isotope composition of bottom waters has nevertheless been derived from slowly growing hydrogenetic ferromanganese crusts (cf. Frank, 2002) and from ferromanganese coatings of bulk marine sediments (cf. Gutjahr et al., 2009).

1.5. Clay minerals

In general, clay minerals consist of tetrahedral and octahedral sheets comprising interlayered cations. A silicon cation is located at the center of each tetrahedron and an alumimium cation sits on the central position of the octahedron. The corners of these structures are occupied by oxygen anions. From the ratio of tetrahedral to octahedral layers, and from the composition and charge of the interlayer sheets, the clay minerals are subdivided into different clay mineral groups and subgroups. The clay minerals commonly used in sedimentological investigations are kaolinite, illite, smectite and chlorite. Kaolinite is the most abundant 1:1 clay mineral (i.e. one tetrahedral sheet, one octahedral sheet), whereas illite and smectite comprise the main clay minerals consisting of 2:1 layer types. Chlorite is considered a 2:1:1 layer structure with an aluminium-hydroxide sheet added to the general 2:1 clay mineral type (cf. Chamley).

Clay minerals originate from physical and chemical weathering processes on rock surfaces and form during pedogenesis. The dominating chemical weathering process is hydrolysis ($5 < pH < 9.6$), which depends largely on precipitation, insolation and temperature and is therefore sensitive to prevailing climate conditions. Exposed rock forming minerals are attacked by water or by weak acids resulting in a progressive subtraction of ions from the parent mineral and finally lead to the formation of clay minerals (Tab. 1.2). During the hydrolytic destruction of the parent mineral major elements are more mobile than transition elements, whereas silicon and aluminium are the least mobile elements (cf. Chamley, 1989).

Weathering of different local lithologies provides clay mineral assemblages that can be characteristic for the respective source area. Surface runoff, river discharge and atmospheric circulation supply the clay particles (particle fraction in sediments < 2 μm) to their sedimentary deposits. Thus, clay mineral assemblages have been widely used as a tool to determine the origin of marine sediments (cf. Biscaye, 1965; Grousset et al., 1988; Guerzoni et al., 1997; Caquineau et al., 1998; Fagel et al., 2001; Hoogakker et al., 2004; Jimenez-Espejo et al., 2007; Hamann et al., 2009).

Tab. 1.2. General chemical weathering reaction during hydrolysis (e.g. weathering of orthoclase; Chamley, 1989).

Primary mineral		Attack solution		Secondary mineral		Leach solution
parent rock	+	ion-depleted water	→	weathering complex	+	ion-enriched water
orthoclase	+	water	→	kaolinite	+	(Si, K)-enriched water

Chapter 2

Material, Methods & Instrumentation

2.1. Core selection and age models

Three gravity cores from sites in the Gulf of Cadiz (M39008) and the Portuguese margin (M39036 and M39058) were used to produce downcore radiogenic isotope and clay mineral assemblage records covering the last ~23 000 yrs. In addition, twelve coretop samples from different water depths along the flow path of MOW were used to calibrate the Nd isotope compositions of the leached ferromanganese coatings to the corresponding present day water mass compositions. The gravity cores were recovered during RV METEOR cruise M39/1 (Schott et al., 1997) and the additional coretops were recovered during RV MARIA S. MERIAN cruise MSM1/3 (Pfannkuche, 2006), RV POSEIDON cruise PO287 (in 2002) and the LIVRA cruise (RV ALMEIDA CARVALHO, 1977; Fig. 3.1, App. Tab. 3.1).

The age models of the sediment cores have been published previously and are based on high-resolution AMS ^{14}C-datings, correlations of planktonic δ^{18}O records and the identification of Heinrich layers. The age model for core M39008, which documents variations of the upper layer of MOW has been published by Cacho et al. (2001) and Löwemark et al. (2004). The age models for cores M39036 and M39058, which recorded variations of the lower layer of MOW, have been published by Löwemark et al. (2004) and Schönfeld & Zahn (2000). The chronology of core M39008 has been based on 14 AMS ^{14}C-datings covering the past 22 000 yrs resulting in an average sedimentation rate at this location of 25.6 cm/kyr. The chronology of core M39036 has been established on the basis of 11 AMS ^{14}C-datings covering the past 25 300 yrs resulting in an average sedimentation rate of 20.3 cm/kyr. Finally, for core M39058, 8 AMS ^{14}C-datings covering the past 20 700 yrs have been produced yielding an average

sedimentation rate of 6.4 cm/kyr. The reported ^{14}C-dating uncertainties for the three cores range from ±25 to ±150 years (1σ). All three cores do not show any indications for the presence of significant bioturbation, sediment reworking or hiatuses during the period of interest. For the coretop samples no direct dating is available but, as discussed in chapter 3, there is evidence that they all represent undisturbed, recently deposited sediments.

2.2. Sample preparation

In order to achieve an effective separation of the different chemical and sedimentary fractions of interest from the bulk sediment, a successive preparation procedure was applied for each sample (Fig. 2.1). First, the ferromanganese coatings were leached from the bulk sediments to obtain modern and paleo seawater isotope compositions. In a second step, the clay-size fraction (< 2 µm) was separated from the remaining detritus by using a centrifuge-based Atterberg method. From an aliquot of the clay-size fraction, filter samples with a preferred clay mineral orientation were produced to determine their clay-mineralogical composition. A second aliquot of the clay-size fraction was totally digested to

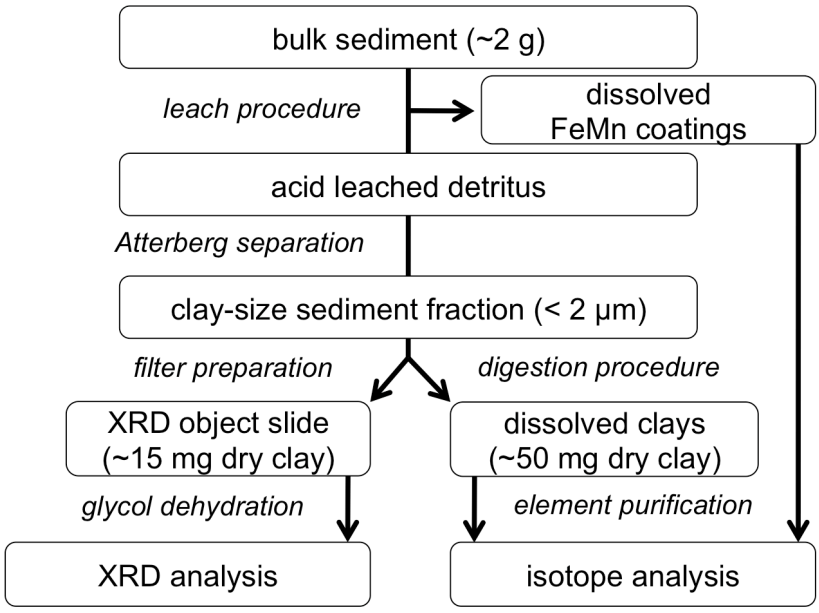

Fig. 2.1. Schematic overview of the successive sample preparation procedure.

analyse the isotopic compositions of Nd, Pb and Sr. These detrital clay-fraction data were used to evaluate potential endmember variability through time. In the following paragraphs, each separation step is described in detail.

2.2.1. Leaching procedure

The authigenic Fe-Mn oxyhydroxide fraction was leached from bulk sediment samples following a modified method for the extraction of seawater Nd and Pb isotopic compositions from Fe-Mn coatings described by Gutjahr et al. (2007; Fig. 2.2). The dry and coarsely ground bulk sediments (~2 g) were rinsed twice with

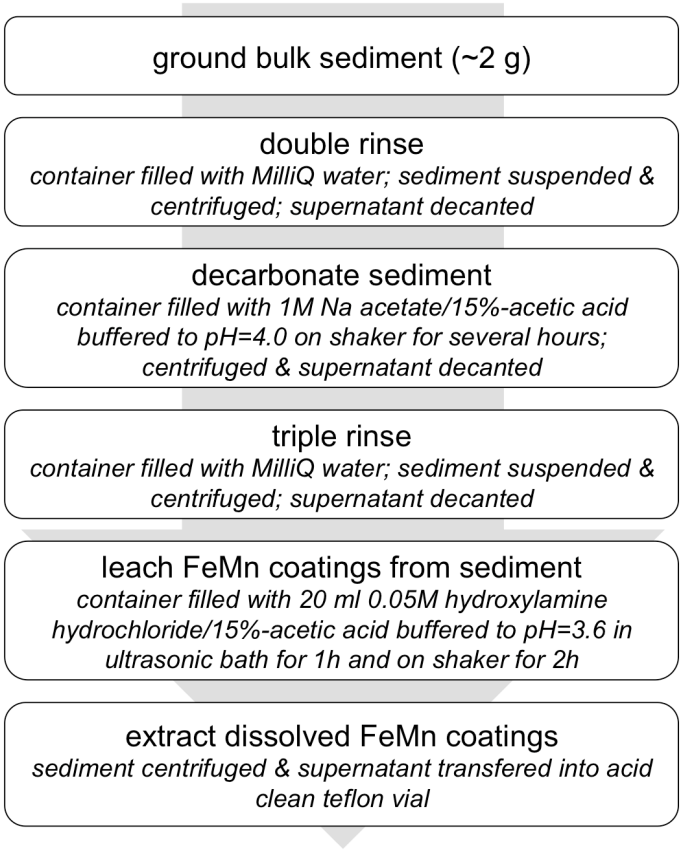

Fig. 2.2. Leaching protocol for the extraction of ferromanganese coatings from bulk sediments (modified from Gutjahr et al., 2007).

de-ionized water (obtained from a Milli-Q system) to eliminate the soluble fraction. Each rinsing cycle included: (i) suspending the sediment in MilliQ-water using a vortex mixer, (ii) centrifuging the suspension until the supernatant was free of particles and (iii) decanting the supernatant. The carbonate fraction was dissolved and removed using a 15%-acetic acid/1M-Na acetate buffer at pH=4.0 with NaOH followed by a triple rinse with de-ionized water. To ensure a complete removal of the carbonate fraction, this step was performed twice for all samples. The FeMn oxyhydroxide coatings were leached for 1 hour in an ultrasonic bath and for 2 hours on a shaker using a 0.05M hydroxylamine hydrochloride/15%-acetic acid solution buffered to pH 3.6 with NaOH. After centrifugation, the supernatant containing the dissolved FeMn coatings was transferred into an acid cleaned teflon vial for further chemical treatment under clean laboratory conditions (chap. 2.4.1). The residual detrital fraction stayed in the remaining leach solution for at least 12 h to achieve complete removal of the coatings, followed by a triple rinse of the sediment with de-ionized water.

2.2.2. Separation of the clay-size fraction

The clay-size fraction (< 2 µm) was separated from the decarbonated and acid-leached bulk sediment samples (chap. 2.2.1) using a centrifuge-based Atterberg method. The required settling time calculations were done by the freely

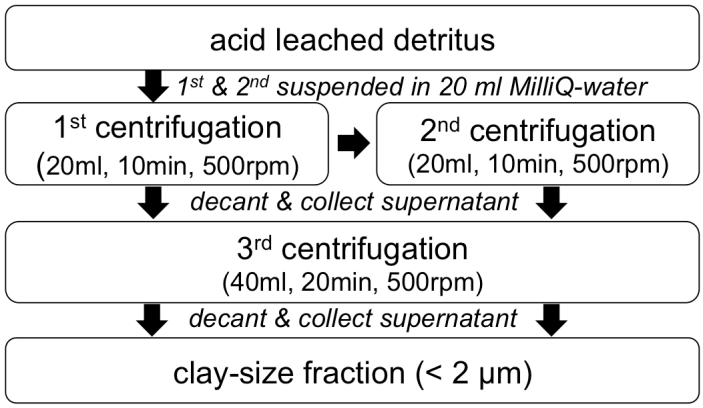

Fig. 2.3. Detailed protocol for the separation of the clay-size fraction using a centrifuge-based Atterberg method (cf. Krumm, 2006). Centrifugation was performed on a Heraeus Megafuge 1.0 in 50 ml Rotilabo® centrifuge tubes.

available software SediCalc (Krumm, 2006). The acid-leached detritus, which represented the residual fraction of the leaching process, was suspended in 20 ml MilliQ-water (in a 50 ml Rotilabo® centrifuge tube) and centrifuged for 10 min at 500 rpm (Heraeus Megafuge 1.0). The supernatant was carefully decanted into a second centrifuge tube. The residual fraction was again treated with the same procedure for a second centrifugation. The collected supernatant was mixed with MilliQ-water to a volume of 40 ml and centrifuged for 20 min to minimize contamination with coarser particles potentially transferred during the previous decanting steps. After centrifugation the supernatant only contained the clay-size fraction < 2 µm (Fig. 2.3), which was successfully cross-checked for a subset of samples on a laser particle-sizer (Fritsch Analysette 22 NanoTec).

2.2.3. Preparation of XRD object slides

About 15 mg of the dried clay fraction (chap. 2.2.2) were suspended in 4 ml of de-ionized water (MilliQ-system) in an ultrasonic bath. Afterwards, the suspended clays were placed on a 0.2 µm filter by applying underpressure. This

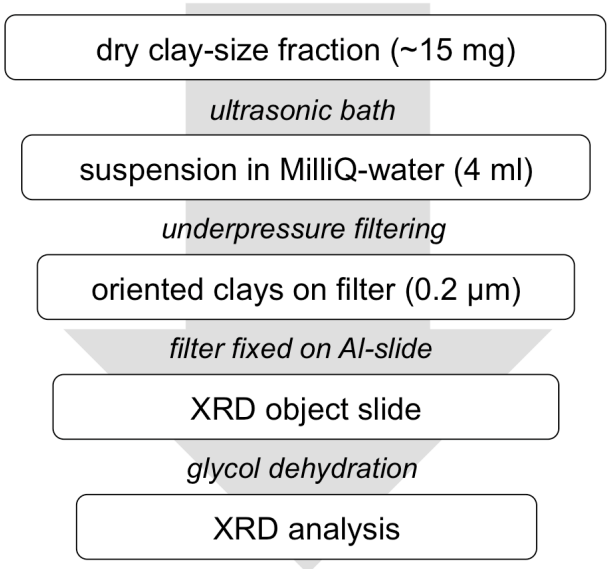

Fig. 2.4. Stepwise description for the production of oriented clay samples on XRD object slides.

resulted in orientation of the clay samples on the filters, which were dried between silicon coated object slides at 50°C in an oven. Finally, the clay-covered filters were fixed on aluminum object slides with double-faced adhesive tape. Prior to x-ray diffraction measurements (Philips PW series) the clay samples were dehydrated with glycol at 50°C for 12 hours.

2.3. XRD analysis

2.3.1. XRD measurements

The XRD measurements were carried out on a Phillips x-ray diffractometer (PW series; CoKα-tube, 40kV, 35mA) at IFM-GEOMAR, Kiel. In a first x-ray scan, the glycol-dehydrated clay samples were measured from 3 to 40°2θ at a step size of 0.01°2θ to get the full range of all mineral reflections of interest. Additionally, a second scan at higher resolution between 27.5 and 30.5°2θ (step size = 0.005°2θ) was performed to achieve a better separation of the kaolinite/chlorite reflections (Fig. 2.5).

2.3.2. Clay mineral quantification

The x-ray diffraction patterns were interpreted using the freely available XRD software MacDiff v4.2.5 (Petschick, 2001). Clay mineral identification and quantification of kaolinite, chlorite, illite and smectite were carried out following Biscaye (1965). The peak positions of all full range XRD patterns (first scans) were normalized to the quartz peak (100) at 4.26Å. The peak areas including the maximum reflections of smectite (001, 17Å), illite (002, 10Å) and kaolinite/chlorite (001, 7.1Å) were used to calculate the clay mineral abundances. From the kaolinite 3.58Å/chlorite 3.54Å peak area ratios (second scan) the respective peak area fractions of kaolinite and chlorite in the combined 7.1Å

reflection were calculated. The sum of the respective peak areas of the four minerals was set to 100% and each mineral was expressed in weighted peak area percentage. Considering the well-known semi-quantitative character of this method, repeated analyses of the XRD patterns were carried out and resulted in a reading error of 2% for the finally calculated peak area percentage of the abundance of each clay mineral.

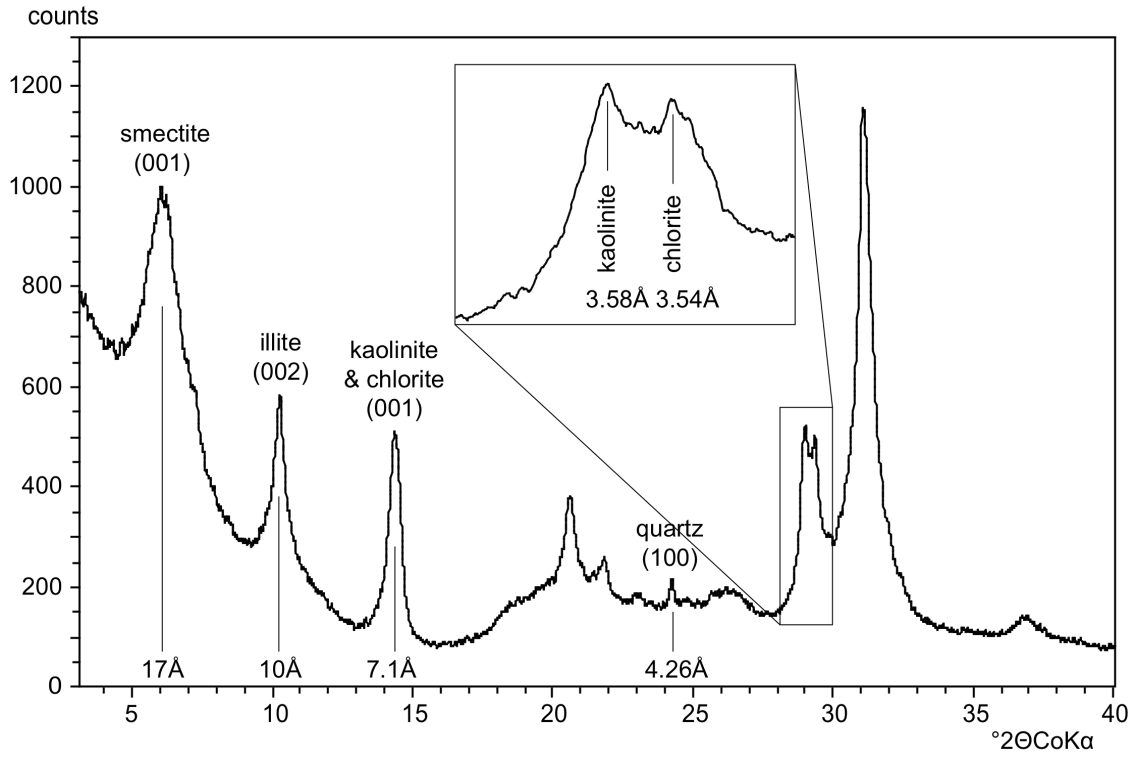

Fig. 2.5. Full range x-ray diffraction scan with the main reflections used for the clay mineral quantification. The inset graph shows the associated high resolution scan from 28 to 30°2θ angles to achieve a more precise kaolinite/chlorite separation.

2.4. Isotope analysis

The chemical procedures applied prior to the isotope measurements described in the following paragraphs were all carried out under clean laboratory conditions at IFM-GEOMAR, Kiel.

2.4.1. Dissolution of the clay-size fraction

Approximately 50 mg of the dried clay fraction were treated with 4 ml aqua regia at 120°C on a hotplate for about 12 hours. Afterwards, the samples were completely dried at 120°C, and the residual sample was treated with a mixture of 4 ml HF (40%) and 1 ml HNO_3 (65%) at 120°C for about 12 hours. After total evaporation of the acid, the residual was totally digested in a mixture of 2 ml HF (40%), 2 ml HNO_3 (65%) and 0.5 ml $HClO_4$ (70%) at 180°C for at least 6 hours. Subsequently, the concentrated acid mixture was evaporated to dryness at 180°C and was subsequently dissolved in 4 ml concentrated HNO_3. The sample was evaporated to dryness again and the residual was carefully dissolved in 100 µl HNO_3 (65%)/100 µl H_2O_2 (30%). After a final evaporation step the residual sample was dissolved in concentrated HNO_3 and transferred into an acid clean teflon vial for further chemical treatment described below.

2.4.2. Element separation and purification

The dissolved Fe-Mn coatings (chap. 2.2.1) and the totally digested clays (chap. 2.4.1) were transferred into nitric form by using concentrated HNO_3. Additionally, all samples were centrifuged to avoid loading undissolved particles onto the ion exchange columns used during the subsequent ion chromatographic procedures (Fig. 2.6). Separation and purification of the respective elements followed previously published standard procedures for Nd (Cohen et al., 1988;

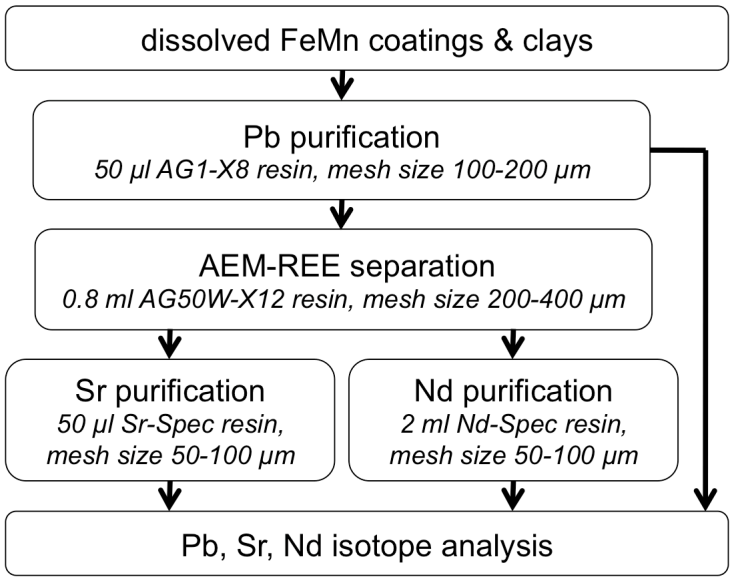

Fig. 2.6. Successive element separation and purification procedure applied for all samples prior to TIMS and MC-ICPMS isotope analysis.

Barrat et al., 1996; Le Fèvre et al., 2005), Pb (Galer and O'Nions, 1989; Lugmair and Galer, 1993) and Sr (Horwitz et al., 1992; Bayon et al., 2002). First, Pb was separated and purified on anion exchange columns (50 µl AG1-X8 resin, mesh size 100-200). After separation of the alkaline earth metals (AEM) from the rare earth elements (REE) on cation exchange columns (0.8 ml AG50W-X12 resin, mesh 200-400), Sr was purified on columns loaded with 50 µl Sr Spec resin (mesh size 50-100), while Nd was separated from the other REEs on columns containing 2 ml Ln Spec resin (mesh size 50-100). The detailed column chemistry recipes for the successive chemical element separations and purifications are listed in the appendix (App. Tab. 2.1-2.4).

2.4.3. Nd isotope analysis

The Nd isotope compositions were determined on a Thermo Scientific TIMS Triton at IFM-GEOMAR, Kiel. Prior to analysis, the purified and dried Nd samples were dissolved in 5 µl 1M HCl/0.35M H_3PO_4 and were loaded and dried on previously degassed rhenium filaments. The measurements were performed at a

minimum ^{144}Nd beam size of 0.5 V using a double filament heating method. The configuration of the detector cups of the instrument and the corresponding isotope masses are shown below (Tab. 2.1). The ^{143}Nd/^{144}Nd ratios were mass bias corrected to ^{146}Nd/^{144}Nd=0.7219 using an exponential fractionation law and were normalized to the accepted value of the JNdi-1 standard of 0.512115 (Tanaka et al., 2000). Repeated measurements of the JNdi-1 standard over a period of several months gave a long-term reproducibility of ±0.35 εNd (2σ). Nd blanks determinations were spiked on mass ^{150}Nd and calculated from the measured ^{150}Nd/^{144}Nd ratio. All procedural blanks were below 50 pg.

Tab. 2.1. Configuration of the detector cups for the Nd isotope measurements on the Thermo Scientific TIMS Triton.

Cup	L4	L3	L2	L1	C	H1	H2	H3	H4
Mass	-	^{142}Nd/^{142}Ce	^{143}Nd	^{144}Nd/^{144}Sm	^{145}Nd	^{146}Nd	^{147}Sm	^{150}Nd	-

2.4.4. Pb isotope analysis

The Pb isotope measurements were carried out on a Nu Plasma HR MC-ICPMS at IFM-GEOMAR, Kiel. All purified Pb samples were adjusted to approximately the same Pb concentration by performing a concentration test prior to the isotope batch runs to achieve comparable Pb beam sizes during the isotope analysis. Accordingly, the purified Pb samples were diluted to a concentration of around 50 ppb in 1 ml HNO_3 (2%). The Pb isotope ratios were determined using a standard bracketing method (Albarède et al., 2004), the configuration of the detector cups and the corresponding isotopes are shown below (Tab. 2.2). All reported Pb isotopic ratios were normalized to the accepted values for NBS981 (Abouchami et al., 1999). The 2σ long-term reproducibility for this standard was ±0.005 for ^{206}Pb/^{204}Pb and ^{207}Pb/^{204}Pb, ±0.015 for ^{208}Pb/^{204}Pb, ±0.0005 for ^{208}Pb/^{206}Pb and ±0.0001 for ^{207}Pb/^{206}Pb. Pb blank concentrations were determined on the Nu Plasma HR MC-ICPMS ion counters by using a standard

calibration based on Pb standard concentrations below 200 ppt. Procedural Pb blanks were below 2.5 ng.

2.4.5. Sr isotope analysis

The Sr isotope measurements were also carried out on a Nu Plasma HR MC-ICPMS at IFM-GEOMAR in Kiel. As described for the Pb isotope analysis above, the Sr samples were diluted to concentrations around 75 ppb in 1 ml HNO_3 (2%) prior to the isotope measurements. Due to variable krypton concentrations in the argon carrier gas used for the inductively coupled plasma (ICP) instruments, the Kr background noise was determined by measuring an additional zero cycle prior to the standard and sample analysis. The configuration of the detector cups and the corresponding isotopes are shown below (Tab. 2.2). Subsequently, the measured $^{87}Sr/^{86}Sr$ isotope ratios were interference (^{86}Kr, ^{87}Rb) and mass bias corrected using an exponential fractionation law (using $^{86}Sr/^{88}Sr$=0.1194, Steiger and Jäger, 1977). The Sr isotope results were normalized to NBS987 $^{87}Sr/^{86}Sr$=0.710245, whereby the 2σ external reproducibility of the repeated standard measurements was ±0.00004. Repeated measurements of a subset of samples showed significantly smaller external reproducibilities of the Sr isotope precision than given by the long-term standard reproducibilities (App. Tab. 4.1). The procedural Sr blanks, which were determined on the ion counters based on a calibration of Sr standards below 250 ppt, were less than 1.7 ng.

Tab. 2.2. Configuration of the detector cups for the Pb and Sr isotope measurements on the Nu Plasma HR MC-ICPMS.

Cup	L4	L3	L2	L1	C	H1	H2	H3	H4
$Mass_{Pb}$	-	-	^{202}Hg	^{203}Tl	^{204}Pb	^{205}Tl	^{206}Pb	^{207}Pb	^{208}Pb
$Mass_{Sr}$	^{83}Kr	$^{84}Sr/Kr$	^{85}Rb	-	$^{86}Sr/Kr$	-	$^{87}Sr/Rb$	-	^{88}Sr

Chapter 3

Late Quaternary variability of Mediterranean Outflow Water from radiogenic Nd and Pb isotopes

Abstract

Mediterranean Outflow Water (MOW) is characterized by higher temperatures and salinities than other ambient water masses. MOW spreads at water depths between 500 and 1500 m in the eastern North Atlantic and has been a source of salinity for the Atlantic Meridional Overturning Circulation in the North Atlantic. We used high-resolution Nd and Pb isotope records of past ambient seawater obtained from authigenic ferromanganese coatings of sediments in three gravity cores at 577, 1 745 and 1 974 m water depth in the Gulf of Cadiz and along the Portuguese margin complemented by a selection of surface sediments to reconstruct the extent and pathways of MOW over the past 23 000 years. The surface and downcore Nd isotope data from all water depths exhibit only a very small variability close to the present day composition of MOW but do not reflect the present day Nd isotopic stratification of the water column as determined from a nearby open ocean hydrographic station. In contrast, the Pb isotope records show significant and systematic variations, which provide evidence for a significantly different pattern of the MOW pathways between 20 000 and 12 000 years ago compared with the subsequent period of time.

this chapter has been published as:

Stumpf, R., Frank, M., Schönfeld, J., Haley, B.A., 2010. Late Quaternary variability of Mediterranean Outflow Water from radiogenic Nd and Pb isotopes. Quaternary Sci. Rev. 29 (19/20), 2462-2472, doi:10.1016/j.quascirev.2010.06.021

3.1. Introduction

3.1.1. Recent hydrography

The Mediterranean Outflow Water (MOW) is a warm (10.5-14 °C) and highly saline (36.5-37.5 psu) water mass, which flows through the Strait of Gibraltar (~ 0.8 Sv) into the Gulf of Cadiz, from where it spreads throughout the North Atlantic Ocean at intermediate water depths between 500 and 1500 m (cf. Schönfeld & Zahn, 2000; Fusco et al., 2008; Sánchez-Román et al., 2009). Waters feeding the MOW in the Mediterranean today are the Levantine Intermediate Water (LIW) and Western Mediterranean Deep Water (WMDW) (Bryden & Stommel, 1984). Differential mixing with the entrained North Atlantic Central Water and the bottom topography in the Gulf of Cadiz lead to a splitting of the MOW into two stability levels: an upper layer with a temperature maximum of >11°C is centred between 500 and 800 m and a lower layer with a salinity maximum of >36.6 prevails between 1000 and 1400 m (Zenk, 1975; Thorpe, 1976; Baringer & Price, 1999). The lower MOW layer expands westwards into the central North Atlantic, while the upper layer is advected northwards along the Iberian continental slope. The latter watermass is still clearly distinguishable in the Irish Sea and the Rockall Trough, and the corresponding density surfaces are found as far north as the Norwegian-Greenland Sea (Reid, 1979; Sparrow et al., 2002). Thus, MOW preconditions North Atlantic Deep Water (NADW) formation and contributes to the Atlantic Meridional Overturning Circulation (AMOC; Bigg et al., 2003). Although the present-day effect on the Atlantic overturning is rather small, enhanced input of MOW supposedly had a stronger and sustaining influence on North Atlantic overturning circulation and thus northern hemisphere climate during the late Quaternary (Rahmstorf, 1998).

3.1.2. Paleoceanography

The spreading, properties and variability of the glacial MOW have been addressed by several studies during the last decade (Schönfeld & Zahn, 2000; Rogerson et al., 2005; Voelker et al., 2006, 2009). From benthic foraminiferal assemblages, stable carbon and oxygen isotope compositions of benthic foraminifera, as well as grain size data it was inferred that MOW was denser and prevailed at greater depths than today at the southern Portuguese continental margin and in the Gulf of Cadiz during the Last Glacial Maximum (Schönfeld & Zahn, 2000; Rogerson et al., 2005). The intensity and composition of the MOW was driven by variations in deep-water formation within the Western Mediterranean Sea, which increased during cold climatic periods (Cacho et al., 2000; Sierro et al., 2005; Cacho et al., 2006). High-resolution grain size analyses from the Gulf of Cadiz also provide evidence for enhanced current strength in the deeper MOW layer during short-term cold events as Dansgaard/Oeschger Stadials and Heinrich Events (Mulder et al., 2002; Llave et al., 2006; Voelker et al., 2006, 2009). Sedimentological and micropaleontological data suggest, however, that lower MOW did not extend further to the north than the Estremadura Plateau north of Lisbon (Schönfeld & Zahn, 2000). The extent of the upper MOW layer was confined to the Gulf of Cadiz during cold periods (Faugères et al., 1984; Sierro et al., 1999; Toucanne et al., 2007).

3.1.3. Radiogenic isotopes

This study aims to reconstruct the variability of late Quaternary flow paths of MOW from its origin in the Strait of Gibraltar, through the Gulf of Cadiz and along the Portuguese margin based on radiogenic Neodymium (Nd) and Lead (Pb) isotopes. These radiogenic isotope systems have increasingly been applied as water mass tracers for the past and present ocean (e.g. Burton et al., 1997; Abouchami et al., 1999; Frank, 2002; Tachikawa et al., 2004; Piotrowski et al.,

2005; Gutjahr et al., 2008, 2009). Dissolved neodymium has a seawater residence time of between 400 and 2000 years (Tachikawa et al., 1999; Frank, 2002; Arsouze et al., 2009) and can be used to trace water mass mixing on ocean basin scales. In contrast, lead is scavenged from the water column by particles much faster and has a seawater residence time of only about 50 years in the Atlantic Ocean and of up to 200 years in the deep Pacific Ocean (Schaule & Patterson, 1981; von Blanckenburg & Igel, 1999). Therefore, Pb isotopes are mainly used as a tracer for local changes in continental inputs into the ocean and short distance water mass mixing.

The content of dissolved trace elements (i.e. Nd, Pb) in the oceans mainly derives from riverine and eolian inputs determined by weathering processes on the adjacent continents. Boundary exchange processes at the seawater/continental margin interface are also considered to contribute to the seawater trace metal budget (Lacan & Jeandel, 2005; Arsouze et al., 2009). Water masses of different origin therefore acquire distinct elemental and isotopic compositions in their source areas, which in the case of Nd isotopes, at a distance from continental inputs, only change through mixing with other water masses. With prevailing oxic conditions in the pore waters, past bottom water isotopic compositions are preserved in early diagenetic, authigenic ferromanganese oxyhydroxide coatings that can be directly extracted from bulk sediments (Rutberg et al., 2000; Bayon et al., 2002; Gutjahr et al., 2007). Even under suboxic conditions it is unlikely that the seawater Nd and Pb isotope signatures of the coatings are significantly modified given the particle reactivity of both elements. This approach has successfully been applied to reconstruct bottom water Nd isotope compositions over the past 150 000 years from locations in the Southern Ocean (Rutberg et al., 2000; Piotrowski et al., 2004, 2005) and in the Northern Indian Ocean (Piotrowski et al., 2009), as well as on longer time scales at several sites in the Indian Ocean (Gourlan et al., 2008). In the North Atlantic there have been so far only two studies on locations from various water depths on the Blake Ridge and on the Bermuda Rise, which were used to reconstruct the evolution of deep and intermediate water masses in the western North Atlantic (Gutjahr et al., 2008; Roberts et al., 2009). Another study focussed on the evolution of intermediate water masses in the western tropical

Atlantic and south Atlantic Ocean (Pahnke et al., 2008). In the eastern Atlantic Ocean no high resolution radiogenic isotope records exist to date.

In the study area, the isotopic compositions of deep waters can mainly be explained by a mixture within the two endmember system of undiluted Mediterranean Outflow Water (MOW) and Atlantic Waters (AW), which for the purpose of this study comprise North Atlantic Central Water and eastern North Atlantic Deep Water. Downcore variations in the Nd and Pb isotope records thus should reflect the variability of the mixing between the predominant water masses at the core site at a given time.

Modern undiluted MOW at the Strait of Gibraltar has an εNd value of -9.4 (Tachikawa et al., 2004). $\varepsilon Nd = [(^{143}Nd/^{144}Nd)sample/(^{143}Nd/^{144}Nd)CHUR-1]x10^4$ with present day CHUR being 0.512638 (Jacobsen & Wasserburg, 1980). Along the flow paths of its different branches, MOW mixes with less radiogenic AW varying from εNd=-11.8 to -12.9 (Spivack & Wasserburg, 1988; Tachikawa et al., 2004). Although there has been a long-term trend towards less radiogenic Nd isotope compositions of water masses in the eastern North Atlantic over the past 3-4 million years (Abouchami et al., 1999; Muiños et al., 2008), the modern range of Nd isotope compositions of AW is considered a reliable endmember for the past 25 000 years (van de Flierdt et al., 2006).

Due to the anthropogenic input of leaded gasoline into the atmosphere the present day dissolved lead isotope composition of seawater has been altered from its natural values (Schaule & Patterson, 1981; Weiss et al., 2003). Information about the preanthropogenic Pb isotope composition of bottom waters has nevertheless been derived from slowly growing hydrogenetic ferromanganese crusts (cf. Frank, 2002). These data show that pre-industrial $^{206}Pb/^{204}Pb$ ratios were ≥ 19.0 for AW and ≤ 18.8 for MOW respectively (Abouchami et al., 1999; Muiños et al., 2008), but it needs to be taken into account that these numbers represent averages covering several 10 000 to more than 100 000 years due to the coarse time resolution of the ferromanganese crust records. A direct comparison of

the above records obtained from ferromanganese crusts to the dataset presented here is therefore not easily practicable because the short-term hydrographic variations (~1 500 yrs) this study focuses on cannot be resolved. In addition, there are no records directly from the immediate MOW flow paths and the Pb isotope signatures obtained from the crusts may therefore not reflect the undiluted endmember composition of MOW. The only high-resolution Pb isotope record of past seawater up to now was obtained from the authigenic ferromanganese coatings of marine sediments from Blake Ridge in the NW Atlantic Ocean by Gutjahr et al. (2009). These data cover the transition from the Last Glacial Maximum (LGM) to the Holocene and document a significant Pb isotope variability of water masses in the western North Atlantic, which was related to weathering inputs released by the retreat of the Laurentide ice sheet.

Here we present the first late Quaternary high-resolution Nd and Pb isotope reconstructions of MOW obtained from several sediment cores in the Gulf of Cadiz and the Portuguese continental margin.

3.2. Material and Methods

Nd and Pb isotope records from three gravity cores from sites in the Gulf of Cadiz and the Portuguese margin have been produced in this study. In addition, twelve coretop samples from different water depths were used to calibrate the Nd

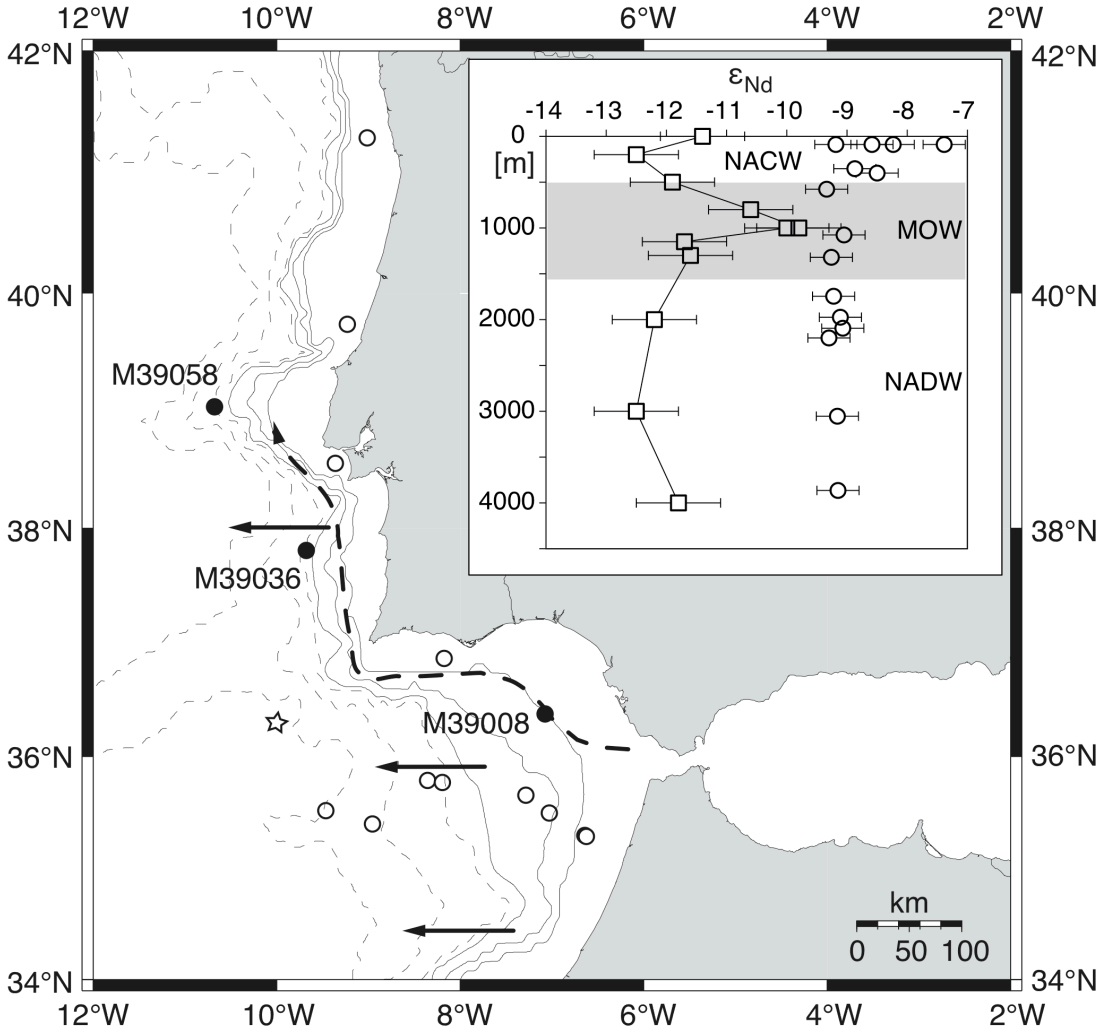

Fig. 3.1. Map of the core locations in the Gulf of Cadiz and along the Portuguese margin and a nearby water column Nd isotope profile (open circles = coretops, filled circles = coretop and downcore samples, asterisk = water column profile). Bathymetry: Solid lines are at 600, 1 000 and 1 600 m (corresponding to the depth of modern MOW); dashed lines represent 2 000, 3 000 and 4 000 m water depth. The dashed line arrow shows the flow path of the upper MOW layer, the solid line arrows show direction and extent of the lower MOW layer. The inset graph shows dissolved ε_{Nd} values vs. water depth for hydrocast station A-II, 109 St. 95 (open squares; Piepgras & Wasserburg, 1983) and coretop leachates (open circles; this study). Present-day MOW depth is highlighted in grey (MOW: Mediterranean Outflow Water; NACW: North Atlantic Central Water; NADW: North Atlantic Deep Water).

isotope composition of the ferromanganese coatings to the present day water mass composition. The gravity cores were recovered during RV METEOR cruise M39/1 (Schott et al., 1997) and the additional coretops were recovered during RV MARIA S. MERIAN cruise MSM1/3 (Pfannkuche, 2006), RV POSEIDON cruise PO287 (in 2002) and the LIVRA cruise (RV ALMEIDA CARVALHO, 1977; Fig. 3.1, App. Tab. 3.1). Seawater isotopic compositions of Nd and Pb were obtained by leaching of the ferromanganese coatings of bulk sediments. To ensure recovery of the authigenic coatings and to avoid contamination by partial leaching of detrital material, the $^{87}Sr/^{86}Sr$ ratios from the same leaching solutions were monitored (Rutberg et al., 2000; Piotrowski et al., 2005; Gutjahr et al., 2007). For Nd isotopes, the coretop leachates are compared to water column Nd isotope signatures of hydrocasts from a location downstream of the Strait of Gibraltar (Piepgras & Wasserburg, 1983; Spivack & Wasserburg, 1988) and from locations around the Strait of Gibraltar itself (Tachikawa et al., 2004) to assess its validity as a water mass tracer at these locations.

3.2.1. Sample preparation

The authigenic Fe-Mn oxyhydroxide fraction was leached from bulk sediment samples following a slightly modified method for the extraction of seawater Nd and Pb isotopic compositions from Fe-Mn coatings described by Gutjahr et al. (2007). The dry and coarsely ground bulk sediments (1-2 g) were rinsed twice with de-ionized water (from a Milli-Q system). The carbonate fraction was dissolved and removed using a 15%-acetic acid/1M-Na acetate buffer followed by a triple rinse with de-ionized water. The Fe-Mn oxide coatings were leached for 1 h in an ultrasonic bath and for 2 h in a shaker using a 0.05M-hydroxylamine hydrochloride/15%-acetic acid solution buffered to pH 3.6 with NaOH. After centrifugation, the supernatant contains the dissolved seawater fraction for further chemical treatment. The detrital fraction stayed for at least 12 h in the remaining leach solution to achieve a complete removal of the coatings, followed by a triple rinse with de-ionized water. Finally, 30 mg of the dried residual fraction

of the bulk sediment was completely dissolved in a mixture of concentrated HF-HNO_3 to determine the isotopic composition of the detrital material for a subset of the samples.

3.2.2. Element separation and purification

Separation and purification of the respective elements in the leachates and the dissolved detritus followed previously published standard procedures for Pb (Galer & O'Nions, 1989; Lugmair and Galer, 1993), Sr (Horwitz et al., 1992; Bayon et al., 2002) and Nd (Cohen et al., 1988; Barrat et al., 1996; Le Fèvre et al., 2005). First, Pb was separated on anion exchange columns (50 µl AG1-X8 resin, mesh 100-200). After separation of the alkaline elements from the rare earth elements on cation exchange columns (0.8 ml AG50W-X12 resin, mesh 200-400), Sr was purified on columns with 50 µl Sr Spec resin (mesh 50-100), while Nd was separated from the other REEs on columns containing 2 ml Ln Spec resin (mesh 50-100).

3.2.3. Isotope analysis

Pb and Sr isotope measurements were carried out on a Nu Plasma MC-ICPMS, whereas Nd isotopes were measured on a TIMS Triton, both at IFM-GEOMAR, Kiel. Lead isotope ratios were determined using a standard bracketing method (Albarède et al., 2004). All reported Pb isotopic data are normalized to the accepted values for NBS981 (Abouchami et al., 1999). The 2σ long-term reproducibility for this standard was ±0.0027 for $^{206}Pb/^{204}Pb$ and $^{207}Pb/^{204}Pb$, ±0.0079 for $^{208}Pb/^{204}Pb$, ±0.0002 for $^{208}Pb/^{206}Pb$ and ±0.0001 for $^{207}Pb/^{206}Pb$. Procedural Pb blanks were below 2.5 ng. $^{87}Sr/^{86}Sr$ isotope ratios were interference (^{86}Kr, ^{87}Rb) and mass bias corrected (using $^{86}Sr/^{88}Sr$=0.1194, Steiger and Jäger, 1977). The Sr isotope results were normalized to NBS987 $^{87}Sr/^{86}Sr$=0.710245,

whereby the 2σ external reproducibility during the measurements for this study was ±0.000033. Procedural Sr blanks were less than 1.7 ng. $^{143}Nd/^{144}Nd$ ratios were mass bias corrected to $^{146}Nd/^{144}Nd=0.7219$ and normalized to the accepted value of the JNdi-1 standard of 0.512115 (Tanaka et al., 2000). Repeated measurements of the JNdi-1 standard over a period of several months gave a long-term reproducibility of ±0.35 εNd (2σ). Procedural Nd blanks were ≤ 25pg.

3.2.4. Core descriptions and age models

The age models of the sediment cores have been published previously and are based on high-resolution AMS ^{14}C-dating, correlation of planktonic $\delta^{18}O$ records and the identification of Heinrich layers. The age model for core M39008, which documents the variations in the upper layer of MOW, was published by Cacho et al. (2001) and Löwemark et al. (2004). The age models for cores M39036 and M39058, which document the variations in the lower layer of MOW, were published by Löwemark et al. (2004) and Schönfeld and Zahn (2000). The chronology of core M39008 is based on 14 AMS ^{14}C-datings covering the past 22 000 yrs and resulting in an average sedimentation rate at this location of 25.6 cm/kyr. The chronology of core M39036 was established with 11 AMS ^{14}C-datings covering the past 25 300 yrs and resulting in an average sedimentation rate of 20.3 cm/kyr. Finally, for core M39058, 8 AMS ^{14}C-datings covering the past 20 700 yrs were produced yielding an average sedimentation rate of 6.4 cm/kyr. The reported ^{14}C-dating uncertainties for the three cores range from ±25 to ±150 years (1σ). All three cores omit any indications for the presence of bioturbation, sediment reworking or hiatuses for the period of interest. For the coretop samples no direct dating is available but, as discussed below, there is evidence that they represent undisturbed, recently deposited sediments.

3.3. Results

The $^{87}Sr/^{86}Sr$ ratios of the leached Fe-Mn coatings are between 0.70838 and 0.70905, on average 0.70870, which is slightly below the modern strontium isotope composition of seawater (0.70916). Similar values are observed for hydroxylamine hydrochloride leachates of sediment particles near the study area (cf. Tachikawa et al., 2004). In contrast, the residual detrital fraction of the sediments shows significantly more radiogenic $^{87}Sr/^{86}Sr$ values above 0.71889. This demonstrates that the applied leaching procedure only dissolves the authigenic ferromanganese coatings of the sediments, and that there is no significant detrital contamination of the leached seawater Nd and Pb isotope signatures (Fig. 3.2, App. Tab. 3.1, App. Tab. 3.3). Any contribution to the Sr isotope signature of the coatings from older pore waters below, which would result in slightly less radiogenic Sr isotope values than present day seawater, cannot be completely excluded but is highly unlikely in view of the relatively young age of the sediments of this study and the prevailing high sedimentation rates.

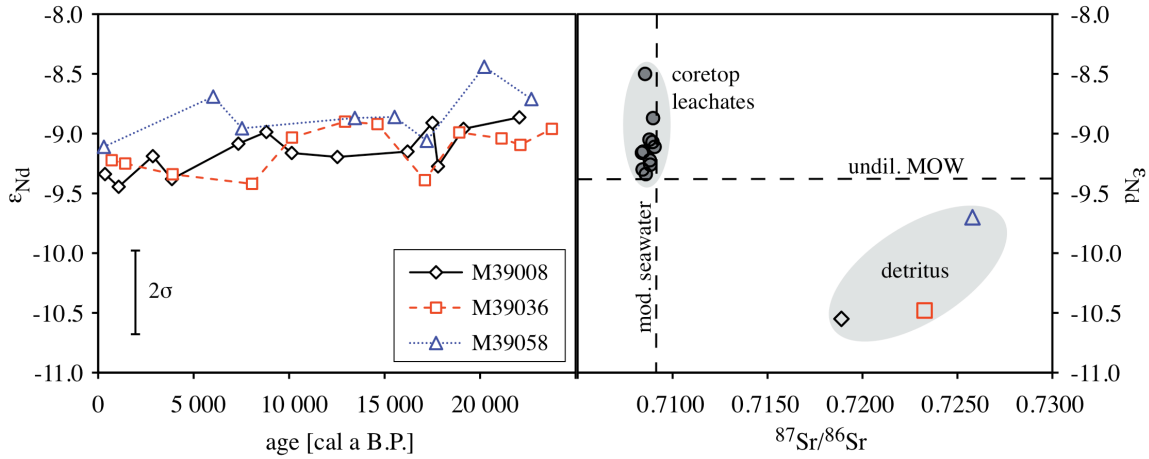

Fig. 3.2. Left: εNd time series for cores M39008 (black solid line, diamonds), M39036 (red dashed line, squares) and M39058 (blue dotted line, triangles). Within the 2σ uncertainties of the measurements, the downcore Nd isotope composition barely changed throughout the late Quaternary. Right: εNd values vs. $^{87}Sr/^{86}Sr$ ratios for coretop leachates and detritus. The coretop leachates plot on modern Sr seawater composition and close to undiluted MOW for the Nd isotopes. The array of the detrital data is shifted to more radiogenic Sr compositions and less radiogenic Nd compositions, documenting that the leachates have not been contaminated by the detrital fraction of the sediments.

The Fe-Mn coatings from the surface and subsurface waters in the study area vary in Nd isotope composition between εNd=-7.7 to -9.3 (Fig. 3.1, App. Tab. 3.1). Since these coretops are located at a short distance to the coast and to river mouths, these values most likely reflect the respective river discharges. However, this lateral variability in Nd isotope composition is not observed in greater water depths at all, suggesting that the coatings formed in surface and subsurface waters do not significantly contribute to the Nd isotope compositions recorded in the underlying water masses.

Below 400 m water depth, the coretop leachates show a very constant εNd =-9.1± 0.35 (Fig. 3.1, App. Tab. 3.1). These data are within error of the measured value of -9.4 for present day undiluted Mediterranean Outflow Water (Spivack & Wasserburg, 1988; Tachikawa et al., 2004). Below the water depths occupied by MOW at present day (below 1 500 m), the seawater εNd values leached from the coretop sediments are, however, also constant at εNd =-9.1 and do not shift to less radiogenic values (i.e. εNd =-11.8 to -12.9 for eastern NADW), which would have reflected the transition to eastern North Atlantic deep water masses. Piepgras & Wasserburg (1983) presented a water column profile from the surface to 4 000 m water depth with εNd values ranging from -11.4 to -12.5 and a pronounced excursion to more radiogenic values of up to -9.8 around 1 000 m water depth corresponding to the core of Mediterranean Outflow Water (Fig. 3.1). This is not observed by the coretop data and the consistency of the neodymium isotopic composition in the leachates with water depth shows that Nd isotopes derived from Fe-Mn coatings do not reflect the different water masses in the Gulf of Cadiz and along the Portuguese margin. The downcore Nd isotope records also barely show any significant variations over time (Fig. 3.2). Furthermore, the most radiogenic εNd record is obtained for core M39058, which is expected to show the most diluted MOW signature (because of its distance to the Strait of Gibraltar) and thus least radiogenic Nd isotope ratios.

The Pb isotope compositions of the coretop leachates are much less radiogenic than the observed downcore ratios (App. Tab. 3.2-3.3) due to the

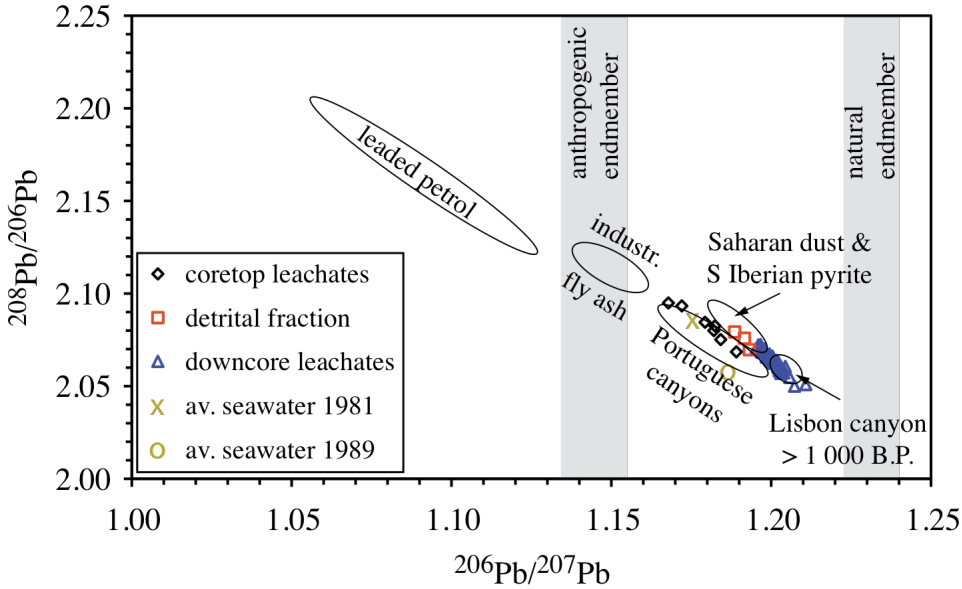

Fig. 3.3. $^{208}Pb/^{206}Pb$ vs. $^{206}Pb/^{207}Pb$ ratios for coretop (black diamonds) and downcore (blue triangles) leachates and the coretop detrital fraction (red squares). Brownish symbols are average seawater Pb isotope compositions from the East Iberian Basin from 1981 (X) and the Central Iberian Basin/North African Basin from 1989 (O) respectively (Weiss et al., 2003). The data are plotted together with various Pb sources interacting on the Portuguese margin published by Richter et al. (2009). Shaded bars show anthropogenic and natural Pb endmember composition estimates, black circles frame predominant lead sources (Richter et al., 2009). The coretop leachates are clearly shifted towards the anthropogenic Pb endmember and correspond to the recent Pb isotopic signatures of Portuguese canyons and the ambient modern seawater. Downcore leachates and detrital data of this study agree well with the preanthropogenic Pb in Lisbon canyon, as well as to Pb isotope signatures of Saharan dust and Iberian pyrite.

anthropogenic input of lead derived from gasoline and industrial emissions. The fact that all coretop samples show anthropogenic contamination confirms their very recent deposition. The predominant source responsible for the modification of the modern Pb isotope compositions along the Portuguese margin is most likely fly ash from industrial waste incinerators (Richter et al., 2009; Fig. 3.3).

The Pb isotope signatures of the downcore leachates agree well with Pb ratios observed in sediments older than 1 000 years from Lisbon canyon, and in part with ratios observed for Saharan dust and the southern Iberian pyrite belt (Richter et al., 2009). The data for the detrital fraction of the coretops is also consistent with Pb isotope compositions of Saharan dust and the Southern Iberian pyrite belt,

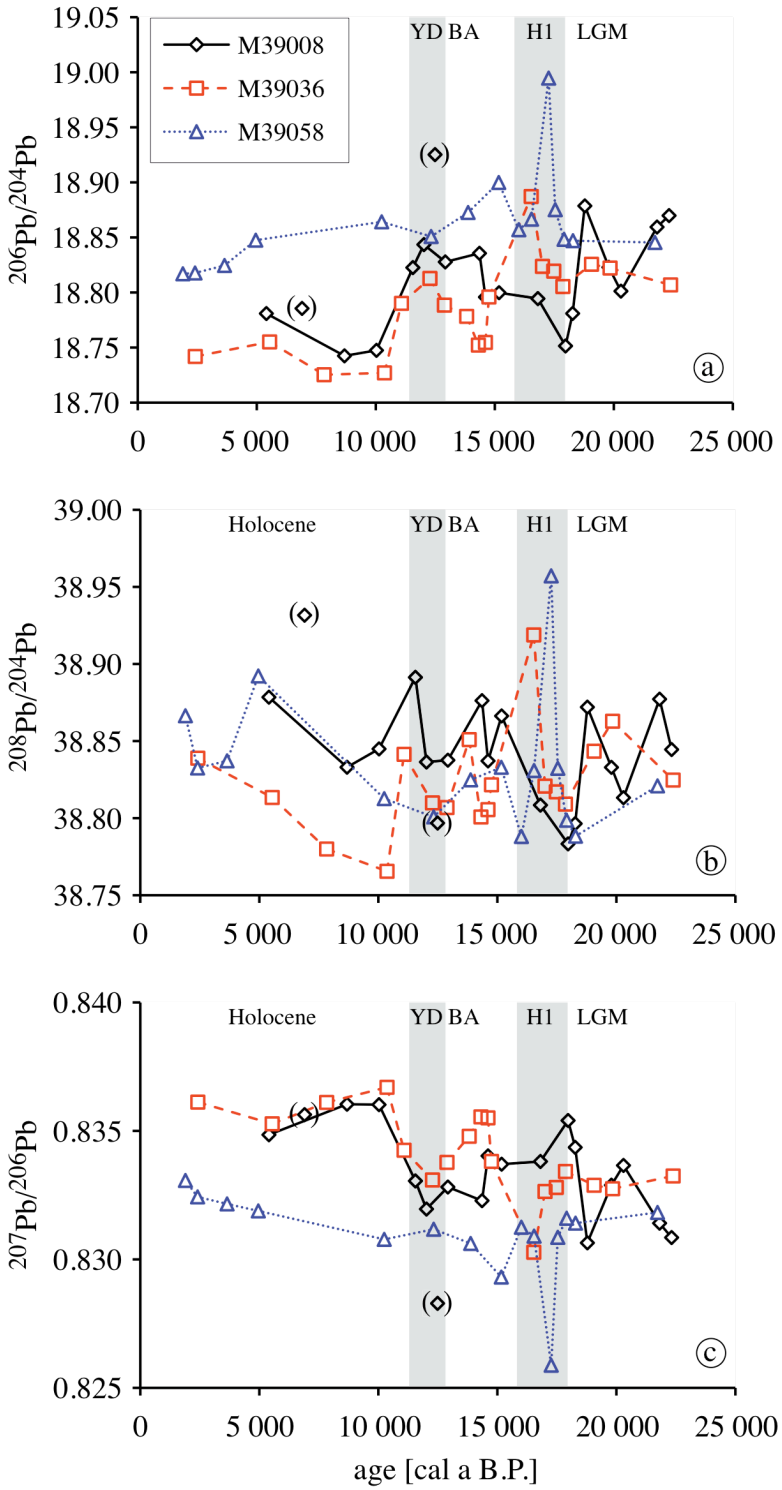

Fig. 3.4. (a) $^{206}Pb/^{204}Pb$, (b) $^{208}Pb/^{204}Pb$ and (c) $^{207}Pb/^{206}Pb$ time series from the LGM to the late Holocene (core M39008 = black solid lines, diamonds; core M39036 = red dashed lines, squares; core M39058 = blue dotted lines, triangles). The two samples that do not plot into the mixing arrays in Fig. 3.5 are excluded from the M39008 time series (diamonds in brackets). Cores M39008 and M39036 show the very similar patterns for all three time series with the strongest variabilities occurring between 15 000 and 20 000 years B.P. (LGM = Last Glacial Maximum; H1 = Heinrich Event 1; BA = Bølling-Allerød interstadial; YD = Younger Dryas stadial). 2σ errors correspond to symbol size for $^{208}Pb/^{204}Pb$ and $^{207}Pb/^{204}Pb$ ratios and are even smaller for $^{207}Pb/^{206}Pb$.

which are likely to have been major contributors to the dissolved Pb in the western Mediterranean and thus for MOW throughout the late Quaternary.

In contrast to Nd isotopes, Pb isotope compositions of past seawater document systematic variations over the past 25 kyrs including a tendency to less radiogenic Pb isotope ratios during the Holocene (Fig. 3.4a, App. Tab. 3.2). During the Last Glacial Maximum (LGM) and the early deglaciation until the onset of the Bølling-Allerød (BA) interstadial, the Pb isotope variability recorded in cores M39008 (representing the upper MOW layer in the Gulf of Cadiz) and M39036 (representing the lower MOW layer) shows significant differences, which is reported in the overlapping of their time series. From around 13.7 ka onwards, in contrast, the Pb isotope variability in these two cores are very similar (Pb isotope evolutions are essentially parallel; Fig. 3.4). The variability observed in cores M39008 and M39036 during the early deglaciation was most likely generated by an intense and rapid fluctuation of the depth of the MOW layer, possibly amplified by a decoupling of the upper and lower outflow paths. During the Holocene, the signatures of the MOW core layers are much more stable. Except for a short excursion to highly radiogenic values during Heinrich Event H1, the time series for the third core M39058 shows essentially invariable Pb isotope compositions throughout the past ~23 000 years (Fig. 3.4).

3.4. Discussion

3.4.1. Evaluating MOW flow paths with Nd isotopes

As described above, the seawater Nd isotope signatures obtained by leaching of the Fe-Mn coatings are inconsistent with corresponding samples from the open ocean water column above and below the depths of MOW (Fig. 3.1). The constant Nd isotope composition of the leachates with water depth may indicate that the Nd isotope composition of bottom water masses at all depths along the Portuguese

margin is essentially the same. Although this possibility appears rather unlikely, there are to date no seawater Nd isotope measurements directly on the Portuguese margin itself and it cannot be completely excluded that boundary exchange processes with the margin sediments (Lacan & Jeandel, 2005) have led to a shift of the dissolved Nd isotope compositions directly above the sediments to values essentially identical to that of MOW. In this case one would, however, have expected a shift towards less radiogenic values given that the Nd isotope compositions of the detrital fractions themselves are significantly less radiogenic (εNd = -10 to -12) than the observed leachate data and the isotopic composition of MOW. Alternatively, and more likely, the different water masses, which at a distance from the continent are clearly distinct (Piegras & Wasserburg, 1983; Spivack & Wasserburg, 1988), cannot be distinguished in their Nd isotope signatures at these sites because they have been strongly influenced by processes other than water mass mixing. Potential processes that might be responsible for the vertical homogenisation of the Nd isotope compositions leached from the sediments of the Gulf of Cadiz and along the Portuguese margin are (a) a steady eolian dust input from North Africa and Iberia which overprints the local water mass signatures and (b) a continuous downslope transport of sediment in the nepheloid layer along the continental margin.

The present-day North African and Iberian dust input into the western Mediterranean Sea, the Gulf of Cadiz and the eastern North Atlantic near Portugal has εNd signatures between -11.0 and -12.0 (Grousset et al., 1998). Thus, a contribution of unradiogenic dust (εNd =-11.0 to -12.0) to even more unradiogenic deeper water masses (εNd =-12 to -13.5) cannot explain the uniformly radiogenic εNd around -9.1 in the coretop leachates at the Portuguese margin below 500 m water depth.

From the above considerations, an influence of downslope sediment transport within the nepheloid layer is the more likely explanation. Gutjahr et al. (2008) described a similar observation for Nd isotope signatures obtained from sediment coatings from the North American continental slope at Blake Ridge,

where the Nd isotope signature of the coatings only represents the present day dissolved seawater signature within the water depths occupied by the high current speed core of the deep western boundary current, whereas above this depth downslope transport of particles coated at shallow depths on the shelf obscured the present day seawater signature. Sediment particles can continuously be transported downslope within the nepheloid layer or by repeated re-suspension without apparently disturbing the chronostratigraphy of the sediments. During each period of redeposition, the coatings can incorporate the isotope composition of the local bottom water if the early diagenetic conditions at the sediment/water interface still allow the formation of ferromanganese coatings. Thus, sediment coatings can acquire isotope compositions that integrate over different water masses at various depths. It is known that the constant shearing of MOW in the Gulf of Cadiz and along the Portuguese margin leads to increased erosion as well as to enhanced nepheloid layer activity (Arzola et al., 2008), and the occurrence of sediment flows and turbidites are reported (Lebreiro et al., 1997; Mulder et al., 2009).

Although this process can explain the mismatch between coatings and corresponding dissolved seawater data, it does not sufficiently explain the uniformity of the εNd signature below 500 m water depth. Given that eastern NADW is the predominant water mass below MOW, the εNd value of downslope transported coatings should thus approximate εNd =-13. Considering that the time scales and conditions of the formation of Fe-Mn coatings are still under debate, our data suggest that the sediment coatings were mainly formed within MOW before they were exported to greater depths. In addition, the high sedimentation rates at the core locations inhibit that the coatings formed in the MOW layer above can incorporate any significant deeper Nd isotope signal. It is also possible, but less likely, that the formation of the coatings stopped while still under the influence of the MOW before they sank to greater depths.

Although there are evident difficulties in distinguishing Nd isotopes of certain water masses, Fe-Mn precipitates and airborne particles in the coastal

areas off NW Africa and on the Portuguese margin (cf. Albarède et al., 1992), MOW can clearly be distinguished from adjacent water masses by its Nd isotope signature at greater distance from its source. Rickli et al. (2009) presented data from a water column profile in the Bay of Biscay where the presence of MOW is clearly reflected by its Nd isotope composition. Ferromanganese crusts several hundred km west of Gibraltar also recorded the Nd isotope composition of MOW at the corresponding water depth (Abouchami et al., 1999; Muiños et al., 2008). Khélifi et al. (2009) were able to trace the Pliocene extension of MOW along the eastern North Atlantic continental margin as far north as SE Ireland using Mg/Ca-based bottom water temperatures, paleo-salinity and paleo-density variations, as well as the Nd isotope compositions of leached Fe-Mn coatings.

In summary, the data of our study suggest that the applicability of Nd isotopes in Fe-Mn coatings as a water mass tracer is limited at locations on continental margins with steep slopes, high sedimentation rates and the presence of downslope transport of suspended material in the nepheloid layer. Nevertheless, the persistent Nd isotope signature at the present and presumably also past MOW depth indicates a constant MOW signature close to the outflow source and a constant prevalence of MOW during the past 25 000 years.

3.4.2. Evaluating MOW flow paths with Pb isotopes

For Pb isotopes the coretop leachates unfortunately cannot be used to directly verify the observations concerning the present day water mass signatures given that both the seawater itself and the coatings in the study area have been overprinted by anthropogenic Pb (Richter et al., 2009; Fig. 3.3). Nevertheless, significant and systematic variations were observed for the preanthropogenic seawater Pb isotope time series obtained from the ferromanganese coatings. Despite the fact that the Nd isotope signatures have been homogenized by the sedimentary processes described above, the Pb isotope variabilities are considered reliable, which is mainly due to the pronounced difference between the Pb isotope compositions of the two water mass endmembers. In addition, the short residence

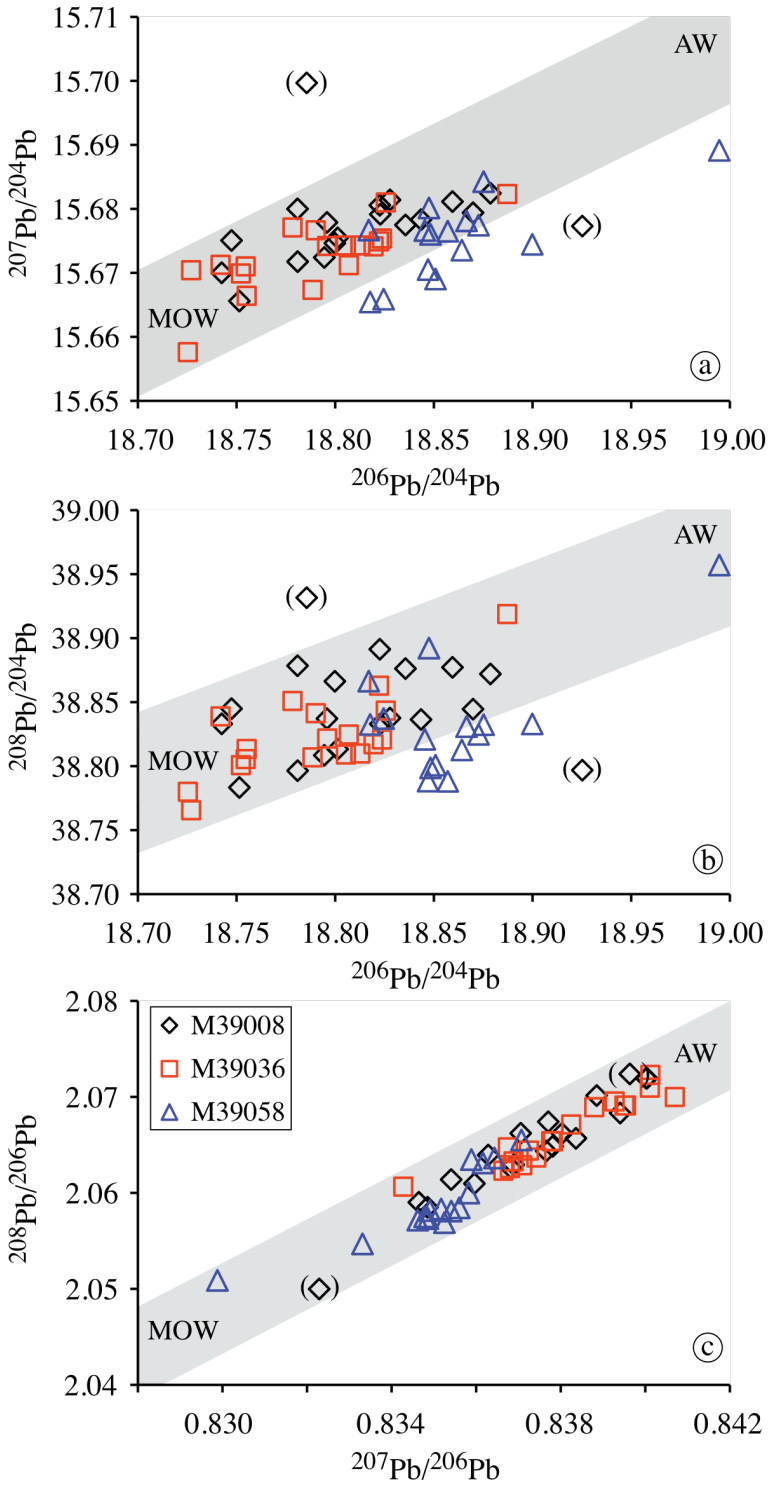

Fig. 3.5. (a) $^{207}Pb/^{204}Pb$ vs. $^{206}Pb/^{204}Pb$, (b) $^{208}Pb/^{204}Pb$ vs. $^{206}Pb/^{204}Pb$ and (c) $^{208}Pb/^{206}Pb$ vs. $^{207}Pb/^{206}Pb$ ratios for cores M39008 (black diamonds), M39036 (red squares) and M39058 (blue triangles). The shaded areas mark the mixing arrays between the two endmembers MOW and AW restricted to the values of cores M39008 and M39036. Samples plotting outside these arrays were most likely influenced by a third Pb source. (a)-(b) Core M39058 was strongly influenced by an additional source, as well as two samples from core M39008 (highlighted by diamonds in brackets; see also Fig. 3.4), and is therefore only of limited use for MOW reconstructions using Pb isotopes. (c) All samples plot within the array specified by the radiogenic Pb isotope ratios (^{208}Pb, ^{207}Pb, ^{206}Pb) suggesting that the Pb sources did not experience very large changes. 2σ errors correspond to symbol size for $^{208}Pb/^{204}Pb$ and $^{207}Pb/^{204}Pb$ ratios and are even smaller for the other Pb isotope ratios.

time of Pb in particle enriched near coastal seawater combined with high sedimentation rates at the site locations benefit records of past seawater Pb isotope compositions, which are particularly sensitive to short-term changes in the composition of the MOW endmember. It is clear that the sediment re-suspension processes on the continental slope inferred for the homogenisation of the Nd isotope signature in the study area must also have affected the Pb isotopes. In particular, the amplitude of the isotopic variations may decrease if signatures from slightly different time slices (i.e. decades) are mixed during redeposition, and the upper and lower boundaries of water masses appear to be at deeper positions due to downslope transport. However, in contrast to Nd isotopes, the Pb isotopic differences between the endmember water masses involved were large enough to provide reliable information about the predominant water masses at the respective sites over time. Thus, the Pb isotope variations can be used to assess the late Quaternary history of MOW in the study area (Fig. 3.6).

3.4.2.1. Past variability of MOW

The Pb isotope ratios for cores M39008 (representing the upper MOW layer) and M39036 (representing the lower MOW layer) plot on a mixing-line between the MOW and AW endmembers except for two samples (Fig. 3.5). The data for the northernmost core M39058 have been significantly influenced by an additional source of Pb over the past 25 000 years (Fig. 3.5a-b). Although the core is located on the western tip of Tagus plateau, the discharge of Tagus river system may have been responsible for the biased Pb isotopic signature. Thus, core M39058 is not applicable for a reconstruction of the history of MOW using lead isotopes.

The Pb isotope variability in the study area over time has been controlled by two processes: (a) variability of the endmember composition of the water masses due to changes in the erosional input in the source regions and (b) changes in the circulation system of MOW. In order to evaluate and isolate the predominant

factors throughout the late Quaternary, both processes will be discussed separately.

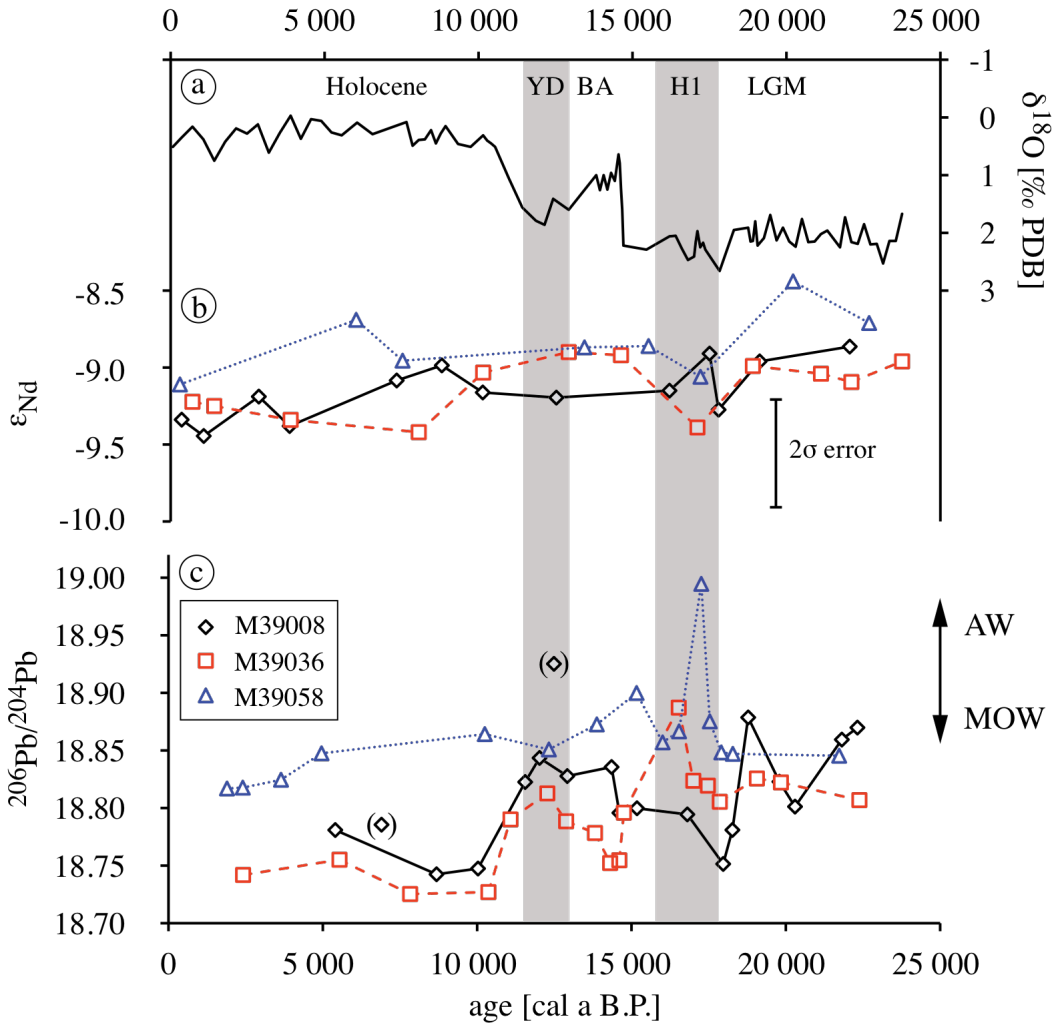

Fig. 3.6. (a) $\delta^{18}O$, (b) ε_{Nd} and (c) $^{206}Pb/^{204}Pb$ records for the LGM to Holocene transition. (a) $\delta^{18}O$ record from core M39036 based on planktonic foraminifera. (b) ε_{Nd} records for cores M39008 (black diamonds), M39036 (red squares) and M39058 (blue triangles). Taking into account the 2σ uncertainty of the Nd isotope measurements (ε_{Nd} ±0.35), there is barely a significant change in Nd isotope composition through time for each core. Interestingly, the most radiogenic ε_{Nd} values are from core M39058, which would have been expected to show the most diluted Nd composition of MOW and thus the least radiogenic Nd isotope compositions. (c) $^{206}Pb/^{204}Pb$ time series for cores M39008 (black solid line), M39036 (red dashed line) and M39058 (blue dotted line). The two unconnected data points (diamonds with brackets) refer to Fig. 3.5. The strongest variability took place during the early deglaciation (LGM = Last Glacial Maximum; H1 = Heinrich Event 1; BA = Bølling-Allerød interstadial; YD = Younger Dryas stadial).

3.4.2.2. Endmember variability

The Pb isotopic composition of the Atlantic endmember (AW) with its large deep water reservoir is expected to show less variability at smaller amplitudes than the Mediterranean one (MOW) during the late Quaternary. The variability of the MOW endmember has been governed by variations in continental weathering regimes. During the LGM, H1 and YD cold events, as well as the earliest deglaciation, arid conditions led to a decrease in riverine inputs and an increased input of dust (Morellón et al., 2009). In contrast, during warmer and more humid periods, chemical weathering dominated the Pb endmember characteristics and the influence of dust input decreased. Since the source regions of Pb most likely did not change significantly over time (Fig. 3.5), the isotopic variability of the MOW endmember was induced by the prevailing riverine inputs controlled by climatic conditions. Colder and drier climatic intervals are depicted as maxima of the $^{206}Pb/^{204}Pb$ record of core M39036 during the LGM, H1 and YD. These maxima alternate with $^{206}Pb/^{204}Pb$ minima representing increased riverine inputs that shifted the ratios towards the composition of MOW during the earliest deglaciation, the BA and the Holocene (Fig. 3.6).

Assuming this, we suggest that the observed Pb isotope variability of the records have mainly been controlled by MOW endmember variabilites during the Younger Dryas and throughout the Holocene, when the Pb isotope time series of cores M39008 and M39036 have changed in phase (Fig. 3.6). We note that the similarity of the Pb isotope variations for the Holocene records may at least partly have resulted from the sediment redeposition processes. However, the Pb isotope records of both cores were decoupled from the LGM to the early YD. For this period of time, we suggest that changes in extent and flow path of MOW were responsible for the observed Pb isotopic variability.

3.4.2.3. Changes in flow paths of MOW

From the above considerations, the Pb isotope data indicate that significant changes in the flow paths and the extent of MOW occurred between the LGM and the onset of the YD stadial. Due to lower temperature and increased salinity, MOW prevailed at a greater water depth than today during the last glacial (Schönfeld & Zahn, 2000; Rogerson et al., 2005). During early deglaciation, the $^{206}Pb/^{204}Pb$ ratios in the upper layer of MOW (Fig. 3.6; core M39008) switched from radiogenic Atlantic-like values to less radiogenic Mediterranean-like values at the onset of Heinrich Event H1 indicating an emplacement of the upper MOW layer, while the lower MOW (Fig. 3.6; core M39036) remained unchanged.

The Pb isotope data further suggest that the lower layer of MOW underwent a short excursion to shallower depths during H1, before re-establishing somewhat deeper around 15 000 calender years B.P. During the same period of time, the upper MOW layer moderately deepened and only showed small fluctuations, which is in good agreement with observations by Cacho et al. (2006). According to these authors, the deep water formation rate in the western Mediterranean Sea (WMDW) decreased immediately before H1 but the salinity was still high resulting in a reduced current speed of the lower MOW and re-establishment of the upper layer of MOW. During H1, the WMDW was less saline, but the formation rates increased again leading to a higher current speed in the upper MOW layer.

With the beginning of the Bølling-Allerød interstadial at 14.8 ka, the Pb isotope data show that both MOW layers deepened, and from 14.5 ka onwards and throughout the Younger Dryas the lower layer of MOW rose again, while the upper one kept its depth and extent. Based on benthic foraminiferal assemblages, an extension of the upper layer to greater depths, as well as a deepening of the lower layer started at 15.8 ka (13 kyrs ^{14}C-age, Schönfeld & Zahn, 2000). This difference in timing between the two approaches may have been caused by sediment redeposition given that fine grained sediment particles are more susceptible than the relatively large foraminifera.

Since the outgoing Younger Dryas stadial and throughout the entire Holocene, the isotopic compositions of both MOW layers have been very similar, whereby the shallower location of core M39008 has always remained more radiogenic. This suggests that the Holocene Pb isotopic variability has mainly been caused by changes in the endmember compositions and that the flow paths of upper and lower MOW have been stable in position and extent over the last 12 000 years. This observation is not in agreement with micropaleontological and sedimentological studies suggesting the establishment of the modern hydrology of the Mediterranean Outflow Water by between 8.3 and 6.8 ka (7.5 - 6 kyrs ^{14}C-age, Schönfeld & Zahn, 2000). It has to be taken into account that the above micropaleontological and sedimentological studies reflect changes in current velocities. The Pb isotope compositions, in contrast, were a consequence of changes in water mass advection, which was not necessarily accompanied by changes in current velocities.

The difficulties in distinguishing between influences of endmember variability and changes in ocean circulation on the recorded Pb isotope variability in the Gulf of Cadiz and along the Portuguese margin, and the fact that only two core records are available, possibly limits the detection of minor changes in the flow paths and intensity of MOW, but the data show that major circulation changes of MOW during the late Quaternary can be traced using Pb isotopes.

3.5. Conclusions

Seawater Nd isotope signatures obtained from leached Fe-Mn coatings from coretop bulk sediment samples in the Gulf of Cadiz and along the Portuguese margin differ from the Nd isotopic composition of water samples from the corresponding water depths at a distance from the coast. Although the Fe-Mn coatings of the sediments within the MOW flow paths (~500 – 1500 m) reflect the Nd isotope composition of the outflow water, the transition to underlying eastern

NADW is not documented in the sediments, most likely due to downslope sediment redeposition processes in the nepheloid layer. The downcore records of leached Nd isotope signatures of all three cores covering the last 23 000 yrs barely show significant variations and thus cannot contribute to the reconstruction of the late Quaternary history of MOW in the study area, although the data confirm a constant Nd isotope signature of MOW over the investigated period of time, which can thus be used to trace the paleo flow path of MOW further downstream.

The variability of Pb isotope composition of the MOW endmember has mainly been controlled by the prevailing climatic conditions. During colder periods eolian input dominated the isotopic endmember composition, whereas warmer climates led to an increased riverine input as a consequence of an enhanced hydrological cycle. Based on the downcore Pb isotope records of cores M39008 and M39036 major changes in MOW flow paths occurred during the early deglaciation. Settled at greater depth during LGM, the upper layer of MOW shallowed significantly or was even established during H1, followed by a moderate deepening. Decoupled from the upper MOW layer, the lower outflow layer moderately rose and fell again during the outgoing H1. Only minor fluctuations in depth of the MOW layers were documented for the BA interstadial and the YD stadial. Based on the Pb isotope records, the present-day hydrography of MOW was established ~12 000 yrs ago.

3.6. Acknowledgments

This work was funded by Deutsche Forschungsgemeinschaft (Project FR1198/3-1). We would like to thank Folkmar Hauff from IFM-GEOMAR for support of the TIMS measurements. We also thank Fatima Abrantes from the Laboratório Nacional de Energia e Geologia, I.P. (LNEG), Portugal, for providing surface sediment samples from ALMEIDA CARVALHO (1977) and POSEIDON (2002) cruises.

Chapter 4

Climatically driven changes in sediment supply on the SW Iberian shelf since the Last Glacial Maximum

Abstract

The assemblages of marine sediments on the SW Iberian shelf consist of the various regional particulate sources that comprise a record of significant environmental changes since the Last Glacial Maximum (LGM), especially regarding prevailing weathering and transport regimes. The relatively rapid, decadal scale Mediterranean overturning circulation permits mixing of suspended particles from the entire Mediterranean Sea. They are entrained into the suspended particulate matter (SPM) carried by Mediterranean Outflow Water (MOW), which enters the Eastern North Atlantic through the Strait of Gibraltar and spreads at intermediate water depth in the Gulf of Cadiz and along the Portuguese continental margin. Other major sediment sources that have potentially contributed to the character and budget of SPM along the flow path of MOW on the SW Iberian shelf are North African dust and river transported particles from the Iberian Peninsula. In order to reconstruct climate and circulation driven changes in the supply of sediments from these sources over the past ~23 000 years, radiogenic Nd, Sr and Pb isotope records from the clay-size sediment fraction were produced from three gravity cores in the Gulf of Cadiz (577 m water depth) and from the Portuguese shelf (1745 m, 1974 m water depth). These records were supplemented by time series analyses of clay mineral abundances from the same set of samples. Contrary to expectations, the transition from the LGM to the Holocene was not marked by very strong changes but significantly different isotopic records reflect Heinrich stadial 1 and the African Humid Period (AHP). The data also suggest that the continental chemical weathering regime changed

with prevailing climate conditions and supplied the SW Iberian shelf with variable clay mineral abundances from essentially the same source rocks.

---

this chapter is going to be submitted as:

Stumpf, R., Frank, M., Schönfeld, J., Haley, B.A. Climatically driven changes in sediment supply on the SW Iberian shelf since the Last Glacial Maximum.

4.1. Introduction

4.1.1. Mediterranean Sea – North Atlantic hydrography

The thermohaline circulation of the Mediterranean Sea is mainly driven by a zonal conveyor belt (Pinardi & Masetti, 2000). At the Strait of Gibraltar, relatively low-salinity (~36‰) Eastern North Atlantic Central Water (ENACW) enters the Western Mediterranean Sea as a surface layer water mass flowing eastward across the Mediterranean Sea. Upon reaching the eastern Mediterranean basin, permanent evaporation has increased the density of this surface water, which is subducted and transformed into Levantine Intermediate Water (LIW). This higher salinity (~38‰) LIW recirculates westwards at mid-depth and, with some contributions from Western Mediterranean Deep Water (WMDW), forms Mediterranean Outflow Water (MOW), which spreads as a bottom water mass from the sill of Gibraltar into the Eastern North Atlantic with a volume flow of about 0.8 Sv (Baringer & Price, 1997, 1999; Fusco et al., 2008; Sánchez-Román et al., 2009).

Mediterranean Outflow Water sinks to water depths between 500 and 1500 m where interactions with both the ENACW and slope bathymetry in the Gulf of Cadiz lead to a splitting of the MOW plume into two branches. A lower layer of MOW at about 1000-1500 m water depth flows westwards into the central North Atlantic, whereas an upper layer of MOW at about 500-800 m water depths flows northwards along the Iberian continental margin (Schönfeld & Zahn, 2000; Fusco et al., 2008). Today, the salinity anomaly and the corresponding density surfaces of the upper branch of the Mediterranean Outflow Water can be traced as far north as the Bay of Biscay, the Rockall Trough and even the Norwegian-Greenland Sea (Reid, 1979; Sparrow et al., 2002; Rickli et al., 2009). Furthermore, it has been argued that the salinity supplied to the North Atlantic by MOW contributes directly to the North Atlantic Deep Water (NADW) formation (Bigg et al., 2003) and thus broader overturning of the Atlantic Ocean.

During the Last Glacial Maximum (LGM) several multi-proxy studies have suggested that Mediterranean Outflow Water prevailed at greater depths along the Iberian slope than today (Schönfeld & Zahn, 2000; Rogerson et al., 2005; Voelker et al., 2006, 2009). The suggestion is that during cold climatic periods, enhanced Western Mediterranean Deep Water formation increased the current strength of the MOW plume leading to variations of its flow paths (Cacho et al., 2000, 2006; Sierro et al., 2005). Moreover, these pulses of enhanced Mediterranean Outflow Water may have increased the salt budget of the Atlantic, thereby impacting the formation of NADW, and thus North Atlantic overturning circulation during the late Quaternary (Rahmstorf, 1998).

4.1.2. Suspended particulate matter

The suspended particulate matter (SPM) in oceanic water masses originate from physical and chemical weathering processes on the adjacent continents. Surface runoff via river discharge and atmospheric circulation supply the particles to the oceans. Therefore, three major particle sources have contributed to the suspended load deposited on the SW Iberian shelf since the LGM: suspended river material from the European and African continents (Grousset et al., 1988; López-Galindo et al., 1999; Hoogakker et al., 2004; Hamann et al., 2009), North African Saharan dust (Guerzoni et al., 1997; Caquineau et al., 1998; Stuut et al., 2009) and, to some minor extent, ice rafted debris (IRD) during Heinrich stadial H1 (Hemming et al., 1998; Hamann et al., 2009).

The zonal circulation of the Mediterranean conveyor occurs on decadal timescales, and the overturning of the meridional cells connecting the Levantine Intermediate Water with the Mediterranean deep water bodies is thought to take around 50-80 yrs (Pinardi & Masetti, 2000). Due to this rapid basin-wide circulation, riverine and eolian particles from the entire Mediterranean region are well mixed and contribute to the load of suspended particulate matter carried by Mediterranean Outflow Water, which are ultimately deposited in the Gulf of Cadiz

and along the Iberian slope. Beyond these Mediterranean-derived sediments, ENACW transports the clay-size particulate load from proximal Atlantic sources into the western Mediterranean Sea, where the particles stay suspended and thus also contribute to the SPM load of MOW (Grousset et al., 1988).

This study focuses on the detrital clay-size fraction of the sediments deposited in the Gulf of Cadiz and on the Portuguese continental margin aiming to reconstruct changes of the contributions from the different source areas of the SPM within the flow path of Mediterranean Outflow Water along the SW Iberian shelf. Radiogenic Nd, Pb and Sr isotope records obtained from the clay-size fraction, as well as clay mineral abundances from the same set of samples have been produced and compared to available data from the entire Mediterranean catchment area in order to characterize endmember variability during the latest Quaternary and the Holocene. These SPM radiogenic isotope records are compared with previously obtained bottom water radiogenic isotope records extracted from ferromanganese oxyhydroxide coatings of the same sediment cores (Stumpf et al., 2010) to provide a better understanding of the late Quaternary changes of the Mediterranean Outflow Water hydrography.

4.1.3. Radiogenic isotopes and clay mineral abundances as source tracers

Weathering of continental source rocks of particular lithogenic origin and age release particles whose distinct mineralogical and radiogenic isotope signature can be used to trace their source areas. Therefore, changes in the isotopic or mineralogical composition of SPM over time can be used to indicate variations in the contributions of provenance endmembers. These changes are generally closely related to climatic changes (Kohfeld & Harrison, 2001; Frigola et al., 2008; Hamann et al., 2009).

The radiogenic isotope compositions of Nd, Pb, and Sr have successfully been applied to reconstruct changes in contributions from different source areas of deposited particles that have either been transported by rivers and oceanic water masses (cf. Grousset et al., 1995, 1998; Hemming et al., 1998; Fagel et al., 2002, 2004; Erel & Torrent, 2010) or through the atmosphere (cf. Goldstein et al., 1984; Krom et al., 1999; Grousset & Biscaye, 2005; Cole et al., 2009). In sediments deposited in the Gulf of Cadiz and on the Portuguese margin, Sr and Pb isotopic signatures of Saharan dust sources are distinctly less radiogenic ($^{87}Sr/^{86}Sr$=0.715; $^{208}Pb/^{206}Pb$=2.075) and weathering contributions from Iberian rocks are more radiogenic for ($^{87}Sr/^{86}Sr$=0.73; $^{208}Pb/^{206}Pb$=2.090; Erel & Torrent, 2010). During the LGM, the radiogenic Nd and Sr isotope ratios of material supplied from North African dust sources were slightly shifted to less radiogenic values (Grousset et al., 1998). In contrast, during Heinrich stadial 1 the southward shift of the IRD belt discharged least radiogenic Nd isotope signatures (εNd=-20), highly radiogenic Sr compositions ($^{87}Sr/^{86}Sr$>0.725) and a wide range of radiogenic Pb compositions into the Eastern North Atlantic (Hemming et al., 1998).

Clay mineral assemblages have also been widely used as a tool to determine the origin of marine sediments (cf. Biscaye, 1965; Grousset et al., 1988; Guerzoni et al., 1997; Caquineau et al., 1998; Fagel et al., 2001; Hoogakker et al., 2004; Jimenez-Espejo et al., 2007; Hamann et al., 2009). In the study area, increasing smectite abundances have been found to originate from fluvial inputs from the Iberian Peninsula (Grousset et al., 1988; López-Galindo et al., 1999), as well as from river discharge into the Levantine Sea (Hamann et al., 2009). Kaolinite, and to a minor extent illite, have mainly been associated with Saharan dust fluxes (Caquineau et al., 1998; Hamann et al., 2009).

Thus, radiogenic isotope signatures of clay-size particles and clay mineral ratios have recorded the variability of the predominant particle transport processes and source areas supplying the SPM on the SW Iberian shelf through time. Given that this study focuses on core sites located near the upper and lower boundaries of MOW, rapid variations of the composition of the SPM, both

isotopically or mineralogically, are also considered to be caused by changes in the hydrography of MOW.

4.1.4. Clay formation by chemical weathering

Sedimentary clays are mainly formed by chemical weathering processes at the surfaces of the source rocks before they are eroded and transported to the ocean. In mid-latitude environments the dominant chemical weathering process is hydrolysis, which largely depends on precipitation and temperature and is therefore sensitive to the prevailing climate conditions (Chamley, 1989). High kaolinite abundances are confined to low latitudes, being preferentially formed in warm and humid climates (Griffin et al. 1968). In contrast, chlorite and illite formation is increased at higher latitudes, where chemical weathering is reduced by the cold-dry climates (Berry & Johns, 1966; Windom, 1976). The formation of smectite occurs under intermediate mid-latitude conditions of variably cold-dry to warm-humid climates (Chamley, 1989). By analogy to these modern observations, chemical weathering changes driven by changing climate conditions can result in the supply of different clay mineral assemblages originating from the same source rocks over time.

4.2. Material and Methods

4.2.1. Core selection and age models

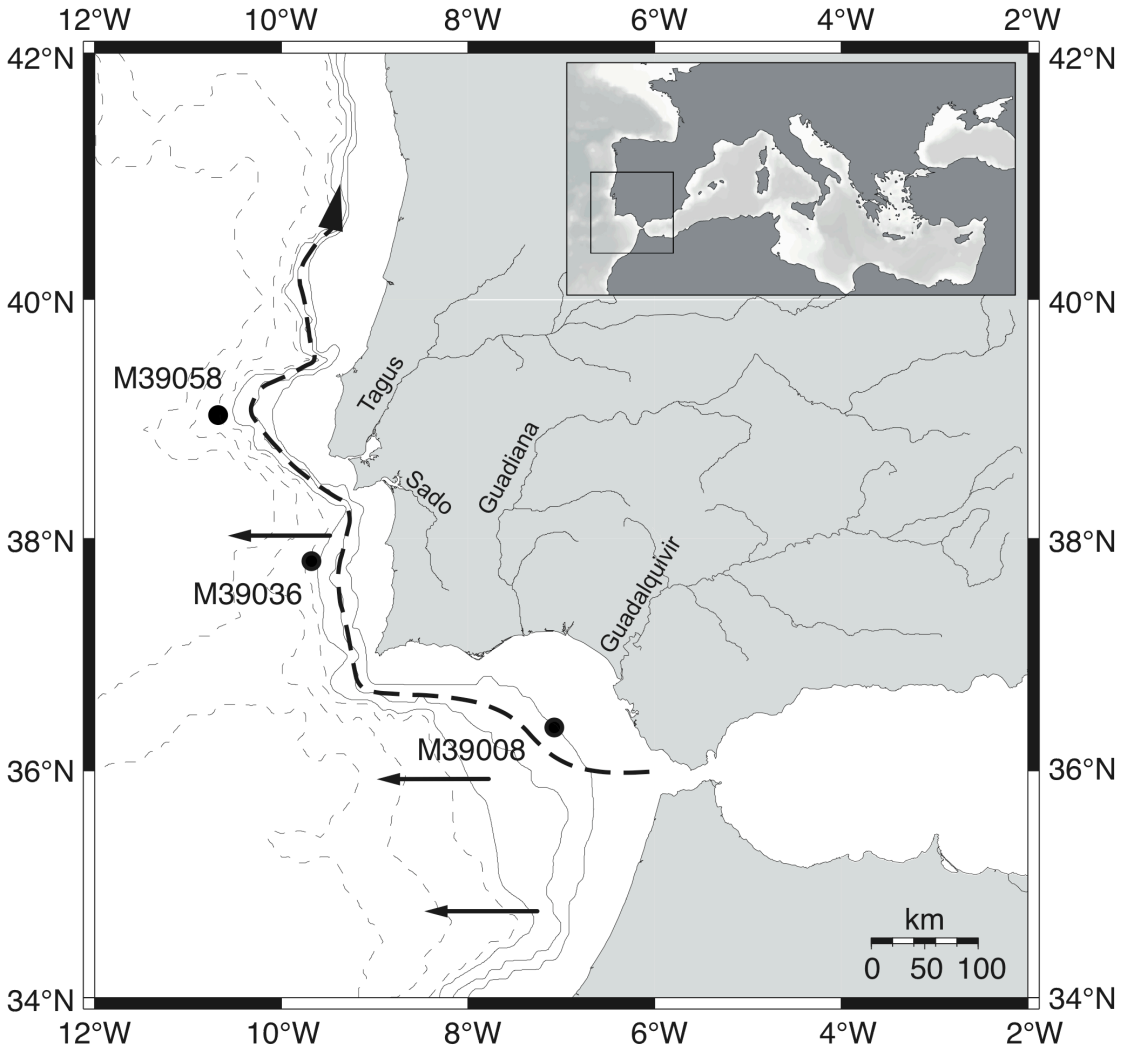

Fig. 4.1. Overview and detailed map of the three core locations (black dots) in the Gulf of Cadiz and on the Portuguese shelf, including the major south Iberian river systems. The Tagus/Sado river system discharges into the Atlantic near Lisbon (~38.5°N), the Guadiana (~7.5°W) and Guadalquivir (~6.5°W) river systems enter the northern Gulf of Cadiz. The dashed line arrow shows the flow path of the upper layer of MOW, the solid line arrows show the direction and extent of the lower layer of MOW. Bathymetry: Solid lines are at 600, 1000 and 1600 m (corresponding to the depth of modern MOW); dashed lines represent 2000, 3000 and 4000 m water depth.

In this study, material from three gravity cores recovered during RV METEOR cruise M39/1 (Schott et al., 1997) from sites in the Gulf of Cadiz and on the Portuguese margin (Fig. 4.1) was used to produce high-resolution records of clay mineralogical composition and radiogenic Nd, Pb, and Sr isotope signatures of the cores clay-size fraction covering the past ~23 000 years. The age models of the sediment cores have been published previously and are based on high-resolution AMS ^{14}C-dating (Fig. 4.2d), correlation of planktonic δ^{18}O records and the identification of Heinrich layers. The age model for core M39008 (at 577 m water depth; representing the upper layer of MOW) has been published by Cacho et al. (2001) and Löwemark et al. (2004). Their ^{14}C-ages cover the last 22 000 yrs and document an average sedimentation rate of 25.6 cm/kyr at this location. The age models for cores M39036 and M39058 from 1 745 m and 1 974 m water depth respectively, which represent the lower layer of MOW, have been published by Löwemark et al. (2004) and Schönfeld & Zahn (2000). Age estimates of core M39036 cover the past 25 300 yrs and yield an average sedimentation rate of 20.3 cm/kyr. ^{14}C-ages of core M39058 cover the last 20 700 yrs and yield an average sedimentation rate of 6.4 cm/kyr. The reported uncertainties of the ^{14}C-dating for the three cores range from ±25 to ±150 years (1σ). For the period of interest, there is no indication for the presence of strong bioturbation or sediment reworking in the cores.

4.2.2. Sample preparation

Prior to the separation of the clay-size fraction (< 2 μm) the sediments were treated with buffered acetic acid and leached with hydroxylamine, following a previously published procedure (modified from Gutjahr et al., 2007; Stumpf et al., 2010). This procedure removes carbonates and authigenic oxides, providing a more pure clay signal for analyses. The clay-size fraction was then separated from the cleaned bulk sediment samples using a centrifuge-based Atterberg method. The required settling times were calculated with the freely available software SediCalc (Krumm, 2006). The grain size intended for isolation (< 2 μm) was

verified using a subset of samples on a laser particle-sizer (Fritsch Analysette 22 NanoTec).

4.2.3. Clay mineralogical analysis

About 15 mg of the dried clay fraction was resuspended in an ultrasonic bath and placed on 0.2 µm filters by applying underpressure below the filters. This oriented the clay samples, which were then dried at 50°C in an oven and positioned on aluminium object slides. Prior to x-ray diffraction (XRD) analyses (Philips PW series) the clay samples were dehydrated using glycol at 50°C for 12 hours (cf. Biscaye, 1965; Winkler, 1999).

The x-ray diffraction patterns were interpreted using the freely available XRD software MacDiff v4.2.5 (Petschick, 2001). Clay mineral identification and quantification of kaolinite, chlorite, illite and smectite were carried out following Biscaye (1965). The sums of the respective peak areas of the four minerals were set to 100% and each individual mineral was expressed as a weighted peak area percentage. Considering the well-known semi-quantitative character of this method, repeated analysis of the XRD patterns were carried out and resulted in a reading error of 2% for the finally calculated abundance of each clay mineral.

4.2.4. Element separation and purification

A second 50 mg aliquot of the dried clay fraction was completely digested using a mixture of concentrated HF-HNO_3-$HClO_4$. Separation and purification of Nd, Pb and Sr from the totally digested clays followed previously published procedures for Nd (Cohen et al., 1988; Barrat et al., 1996; Le Fèvre et al., 2005), Pb (Galer and O'Nions, 1989; Lugmair and Galer, 1993) and Sr (Horwitz et al., 1992; Bayon et al., 2002), which is outlined in Stumpf et al. (2010).

4.2.5. Isotope analysis

Nd isotope compositions were measured on a Triton TIMS at IFM-GEOMAR, Kiel. $^{143}Nd/^{144}Nd$ ratios were mass bias corrected to $^{146}Nd/^{144}Nd=0.7219$ and were then normalized to the accepted value of the JNdi-1 standard of 0.512115 (Tanaka et al., 2000). For convenience, the $^{143}Nd/^{144}Nd$ ratios were expressed in the ε-notation with $\varepsilon Nd = [(^{143}Nd/^{144}Nd)_{sample}/(^{143}Nd/^{144}Nd)_{CHUR} - 1] \times 10^4$ using CHUR = 0.512638 (Jacobsen & Wasserburg, 1980). Repeated measurements of the JNdi-1 standard over a period of several months gave a long-term external reproducibility of ±0.35 εNd units (2σ). Procedural Nd blanks were ≤ 50 pg. Pb and Sr isotope measurements were carried out on a Nu Plasma MC-ICPMS, also at IFM-GEOMAR in Kiel. Pb isotope ratios were determined using a standard bracketing method (Albarède et al., 2004). All reported Pb isotope data have been normalized to the accepted values for NBS981 (Abouchami et al., 1999). The 2σ long-term reproducibility of the measurements of this standard was ±0.005 for $^{206}Pb/^{204}Pb$ and $^{207}Pb/^{204}Pb$, ±0.015 for $^{208}Pb/^{204}Pb$, ±0.0005 for $^{208}Pb/^{206}Pb$ and ±0.0001 for $^{207}Pb/^{206}Pb$. Procedural Pb blanks were below 0.5 ng. Measured $^{87}Sr/^{86}Sr$ isotope ratios were interference (^{86}Kr, ^{87}Rb) and mass bias corrected (using $^{86}Sr/^{88}Sr=0.1194$, Steiger and Jäger, 1977). The Sr isotope results were normalized to NBS987 $^{87}Sr/^{86}Sr=0.710245$, and the 2σ external reproducibility during the measurements for this study was ±0.00004. Procedural Sr blanks were less than 0.7 ng. Repeated measurements of a subset of samples revealed a significantly better precision of the Nd and Sr isotope data than the long-term standard reproducibilities (App. Tab. 4.1).

4.3. Results

4.3.1. Nd, Pb and Sr isotope time series

The Nd isotope compositions of the clay-size fraction range from εNd=-9.0 to -11.5 (Fig. 4.2b). Following a common pattern for the last ~23 000 years, the εNd values are more radiogenic overall for the northernmost core (M39058) and become less radiogenic approaching the Strait of Gibraltar. Between 15.5-17.5 ka this pattern was inverted to least radiogenic εNd values at the northernmost site. However, the LGM and Holocene Nd isotope compositions agree well with Nd isotope signatures of adjacent continental rocks (Jeandel et al., 2007), and North African sources, which have likely been major contributors to the suspended particulate matter (SPM) load of MOW and the Iberian continental margin via eolian dust transport (Grousset et al., 1988, 1998; Grousset & Biscaye, 2005).

The clays' $^{206}Pb/^{204}Pb$ isotope compositions became continuously less radiogenic from the Last Glacial Maximum (LGM) to late Holocene times (Fig. 4.2c) for all three cores. However, while the two cores closest to the Gulf of Cadiz (M39008 and M39036) have a similar Pb isotope evolution, those of core M39058 are significantly more radiogenic. This observation is in agreement with previously published Pb isotope data of past ambient bottom waters obtained from ferromanganese coatings of sediment particles from the same cores (Stumpf et al., 2010). The offset of core M39058 is also apparent in the $^{208}Pb/^{206}Pb$ vs. $^{206}Pb/^{207}Pb$ three-isotope plot (Fig. 4.6). There is also a distinct difference in the $^{208}Pb/^{204}Pb$ ratios, although less radiogenic than the two other cores, whereas there is no significant difference in the $^{207}Pb/^{204}Pb$ ratios (App. Tab. 4.1).

At all three locations, the $^{87}Sr/^{86}Sr$ ratios of the clay-size fraction were most radiogenic during the early deglaciation around H1 at ~16.5 ka, then decreased to become least radiogenic at ~10 000 years ago to change again to slightly more radiogenic values during the Holocene (Fig. 4.2a). A similar radiogenic Sr isotope

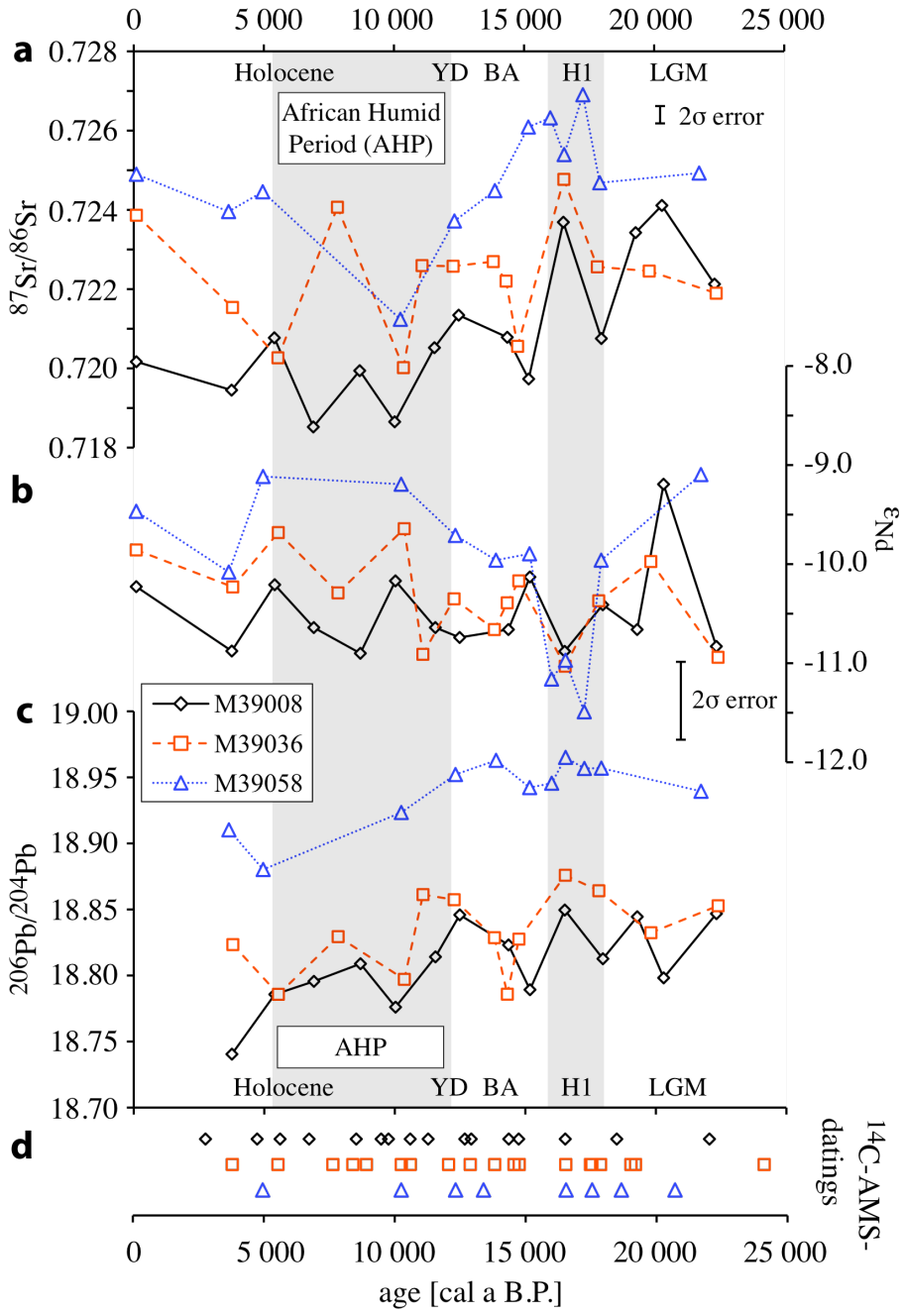

Fig. 4.2. (a) $^{87}Sr/^{86}Sr$, (b) εNd and (c) $^{206}Pb/^{204}Pb$ isotope records, as well as (d) ^{14}C-AMS dating points for the last ~ 23 000 cal yrs B.P. for cores M39008 (black diamonds, solid line), M39036 (red squares, dashed line) and M39058 (blue triangles, dotted line). The $^{206}Pb/^{204}Pb$ 2σ error in (c) is below dot size. The time interval covering the African Humid Period (AHP) is from Cole et al., (2009) (LGM=Last Glacial Maximum; H1=Heinrich Event 1; BA=Bølling-Allerød interstadial; YD=Younger Dryas stadial).

evolution has been observed at a core location off northwestern Africa (Cole et al., 2009). As with the Pb and Nd data, core M39058 consistently shows the most

radiogenic Sr isotopic composition and a slightly different evolution through time than the other two cores. The $^{87}Sr/^{86}Sr$ values during H1 are in good agreement with data reported for the North Atlantic IRD belt (Hemming et al., 1998). Holocene Sr isotope ratios compare well to data from North African Saharan dust (Grousset & Biscaye, 2005) and weathered Iberian soils (Erel & Torrent, 2010). However, the more radiogenic Sr isotope ratios observed during the LGM contrast with data from Grousset et al. (1998), who reported a shift towards less radiogenic Sr isotope compositions during that period of time.

4.3.2. Clay mineralogy

Overall, the abundance of illite+smectite (∅=67%) dominates the kaolinite+chlorite content (∅=33%) in all three cores through time (Fig. 4.3, App. Tab. 4.2), which is in good agreement with previously published clay assemblage data in the Gulf of Cadiz and from the Portuguese margin (Biscaye, 1965; Grousset et al., 1988; Lopez-Galindo, 1999). Illite, and especially kaolinite and chlorite abundances, show only little significant variations. Only the illite/kaolinite record shows a tendency towards lower ratios from the LGM to the Holocene (Fig. 4.4, right panel). The smectite abundance shows the highest variability with time in all cores and it is most dominant in shallow core M39008 in the Gulf of Cadiz (cf. Schönfeld, 1997). A prominent short-term increase of 10 to 20% in smectite content is documented in every core. Interestingly, this excursion occurred in cores M39036 and M39058 between 16.5 and 15.0 ka, and appeared in core M39008 at 12.5 ka (Fig. 4.3). This phase lag is also documented in the clay mineral ratio time series (Fig. 4.4).

However, the time series of both the clay mineral abundances and the clay mineral ratios show only minor variation around Heinrich stadial 1 at 16.5 ka (Fig. 4.3, Fig. 4.4), when the distinct excursions in the radiogenic isotope compositions of the clay-size fraction occurred.

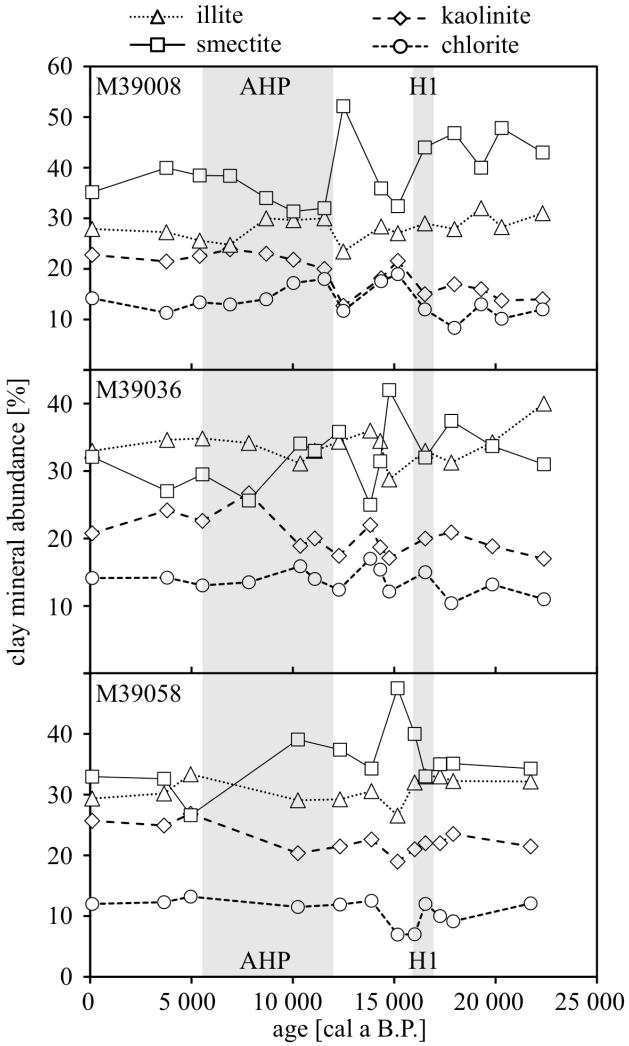

Fig. 4.3. Clay mineral abundance time series covering the past ~23 kyrs for cores M39008, M39036 and M39058. The abundances of smectite, illite, kaolinite and chlorite are given in weighted peak area percentage based on the sums of the four peak areas from the respective XRD measurements. The reading error is about 2%. H1 marks the samples at 16.5 ka representing the maximum of Heinrich stadial 1 in these cores, AHP refers to the African Humid Period.

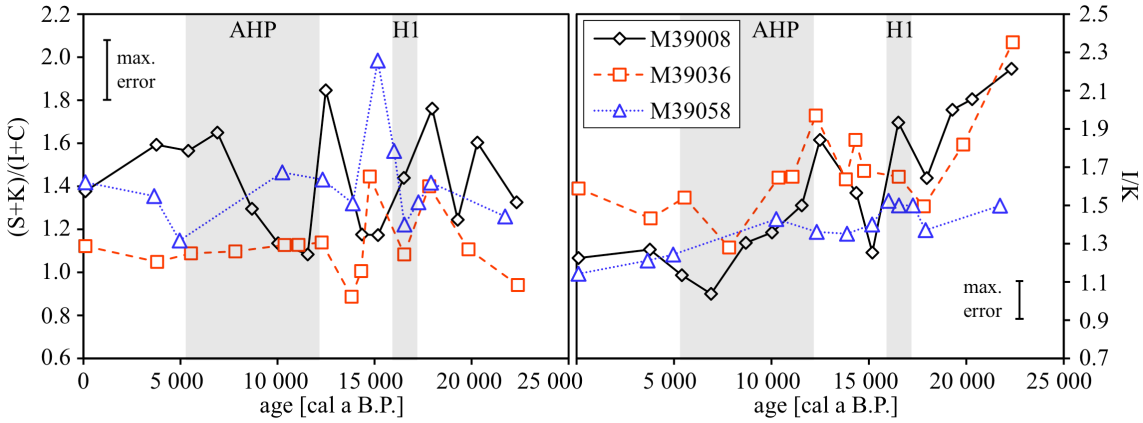

Fig. 4.4. Clay mineral ratio time series for the LGM to Holocene transition for all three cores. The (smectite+kaolinite)/(illite+chlorite) record on the left panel has an estimated error of ±0.15, the illite/kaolinite ratios on the right panel have an estimated error of ±0.10. Error estimations are based on the 2% uncertainty during the semi-quantitative determination of the clay mineral abundances. H1 again marks the samples at 16.5 ka representing the maximum of Heinrich stadial 1 and AHP refer to the African Humid Period.

4.4. Discussion

4.4.1. Present-day endmember compositions

The Nd isotope compositions of coastal rocks from the entire Mediterranean catchment range from εNd=-5.0 to -15.0, wherein highly radiogenic values only occur in the eastern Mediterranean basin (Jeandel et al., 2007). Grousset & Biscaye (2005) reported radiogenic Nd isotope values of εNd=-4.5 for SPM collected within the Mediterranean Sea compared to less radiogenic suspended particulate matter of εNd < -10.0 for the Eastern North Atlantic region. North African aerosols, mainly Saharan dust, are also characterized by less radiogenic Nd isotope signatures of εNd=-10.0 to -15.0 (Grousset & Biscaye, 2005; Cole et al., 2009).

The average particulate $^{87}Sr/^{86}Sr$ composition within the Mediterranean Sea is about 0.71 (Grousset & Biscaye, 2005), which most likely reflects unradiogenic Sr input ($^{87}Sr/^{86}Sr<0.71$) originating from the Nile river particulate discharge into

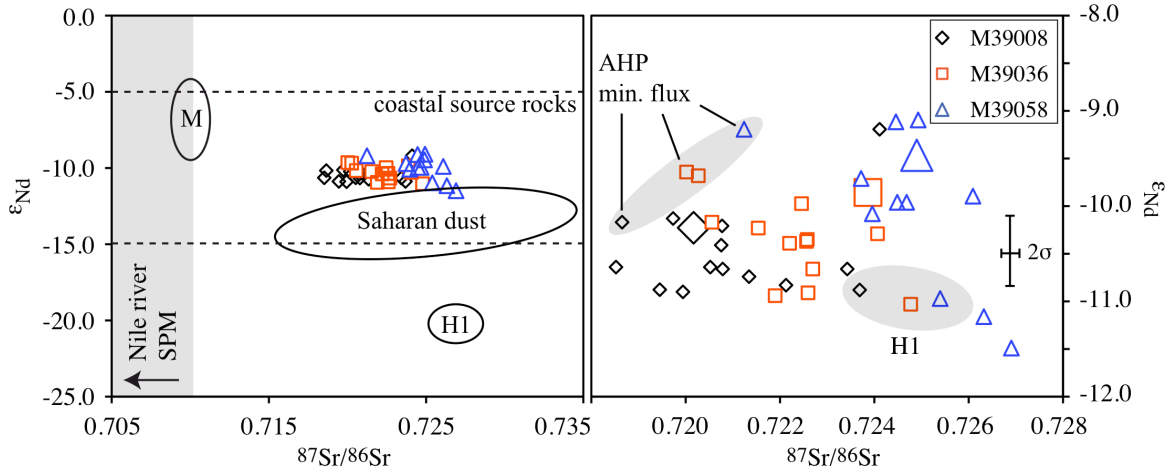

Fig. 4.5. Left: $^{87}Sr/^{86}Sr$ vs. εNd plot including the data from this study and potential modern endmember sources. Average Mediterranean SPM isotope compositions (M) are from Grousset & Biscaye (2005), Heinrich stadial 1 (H1) compositions are from Hemming et al. (1998), Nile river suspended particle Sr data is from Krom et al. (1999), the εNd range for coastal source rocks is from Jeandel et al. (2007) and the wide range of Saharan dust isotope compositions comes from Grousset & Biscaye (2005) and Cole et al. (2009). Right: Focus on the three cores $^{87}Sr/^{86}Sr$ vs. εNd downcore data from this study with marked areas for Heinrich stadial 1 (H1 ~16.5 ka) and the African Humid Period (AHP ~10.0 ka; minimum of dust flux) provinces (core M39008=black diamonds, core M39036=red squares, core M39058=blue triangles; large symbols refer to the three coretop samples).

the Eastern Mediterranean Sea (Krom et al., 1999). In contrast, North Atlantic SPM and Iberian weathered soils have reported $^{87}Sr/^{86}Sr$=0.72-0.73 (Grousset & Biscaye, 2005; Erel & Torrent, 2010). The radiogenic Sr isotope signatures of North African aerosols cover a wide range of values more radiogenic than 0.72 (Krom et al., 1999; Grousset & Biscaye, 2005; Cole et al., 2009).

In a combined εNd vs. $^{87}Sr/^{86}Sr$ plot, these published data demonstrate two distinct endmembers: a Mediterranean SPM endmember, with radiogenic Nd and unradiogenic Sr isotope ratios, and a North African dust/Iberian SPM endmember, characterized by less radiogenic Nd and radiogenic Sr isotope ratios (Fig. 4.5, left panel). The coretop Nd-Sr isotope compositions obtained from the clay-size sediments in the Gulf of Cadiz and from the Portuguese margin form an array between these endmembers, although more similar to the North African dust/Iberian particles field.

As indicated by the combined Sr and Nd isotope data (Fig. 4.5, left panel), the suspended particulate matter deposited on the Iberian shelf contains contributions from all over the Mediterranean Sea, because there are no other source rocks than in the eastern Mediterranean region with a highly radiogenic Nd isotope composition suitable to produce the offset towards more radiogenic Nd signatures than the Saharan dust endmember.

The present-day Pb isotope composition of airborne particles and hence recently deposited sediments has been altered by anthropogenic input of leaded petrol into the atmosphere (Schaule & Patterson, 1981; Weiss et al., 2003). This modern alteration can be recognized in the acid-leached clay-size sediment fraction (Fig. 4.6). In this ^{208}Pb-^{207}Pb-^{206}Pb space, the coretop data plot within the array of Iberian ores/soils (Richter et al., 2009; Erel & Torrent, 2010), and are thus significantly shifted towards the anthropogenic endmember compositions compared to the downcore Pb ratios. Furthermore, the anthropogenic alteration appears to decrease with water depth and distance off the Iberian coast, which suggests that local Iberian Pb inputs are the major contaminant source for the modern particulate Pb isotope compositions.

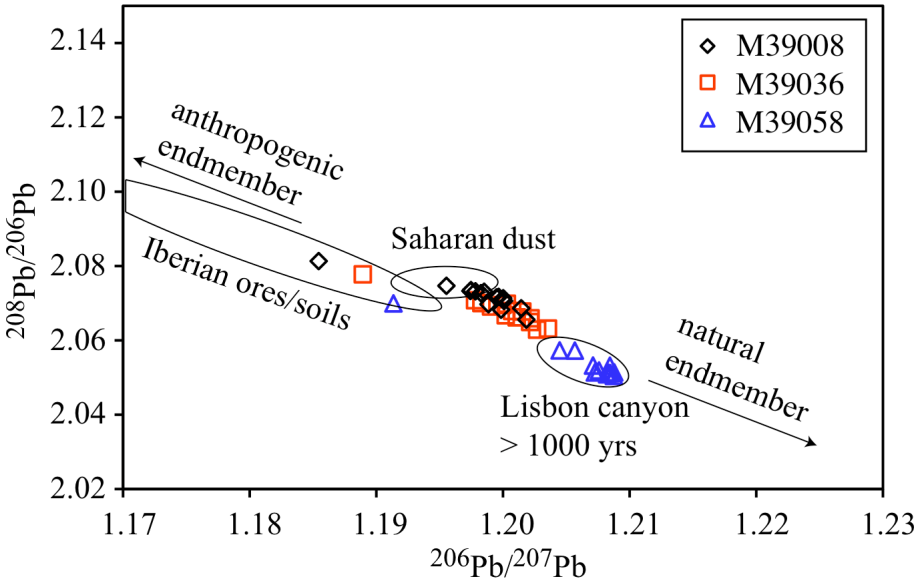

Fig. 4.6. $^{208}Pb/^{206}Pb$ vs. $^{206}Pb/^{207}Pb$ plot for all three cores from this study and potential endmember sources. The three coretop samples are clearly shifted towards the anthropogenic endmember. Natural and anthropogenic endmembers, as well as the data for older Lisbon canyon sediments are from Richter et al. (2009), Saharan dust and Iberian ores/soils data are from Richter et al. (2009) and Erel & Torrent (2010). The 2σ uncertainty is below dot size (core M39008=black diamonds, core M39036=red squares, core M39058=blue triangles).

The present-day endmember clay mineral assemblages are characterized by major variations in smectite (5-83%) and illite (12-55%), and at the same time less variable kaolinite (<29%) and chlorite (<20%) contents (Fig. 4.7). The potential endmembers can be clustered into three groups: (I) dust assemblages and western Mediterranean Sea SPM (Grousset et al., 1988; Guerzoni et al., 1997; Hamann et al., 2009), (II) Iberian Peninsula SPM (Grousset et al., 1988; Erel & Torrent, 2010) and (III) a mixture of Iberian/SE Mediterranean SPM (Hamann et al., 2009; Erel & Torrent 2010). The dust assemblages (I) are characterized by low smectite and high kaolinite+chlorite contents, while the mostly river transported particles (II+III) are enriched in smectite and depleted in kaolinite+chlorite. The three coretops from the sites in the Gulf of Cadiz and the Portuguese margin show an average clay mineral composition plotting between the endmembers discussed above. Therefore, the particles deposited on the SW Iberian shelf appear to be a mixture of all discussed endmembers without one particular dominant source. It is noted though that the coretops' illite/kaolinite ratios (1.1-1.6; Fig. 4.4, right panel)

match well to illite/kaolinite ratios from the Saharan desert (Caquineau et al., 1998), which most likely has been the major contributor of dust to the SW Portuguese margin.

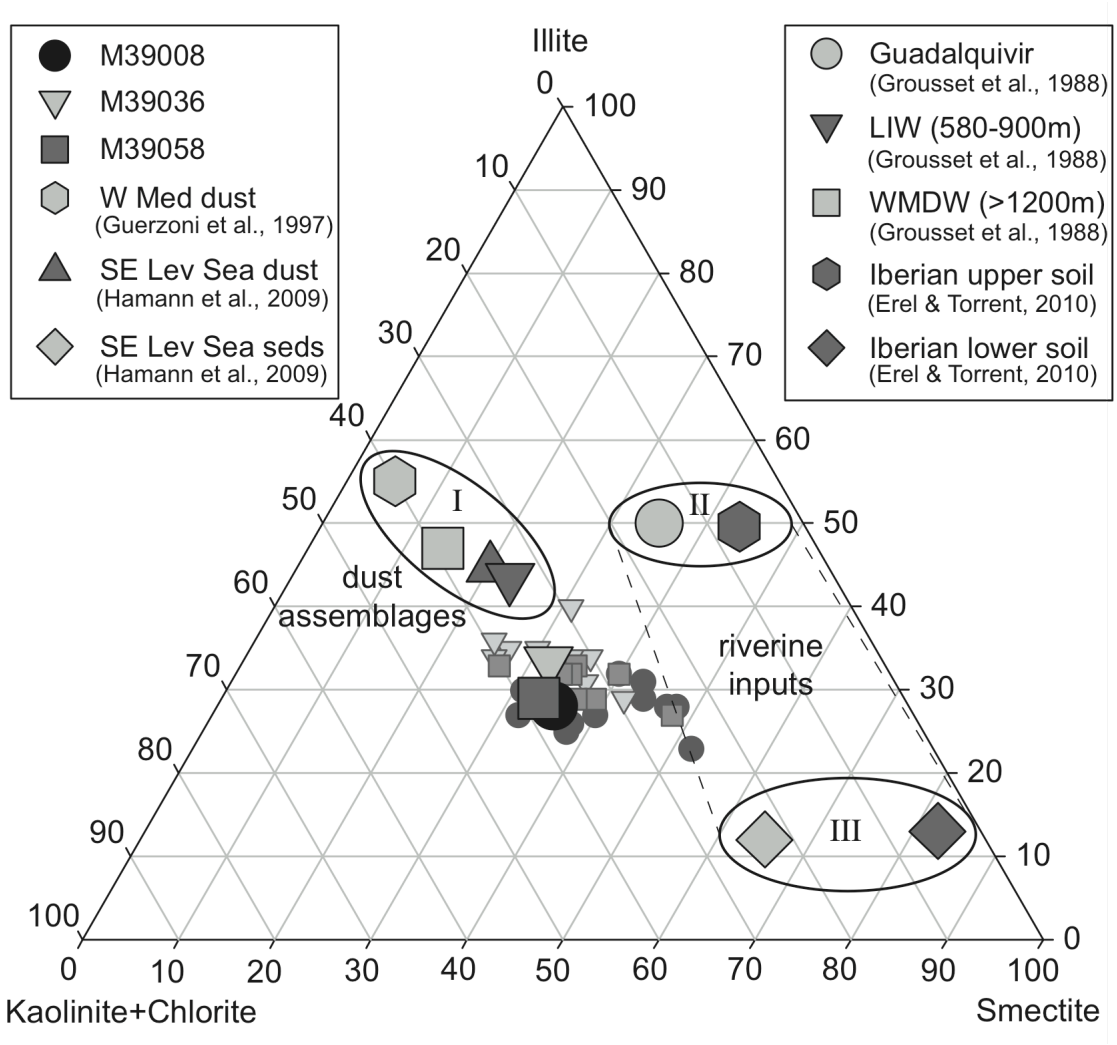

Fig. 4.7. Smectite vs. illite vs. kaolinite+chlorite ternary plot for all samples from this study and potential endmembers. Large symbols refer to data of modern age, the small symbols show the downcore data. The endmember compositions are averages of previously published records (Grousset et al., 1988; Guerzoni et al., 1997; Hamann et al., 2009; and Erel & Torrent, 2010).

4.4.2. LGM to Holocene endmember variability

With the exception of highly unradiogenic Nd compositions during H1 at 16.5 cal years B.P., the Nd isotope composition of source rock contributions from the Mediterranean region has not changed significantly since the LGM. This constancy is clearly documented in the Nd isotope time series for all three cores (Fig. 4.2b) and fits well to North African/Saharan aerosol supplies that have been constant at about εNd=-15.0 for the last 20 kyrs (Cole et al., 2009). The consistent overall εNd offset to more radiogenic ratios at the northernmost core location, in particular during the Holocene, may result from a more limited supply of unradiogenic Saharan aerosols with greater distance from the source area (Grousset et al., 1988). Alternatively, local more radiogenic Nd sources along the Iberian margin may also have contributed to the Nd isotope offset.

The late Quaternary records of the Sr isotope compositions show higher variability, and thus more variable endmember contributions (Fig. 4.2a). Cole et al. (2009) report highly radiogenic $^{87}Sr/^{86}Sr$ ratios (0.722-0.723) during the LGM, as well as for modern Saharan dust assemblages from a core location off NW Africa, which have been correlated to arid climate conditions and thus an increased terrigenous dust flux. A strong correlation of elevated Saharan dust fluxes during arid climate conditions was also observed for Alboran Sea sediments during the stadial periods of Dansgaard/Oeschger cycles and Heinrich Events 28 000 – 48 000 cal yrs B.P. (Moreno et al., 2002). A similar pattern is also documented in the cores in the Gulf of Cadiz and along the Iberian margin: elevated $^{87}Sr/^{86}Sr$ ratios (more dust supply) during more arid conditions in LGM and in recent times and lower $^{87}Sr/^{86}Sr$ ratios (less dust supply) during humid climates, especially during the African Humid Period (AHP). The Sr isotope signature of the Gulf of Cadiz core (M39008) does not reach its LGM value again during the late Holocene. This may indicate the permanent influence of the Guadalquivir and Guadiana river systems in the Gulf of Cadiz throughout the entire Holocene (cf. Grousset et al., 1988; Schönfeld, 1997; Mendes, 2010). Alternatively, the constant Sr isotope compositions at this core location may result from a persistently strong influence of less radiogenic material from the Mediterranean Sea throughout the Holocene.

The downcore data from each core form distinct clusters in the Nd-Sr plot (Fig. 4.5), which are likely to reflect the constantly decreasing influence of the relative amount of SPM carried by the Mediterranean Outflow Water deposited at distance from the source areas. However, there is a clear discrepancy between the Sr-Nd values of the modern Mediterranean SPM endmember and all the Sr-Nd isotope data presented here (Fig. 4.5, left panel), which is most likely due to generally large contributions of suspended particulate matter originating from the Iberian Peninsula.

An overall shift to less radiogenic Nd and Sr isotope composition during the LGM in comparison to the present-day sediments reported by Grousset et al. (1998) is not observed in the data of this study, though it has to be taken into account that the data from Grousset et al. (1998) were obtained from a coarser sediment fraction (< 30 μm) that included source regions at much lower latitudes.

The Pb isotope composition of the deepest and northernmost core location (core M39058) has been influenced by Pb isotope compositions significantly different from the two other core sites, which have apparently been supplied by similar Pb signatures over time. The radiogenic Pb isotope signatures of the clay-size M39058 record are indistinguishable from Pb isotope compositions from Lisbon canyon sediments (Richter et al., 2009), while cores M39008 and M39036 form a distinct array within three-isotope plot (^{208}Pb-^{207}Pb-^{206}Pb, Fig. 4.6). This difference between the cores' Pb sources is also documented by the constant offset of core M39058 in the ^{206}Pb/^{204}Pb time series (Fig. 4.2c). The pre-industrial records show Pb isotope ratios close to values found for European/Pan-African crust and European/Variscan crust, which have been considered the dominant Pb sources within the western Mediterranean Sea region (Fagel et al., 2004).

Although the paleo Pb isotope composition of the Mediterranean SPM endmember remains unknown, it was certainly less radiogenic than the particulate contributions from the Iberian rivers. In comparison with paleo seawater records from the same set of samples (Stumpf et al., 2010), the ^{206}Pb/^{204}Pb time series of Mediterranean Outflow Water has been significantly less radiogenic than the

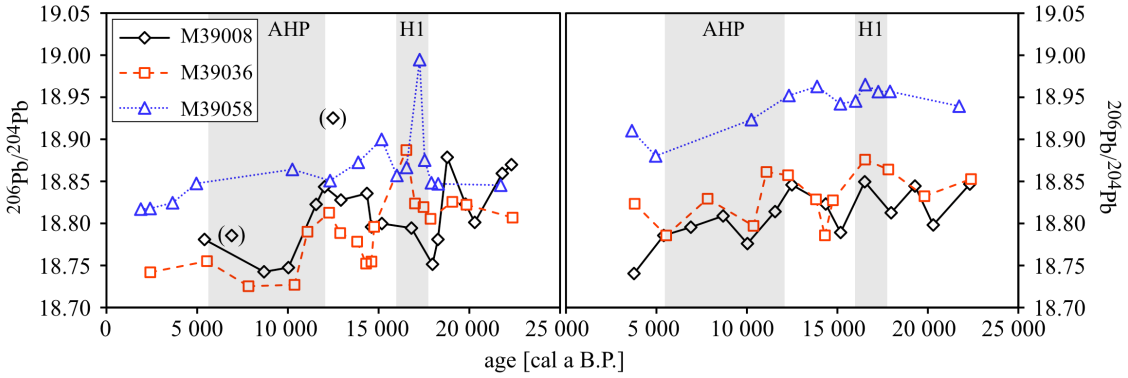

Fig. 4.8. Left: $^{206}Pb/^{204}Pb$ seawater record for the LGM to Holocene transition from leached ferromanganese coatings (Stumpf et al., 2010). Right: $^{206}Pb/^{204}Pb$ time series of the detrital clay-size fraction from a subset of the same samples (this study). The 2σ uncertainty is around dot size (AHP=African Humid Period; H1=Heinrich Event 1).

corresponding detrital fractions, suggesting that the source that preconditioned this water mass has been less radiogenic in Pb isotope composition (Fig. 4.8).

However, the three clay-size $^{206}Pb/^{204}Pb$ records, as well as the Nd and Sr isotopes, changed essentially in phase over time (Fig. 4.2), which suggests that the local source variability has likely been controlled by the regionally prevailing climate conditions and associated particle transport regimes.

In contrast to the radiogenic Sr-Nd isotopes, the late Quaternary records of clay mineral abundances do not show distinct provinces that can be directly correlated with climatic events (i.e. Heinrich stadial 1 or African Humid Period; Fig. 4.7), although each of the three cores document significant variations, mainly in smectite content (Fig. 4.3, Fig. 4.4). The (smectite+kaolinite)/(illite+chlorite) records show the highest amplitude variability in the Gulf of Cadiz (core M39008) with its minima and maxima out of phase with the remaining cores, which also show a smaller amplitude of their changes (Fig. 4.4, left panel). Assuming that smectite is preferentially formed during humid climates and supplied by rivers, the maxima of cores M39036 and M39058 document an enhanced riverine input of suspended material to the SW Iberian shelf during the early deglaciation, shortly interrupted by Heinrich stadial 1. The highly variable record of shallow core M39008, which may not have been affected by MOW during the Last Glacial Maximum and the earliest deglaciation until H1, thus reflects river discharge into

the Gulf of Cadiz interfering with the ongoing transgression continuously alternating the shallow sedimentary environment at this site. Grousset et al. (1988) correlate maxima of this specific clay mineral ratio (Fig. 4.4, left panel) to intensifications of the Atlantic-Mediterranean water mass exchange in the Strait of Gibraltar throughout the last 18 kyrs B.P. Interestingly, these variations are not in phase with any of the clay mineral records presented in this study. The decoupled downcore variability of the three locations is also recorded in the illite/kaolinite clay mineral ratio time series (Fig. 4.4, right panel). Further, the illite/kaolinite ratios document a clearly resolved progressive decrease since the LGM in the two cores closest to the Strait of Gibraltar and to a lesser extent in the deepest and most distant core in the north, which may result from a southward shift of the Saharan dust sources (Caquineau et al., 1998) associated with the chemical weathering regime in a developing warm-humid climate (Griffin et al., 1968).

4.4.2.1. Heinrich stadial 1 (H1)

At ~16.5 ka a prominent excursion in the radiogenic isotope time series of Nd and Sr is recorded (Fig. 4.2), which clearly documents the deposition of ice rafted debris (IRD) originating from ancient terrains surrounding the Labrador Sea during Heinrich Event H1 (Hemming et al., 1998). This pulse of IRD contributed unradiogenic Nd isotope compositions (εNd=-20) and radiogenic Sr isotope compositions ($^{87}Sr/^{86}Sr$=0.725-0.728) to the eastern North Atlantic (Hemming et al., 1998), which obviously is also documented in the clay-size fraction of the detrital material. In the Nd isotope records (Fig. 4.2b), the excursion to less radiogenic values during H1 is least pronounced in the core in the Gulf of Cadiz, which suggests that less IRD reached the southernmost site (cf. Eynaud et al., 2009).

The radiogenic Sr isotope composition time series also clearly show the deposition of IRD, though the excursion aims to more radiogenic $^{87}Sr/^{86}Sr$ ratios. This is evident at all three core sites, although core M39008 shows similar Sr

isotope compositions during the LGM and at H1, which once again suggests a decreased supply of IRD at this site. Furthermore, in the combined Sr-Nd data the H1 (~16.5 ka) sediments from all three core locations are constrained to a separate array (Fig. 4.5), which also strongly suggests a common source.

Interestingly, there is no significant change in the Pb isotope composition during H1 in any core, as has been observed for the Nd and Sr isotope systems (Fig. 4.2). This is probably due to the highly variable Pb isotope compositions reported for the IRD sediments of H1 ($^{206}Pb/^{204}Pb$=12-24; Hemming et al., 1998), which on average is very close to the Pb isotope data of our sediments ($^{206}Pb/^{204}Pb$=18.7-19.0).

Although Fagel et al. (2001) reported illite+smectite abundances of up to ~80% for Heinrich Event 1 layers in the North Atlantic, the clay mineral abundance records barely show variations at ~16.5 ka (Fig. 4.3, Fig. 4.4), most likely due to the overall high smectite+illite abundances in the sediments on the SW Iberian shelf.

4.4.2.2. African Humid Period (AHP)

Cole et al. (2009) correlated a significant drop to less radiogenic Sr compositions at a core location off NW Africa from ~12-5.5 kyrs B.P., with a minimum of $^{87}Sr/^{86}Sr$=0.7125 at around 12-10 kyrs B.P., to the African Humid Period (AHP), which has been characterized by humid climatic conditions and a decreased dust flux. The Sr isotope compositions from all three sites on the SW Iberian shelf also show the least radiogenic Sr signatures at the onset of the AHP documenting an rapid decrease of dust supply from North Africa, most pronounced at the northern core location (Fig. 4.2a). In the combined Sr-Nd isotope plot, the downcore records are distributed between the fields comprising the AHP data and the H1 data (Fig. 4.5, right panel). Given that the sediments deposited during the AHP most likely contain the smallest contribution of North

African dust due to generally more humid climate conditions, the sediments deposited on the SW Iberian shelf at ~10 ka were dominated by the SPM in MOW and the Iberian riverine inputs.

The illite/kaolinite time series decrease massively and reach their smallest ratios during the African Humid Period (Fig. 4.4). In addition to the overall decrease in dust supply, this may indicate that the remaining dust flux was provided by more southern Saharan sources than during dryer climatic periods (Caquineau et al., 1998).

4.4.3. Implications for the late Quaternary hydrography of MOW

According to several studies throughout the last decade, the Atlantic-Mediterranean exchange and thus MOW have undergone significant hydrographic changes in terms of flow paths and current velocity since the Last Glacial Maximum (Cache et al., 2000, 2006; Schönfeld & Zahn, 2000; Rogerson et al., 2005; Voelker et al., 2006, 2009). Therefore, it has to be considered that, even in the absence of any changes in endmember compositions, the distribution of sediments from different sources in the area of interest may have been affected significantly. Changes in MOW current speed control the transportation distance of the clay-size particles, and changes of MOW layer depth inhibit or enable the deposition of suspended particles contributed from the Mediterranean Sea at a particular site location. The downcore records of the shallowest core in the Gulf of Cadiz are likely to be affected most by changes in hydrography, due to its proximity to discharging river systems, sediment resuspension and downslope transport in the nepheloid layer on the Iberian margin (Arzola et al., 2008) combined with the transgression during the last deglaciation. While the radiogenic isotope time series vary in phase with only minor exceptions (Fig. 4.2), the records of the clay mineral abundances and ratios correspond less well, especially in pre-Holocene times (Fig. 4.3, Fig. 4.4, Fig. 4.8). This might be a consequence of hydrographic changes of MOW during the

deglaciation until the early Holocene, which would be in agreement with paleo seawater data from the same set of samples (Stumpf et al., 2010; Fig. 4.8).

4.5. Conclusions

The clay-size sediment fraction deposited on the SW Iberian shelf in water depths occupied by the Mediterranean Outflow Water and below consists of assemblages from the Mediterranean Sea suspended particulate matter, North African aerosols and fluvial inputs from the Iberian Peninsula, with no evidently dominant endmember. The radiogenic isotope records and the clay mineral ratios document a northwards decreasing influence of the dust fraction throughout the entire period of interest. The supply of IRD into the Eastern North Atlantic during Heinrich stadial 1 (~16.5 ka) is clearly documented in the Nd and Sr records, though less material reached the southernmost site in the Gulf of Cadiz. Additionally, the radiogenic Sr and Nd isotopes document a decreased deposition of North African aerosols during the African Humid Period (12-5.5 ka B.P.) reaching its minimum dust flux at about 12-10 ka B.P. At this time, the sediment deposition on the SW Iberian shelf was dominated by fluvial inputs or particles carried by MOW. Furthermore, the records suggest a significant contribution of SPM from river discharge from the Iberian Peninsula into the Gulf of Cadiz throughout the Holocene.

The clay mineral abundances in the area of interest have also been a mixture of the endmembers discussed above. Furthermore, the clay mineral abundances and ratios suggest changes in the chemical weathering regime sensitive to prevailing climate conditions over time, which is reflected in the decoupled variability in pre-Holocene times. In addition, significant hydrographic changes of Mediterranean Outflow Water during the deglaciation could have caused the recorded variabilities to some extent.

Although no dramatic changes in the SPM endmember variability along the MOW flow path have been observed, the SW Iberian shelf sediments have been fed by a complex mixture of different sources, in particular from the Iberian Peninsula.

4.6. Acknowledgments

This work has been funded by Deutsche Forschungsgemeinschaft (Project FR1198/4-1). We would like to thank our colleagues at IFM-GEOMAR in Kiel, for providing and maintaining all the instrument and laboratory facilities (i.e. TIMS, MC-ICPMS, XRD, laser particle-sizer, cleanlab).

Chapter 5

Summary and Outlook

This study focused on a reconstruction of the late Quaternary variability of the Mediterranean Outflow Water flow path, as well as changes in the endmember composition of the detrital weathering inputs to the SW Iberian shelf covering the last ~ 23 000 cal a B.P. The hydrographic changes were evaluated using paleo seawater records of radiogenic Nd and Pb isotope compositions obtained from the authigenic ferromanganese coatings of the bulk sediments from three gravity cores in the Gulf of Cadiz and from the Portuguese continental margin. From the same cores, the detrital clay-size fraction was separated and records of the clay's radiogenic Nd, Pb and Sr isotope compositions were produced to identify the source areas, and the changing contributions throughout the latest Quaternary, supplying the fine-fraction to the SW Iberian shelf sediments. These records were supplemented by time series of the abundances of the clay minerals kaolinite, chlorite, illite and smectite, as well as specific clay mineral ratios, which in combination with the radiogenic isotope records document the changes of the weathering regime prevailing along the flow path of Mediterranean Outflow Water and in the ambient source areas through time.

The main findings and conclusions of this thesis are summarized below in correspondence to the objectives raised in the introductory chapter:

Calibration of the present-day Nd isotope compositions in coretop sediments to the bottom water Nd isotope compositions:

The seawater Nd isotope compositions obtained from leached ferromanganese coatings of coretop bulk sediments in the Gulf of Cadiz and along the Portuguese margin differ significantly from the Nd isotope composition of water samples from the corresponding water depths of a nearby water column profile. Although the Fe-Man coatings of the sediments on the SW Iberian shelf

within the depth of the Mediterranean Outflow Water (~ 500 – 1500 m) precisely reflect the Nd isotope composition of the outflowing water mass, the transition to underlying Eastern North Atlantic Deep Water is not documented in the sediments, most likely due to downslope sediment redeposition processes in the nepheloid layer.

Late Quaternary hydrographic variability of the Mediterranean Outflow Water from leached Nd and Pb isotope compositions:

The three downcore records of the extracted paleo seawater Nd isotope compositions do not show significant variations. The invariant isotope signatures close to the outflow source indicate a constant and continuous prevalence of the Mediterranean Outflow Water during the past 25 000 years.

The downcore Pb isotope records of cores M39008 and M39036 suggest major changes in the flow path of Mediterranean Outflow Water during the early deglaciation. Settled at greater depth during the Last Glacial Maximum, the upper layer of MOW shallowed significantly or was even only established during Heinrich stadial 1, followed by a moderate deepening until ~15 ka. Decoupled from the upper layer of MOW, the lower outflow layer moderately rose during the end of H1 and dropped again until about 15 000 cal a B.P. Based on the Pb isotope records, the present-day hydrography of MOW was established ~12 000 yrs ago.

Changes in endmember contributions to the SW Iberian shelf clay-size sediments since the Last Glacial Maximum from their radiogenic Nd, Sr and Pb isotope compositions, clay mineral abundances, and clay mineral ratios:

The clay-size sediment fraction deposited in the Gulf of Cadiz and along the Portuguese shelf in water depths occupied by the Mediterranean Outflow Water and below consists of assemblages originating from the Mediterranean Sea suspended particulate matter, North African aerosols and fluvial inputs from the Iberian Peninsula, with no evidently dominant endmember, which is documented in both the radiogenic isotope and clay mineral records. The radiogenic isotope records and the clay mineral ratios show a northwards decreasing influence of the North African dust fraction to the three endmember mixture on the SW Iberian

shelf. During Heinrich stadial 1 at about 16.5 ka, the supply of IRD into the Eastern North Atlantic is clearly documented in the Nd and Sr isotope records, most pronounced in the northernmost location of this study. The Sr isotope time series of the clay-size fraction suggests a minimum deposition of North African dust during the onset of the African Humid Period (12-10 ka B.P.). Furthermore, the clay-size radiogenic isotope records indicate a permanent and ongoing influence of the Guadalquivir and Guadiana river systems on the sediment composition of the Gulf of Cadiz throughout the entire Holocene.

Changes in the chemical weathering regime associated to climatic conditions from a comparison of the isotopic and mineralogical records of the clay-size fraction:

Variation of the radiogenic isotope compositions of the clay-size fraction has only depended on endmember source mixing, which has mainly been controlled by varying dust supply since the Last Glacial Maximum, and was thus closely correlated to climatic changes. Clay mineral abundances and ratios vary out-of-phase with the radiogenic isotope records suggesting other factors than pure endmember source mixing to affect the clay mineral abundances. Due to the sensitivity of clay formation to the prevailing climate conditions over time, changes in the chemical weathering regime may result in varying clay mineral abundances from essentially the same source rock. This is possibly reflected in the decoupled variability of the clay mineral abundances and ratios mainly in pre-Holocene times. However, it is noted that locally sourced inputs, supposedly biased by the rising sea-level affecting the SW Iberian river mouths, or the significant hydrographic changes of Mediterranean Outflow Water during the deglaciation may have influenced the records.

The data and interpretations presented in this thesis clearly demonstrate the limited applicability of paleo seawater radiogenic isotope records extracted from ferromanganese coatings from marine bulk sediments as a water mass tracer in particle-rich coastal areas with relatively steep continental slopes and high sedimentation rates. Although no dramatic changes in the endmember variability of suspended particulate matter along the Mediterranean Outflow Water flow path

were observed, the data suggest that the SW Iberian shelf sediments have been fed by a complex endmember mixing system, including various sources from the Iberian Peninsula. However, the direct comparison of radiogenic isotope records to mineralogical records from the same set of clay-size samples appear to be a promising tool for distinguishing changes of source areas from changes influenced by chemical weathering.

Outlook:

In order to better resolve and reconstruct the present-day water mass mixing in the Gulf of Cadiz and on the SW Iberian shelf with the radiogenic isotope systems of Nd and Pb, additional water column profiles along the pathway of Mediterranean Outflow Water need to be sampled. From such data it would be possible to obtain a detailed picture of the dynamics of the dilution of MOW isotopic composition distributing into the Eastern North Atlantic. It would also be helpful to gain more information on the isotopic signatures of the major river systems discharging dissolved and particulate radiogenic isotope signatures into the ambient oceanic water masses. This is in particular important for the amount of such tracers immobilised at the mouths of these rivers. In order to reconstruct the paleoceanography of MOW on the SW Iberian shelf in more detail, further archives beyond the ferromanganese oxyhydroxyide coatings of the sediments should be investigated. Cold water corals, for example, dwelling at the present day within the flow path and water depth of MOW and which are supposedly not affected by the sediment redistribution processes occurring on steep continental slopes presumably conserved unbiased bottom water signals.

For future work it would be crucial to supplement the existing radiogenic and mineralogical detrital data sets with respect to the immediate particle sources from the Iberian Peninsula, especially from river sediments of the large river systems entering the Eastern North Atlantic along the flow path of the Mediterranean Outflow Water. It would also be of great advantage to better constrain the endmember composition of North African dust, as well as the

composition of the suspended particulate matter of MOW at its source in the Strait of Gibraltar and in the Western Alboran Sea. The exact knowledge of the various endmember compositions of both the radiogenic isotopes and the clay mineralogy would improve the interpretations of the prevailing differential source mixing that has occurred on the SW Iberian shelf between the Last Glacial Maximum and the present.

References

Abouchami, W., Galer, S.J.G., Koschinski, A., 1999. Pb and Nd isotopes in NE Atlantic Fe-Mn crusts: Proxies for trace metal paleosources and paleocean circulation. Geochim. Cosmochim. Ac. 63(10), 1489-1505.

Albarède, F., Goldstein, S.L., 1992. World map of Nd isotopes in sea-floor ferromanganese deposits. Geology 20(8), 761-763.

Albarède, F., Telouk, P., Blichert-Toft, J., Boyet, M., Agranier, A., Nelson, B., 2004. Precise and accurate isotopic measurements using multiple-collector ICPMS. Geochim. Cosmochim. Ac. 68(12), 2725-2744.

Arsouze, T., Dutay, J.-C., Lacan, F., Jeandel, C., 2009. Reconstructing the Nd oceanic cycle using a coupled dynamical-biogeochemical model. Biogeosciences 6, 2829-2846.

Arzola, R.G., Wynn, R.B., Lastras, G., Masson, D.G., Weaver, P.P.E., 2008. Sedimentary features and processes in the Nazaré and Sétubal submarine canyons, west Iberian margin. Mar. Geol. 250(1-2), 64-88.

Baringer, M.O., Price, J.F., 1997. Mixing and Spreading of the Mediterranean Outflow. J. Phys. Oceanogr. 27, 1654-1677.

Baringer, M.O., Price, J.F., 1999. A review of the physical oceanography of the Mediterranean outflow. Mar. Geol. 155(1-2), 63-82.

Barrat, J.A., Keller, F., Amossé, J., 1996. Determination of rare earth elements in sixteen silicate reference samples by ICP-MS after Tm addition and ion exchange separation. Geostandard. Newslett. 20, 133-139.

Bayon, G., German, C.R., Boella, R.M., Milton, J.A., Taylor, R.N., Nesbitt, R.W., 2002. An improved method for extracting marine sediment fractions and its application to Sr and Nd isotopic analysis. Chem. Geol. 187, 179-199.

Berry, R.W., Johns, W.D., 1966. Mineralogy of the clay-sized fractions of some North Atlantic-Arctic ocean bottom sediments. Geol. Soc. Am. Bull. 77, 183-196.

Bigg, G.R., Jickells, T.D., Liss, P.S., Osborn, T.J., 2003. The role of the oceans in climate. Int. J. Climatol. 23, 1127-1159.

Biscaye, P., 1965. Mineralogy and Sedimentation of Recent Deep-Sea Clay in the Atlantic Ocean and Adjacent Seas and Oceans. Geol. Soc. Am. Bull. 76, 803-832, doi:10.1130/0016-7606.

Burton, K.W., Ling, H.-F, O'Nions, R.K., 1997. Closure of the Central American Isthmus and its effect on deep-water formation in the North-Atlantic, Nature 386, 382-385.

Bryden, H.J., Stommel, H.M., 1984. Limiting processes that determine the basic features of the circulation in the Mediterranean Sea. Oceanol. Acta 7, 289-296.

Cacho, I., Grimalt, J.O., Sierro, F.J., Shackleton, N., Canals, M., 2000. Evidence for enhanced Mediterranean thermohaline circulation during rapid climatic coolings. Earth Planet. Sc. Lett. 183(3-4), 417-429.

Cacho, I., Grimalt, J.O., Canals, M., Sbaffi, L., Shackleton N.J., Schönfeld, J., Zahn, R., 2001. Variability of the western Mediterranean Sea surface temperature during the last 25 000 years and its connection with the Northern Hemisphere climatic changes. Paleoceanography 16(1), 40-52.

Cacho, I., Shackleton, N., Elderfield, H., Sierro, F.J., Grimalt, J.O., 2006. Glacial rapid variability in deep-water temperature and $\delta^{18}O$ from the Western Mediterranean Sea. Quaternary Sci. Rev. 25, 3294-3311.

Caquineau, S., Gaudichet, A., Gomes, L., Magonthier, M.-C., Chatenet, B., 1998. Saharan dust: Clay ratio as a relevant tracer to assess the origin of soil-derived aerosols. Geophys. Res. Lett. 25(7), 983-986.

Chamley, H., 1989. Clay sedimentology. Springer-Verlag Berlin Heidelberg, ISBN 3-540-50889-9, 623 pp.

Cohen, A.S., O'Nions, R.K., Siegenthaler, R., Griffin, W.L., 1988. Chronology of the pressure-temperature history recorded by a granulite terrain. Contrib. Mineral. Petrol. 98, 303-311.

Cole, J.M., Goldstein, S.L., deMenocal, P.B., Hemming, S.R., Grousset, F.E., 2009. Contrasting compositions of Saharan dust in the eastern Atlantic Ocean during the last deglaciation and African Humid Period. Earth Planet. Sc. Lett. 278, 257-266.

Erel, Y., Torrent, J., 2010. Contribution of Saharan dust to Mediterranean soils assessed by sequential extraction and Pb and Sr isotopes. Chem. Geol. 275, 19-25.

Eynaud, F., de Abreu, L., Voelker, A., Schönfeld, J., Salgueiro, E., Turon, J.-L., Penaud, A., Toucanne, S., Naughton, F., Sánchez Goñi, M.F., Malaizé, B., Cacho, I., 2009. Position of the Polar Front along the western Iberian margin during key cold episodes of the last 45 ka. Geochem. Geophy. Geosy. 10(7), Q07U05, doi:10.1029/2009GC002398.

Fagel, N., Robert, C., Preda, M., Thorez, J., 2001. Smectite composition as a tracer of deep circulation: the case of the North Atlantic. Mar. Geol. 172, 309-330.

Fagel, N., Innocent, C., Gariepy, C., Hillaire-Marcel, C., 2002. Sources of Labrador Sea sediments since the last glacial maximum inferred from Nd-Pb isotopes. Geochim. Cosmochim. Ac. 66(14), 2569-2581.

Fagel, N., Hillaire-Marcel, C., Humblet, M., Brasseur, R., Weis, D., Stevenson, R., 2004. Nd and Pb isotope signatures of the clay-size fraction of Labrador Sea sediments during the Holocene: Implications for the inception of the modern deep circulation pattern. Paleoceanography 19, PA3002, doi:10.1029 /2003PA000993.

Faugères, J.-C., Gonthier, E., Stow, D.A.V., 1984. Contourite drift molded by deep Meditarranean outflow. Geology 12, 296-300.

Foster, G.L., Vance, D., Prytulak, J., 2007. No change in the neodymium isotope composition of deep water exported from the North Atlantic on glacial-interglacial time scales. Geology 35(1), 37-40.

Frank, M., 2002. Radiogenic isotopes: Tracers of past ocean circulation and erosional input. Rev. Geophys. 40(1), 1001, doi:10.1029/2000RG000094.

Frigola, J., Moreno, A., Cacho, I., Canals, M., Sierro, F.J., Flores, J.A., Grimalt, J.O., 2008. Evidence of abrupt changes in Western Mediterranean Deep Water circulation during the last 50 kyr: A high-resolution marine record from the Balearic Sea. Quatern. Int. 181, 88-104.

Fusco, G., Artale, V., Cotroneo, Y., Sannino, G., 2008. Thermohaline variability of Mediterranean Water in the Gulf of Cadiz, 1948-1999. Deep-Sea Res. Pt. I 55, 1624-1638.

Galer, S.J.G, O'Nions, R.K., 1989. Chemical and isotopic studies of ultramafic inclusions from the San Carlos volcanic field, Arizona: A bearing on their petrogenesis. J. Petrol. 30(4), 1033-1064.

Goldstein, S.L., O'Nions, R.K., Hamilton, P.J., 1984. A Sm-Nd isotopic study of atmospheric dusts and particulates from major river systems. Earth Planet. Sc. Lett. 70, 221-236.

Gourlan, A.T., Meynadier, L., Allègre, C.J., 2008. Tectonically driven changes in the Indian Ocean circulation over the last 25 Ma: Neodymium isotope evidence. Earth Planet. Sc. Lett. 267, 353-364.

Griffin, J.J., Windom, H.L., Goldberg, E.D., 1968. The distribution of clay minerals in the worlds oceans. Deep-Sea Res. 15, 433-459.

Grousset, F.E., Joron, J.L., Biscaye, P.E., Latouche, C., Treuil, M., Maillet, N., Faugères, J.C., Gonthier, E., 1988. Mediterranean Outflow through the Strait of Gibraltar since 18 000 years B.P.: Mineralogical and Geochemical Arguments. Geo-Mar. Lett. 8, 24-34.

Grousset, F.E., Quetel, C.R., Thomas, B., Donard, O.F.X., Lambert, C.E., Guillard, F., Monaco, A., 1995. Anthropogenic vs. Lithogenic origins of trace elements (As, Cd, Pb, Rb, Sb, Sc, Sn, Zn) in water column particles: northwestern Mediterranean Sea. Mar. Chem. 48, 291-310.

Grousset, F.E., Parra, M., Bory, A., Martinez, P., Bertrand, P., Shimmield, G., Ellam, R.M., 1998. Saharan wind regimes traced by the Sr-Nd isotopic composition of subtropical Atlantic sediments: Last Glacial Maximum vs today. Quaternary Sci. Rev. 17, 395-409.

Grousset, F.E., Biscaye, P.E., 2005. Tracing dust sources and transport patterns using Sr, Nd and Pb isotopes. Chem. Geol. 222, 149-167.

Guerzoni, S., Molinaroli, E., Chester, R., 1997. Saharan dust inputs to the western Mediterranean Sea: depositional patterns, geochemistry and sedimentological implications. Deep-Sea Res. Pt. II 44(3-4), 631-654.

Gutjahr, M., Frank, M., Stirling, C.H., Klemm, V., van de Flierdt, T., Halliday, A.N., 2007. Reliable extraction of a deepwater trace metal isotope signal from Fe-Mn oxyhydroxide coatings of marine sediments. Chem. Geol. 242, 351-370.

Gutjahr, M., Frank, M., Stirling, C.H., Keigwin, L.D., Halliday, A.N., 2008. Tracing the Nd isotope evolution of North Atlantic Deep and Intermediate Waters in the western North Atlantic since the Last Glacial Maximum from Blake Ridge sediments. Earth Planet. Sc. Lett. 266, 61-77.

Gutjahr, M., Frank, M., Halliday, A.N., Keigwin, L.D., 2009. Retreat of the Laurentide ice sheet tracked by the isotopic composition of Pb in western North Atlantic seawater during termination 1. Earth Planet. Sc. Lett. 286, 546-555.

Hamann, Y., Ehrmann, W., Schmiedl, G., Kuhnt, T., 2009. Modern and late Quaternary clay mineral distribution in the area of the SE Mediterranean Sea. Quaternary Res 71, 453-464.

Hemming, S.R., Broecker, W.S., Sharp, W.D., Bond, G.C., Gwiazda, R.H., McManus, J.F., Klas, M., Hajdas, I., 1998. Provenance of Heinrich layers in core V28-82, northeastern Atlantic: $^{40}Ar/^{39}Ar$ ages of ice-rafted hornblende, Pb isotopes in feldspar grains, and Nd-Sr-Pb isotopes in the fine sediment fraction. Earth Planet. Sc. Lett. 164, 317-333.

Hoogakker, B.A.A., Rothwell, R.G., Rohling, E.J., Paterne, M., Stow, D.A.V., Herrle, J.O., Claytom, T., 2004. Variations in terrigenous dilution in western Mediterranean Sea pelagic sediments in response to climate change during the last glacial cycle. Mar. Geol. 211, 21-43.

Horwitz, E.P., Chiarizia, R., Dietz, M.L., 1992. A novel strontium-selective extraction chromatographic resin. Solvent Extr. Ion Exc. 10(2), 313-336.

Jacobsen, S.B., Wasserburg, G.J., 1980. Sm-Nd isotopic evolution of chondrites. Earth Planet. Sc. Lett. 50, 139-155.

Jeandel, C., Arsouze, T., Lacan, F., Téchine, P, Dutay, J.-C., 2007. Isotopic Nd compositions and concentrations of the lithogenic inputs into the ocean: A compilation, with an emphasis on the margins. Chem. Geol. 239, 156-164.

Jimenez-Espejo, F.J., Martinez-Ruiz, F., Sakamoto, T., Iijima, K., Gallego-Torres, D., Harada, N., 2007. Paleoenvironmental changes in the western Mediterranean since the last glacial maximum: High resolution multiproxy record from the Alegro-Balearic basin. Palaeogeogr. Palaeocl. 246, 292-306.

Khélifi, N., Sarnthein, M., Andersen, N., Blanz, T., Frank, M., Garbe-Schönberg, D., Haley, B.A., Stumpf, R., Weinelt, M., 2009. A major and long-term Pliocene

intensification of the Mediterranean outflow, 3.5-3.3 Ma ago. Geology 37(9), 811-814.

Klevenz, V., Vance, D., Schmidt, D.N., Mezger, K., 2008. Neodymium isotopes in benthic foraminifera: Core-top systematics and a down-core record from the Neogene south Atlantic. Earth Planet. Sc. Lett. 265, 571-587.

Kohfeld, K.E., Harrison, S.P., 2001. DIRTMAP: the geological record of dust. Earth-Sci. Rev. 54, 114.

Krom, M.D., Cliff, R.A., Eijsink, L.M., Herut, B., Chester, R., 1999. The characterisation of Saharan dusts and Nile particulate matter in surface sediments from the Levantine basin using Sr isotopes. Mar. Geol. 155, 319-330.

Krumm, S., 2006. SediCalc (free geological software). GeoZentrum Nordbayern, Universität Erlangen-Nürnberg. http://www.geol.uni-erlangen.de/sedicalc.

Kuhlbrodt, T., Griesel, A., Montoya, M., Levermann, A., Hofmann, M., Rahmstorf, S., 2007. On the driving processes of the Atlantic meridional overturning circulation. Rev. Geophys. 45, RG2001, doi:10.1029/2004RG000166.

Lacan, F., Jeandel, C., 2005. Neodymium isotopes as a tool for quantifying exchange fluxes at the continent-ocean interface. Earth Planet. Sc. Lett. 232, 245-257.

Lebreiro, S.M., McCave, I.N., Weaver, P.P.E., 1997. Late Quaternary turbitite emplacement on the Horseshoe abyssal plain (Iberian margin). J. Sediment. Res. 67(5), 856-870.

Le Fèvre, B., Pin, C., 2005. A straightforward separation scheme for concomitant Lu-Hf and Sm-Nd isotope ratio and isotope dilution analysis. Anal. Chim. Acta 543, 209-221.

Llave, E., Schönfeld, J., Hernández-Molina, F.L., Mulder, T., Somoza, L., Díaz del Río, V., Sánchez-Almazo, I., 2006. High-resolution stratigraphy of the Mediterranean outflow contourite system in the Gulf of Cadiz during the late Pleistocene: The impact of Heinrich events. Mar. Geol. 227, 241-262.

López-Galindo, A., Rodero, J., Maldonado, A., 1999. Surface facies and sediment dispersal patterns: southeastern Gulf of Cadiz, Spanish continental margin. Mar. Geol. 155, 83-98.

Löwemark, L., Schönfeld, J., Werner, F., Schäfer, P., 2004. Trace fossils as a paleoceanographic tool: evidence from Late Quaternary sediments of the southwestern Iberian margin. Mar. Geol. 204, 27-41.

Lugmair, G.W., Galer, S.J.G., 1992. Age and isotopic relationships among the angrites Lewis Cliff 86010 and Angra dos Reis. Geochim. Cosmochim. Ac. 56, 1673-1694.

Martin, E.E., Blair, S.W., Kamenov, G.D., Scher, H.D., Bourbon, E., Basak, C., Newkirk, D.N., 2010. Extraction of Nd isotopes from bulk deep sea sediments for paleoceanographic studies on Cenozoic time scales. Chem. Geol. 269(3-4), 414-431.

Mendes, I., Rosa, F., Dias, J.A., Schönfeld, J., Ferreira, O., Pinheiro, J., 2010. Inner shelf paleoenvironment evolution as a function of land-ocean interactions in the vicinity of the Guadiana River, SW Iberia. Quatern. Int. 221, 58-67.

Morellón, M., Valero-Garcés, B., Vegas-Vilarrúbia, T., González-Sampériz, P., Romero, Ó., Delgado-Huertas, A., Mata, P., Moreno, A., Rico, M., Corella, J.P., 2009. Lateglacial and Holocene palaeohydrology in the western Mediterranean region: the Lake Estanya record (NE Spain). Quaternary Sci. Rev. 28, 2582-2599.

Moreno, A., Cacho, I., Canals, M., Prins, M.A., Sánchez-Goñi, M.-F., Grimalt, J.O., Weltje, G.J., 2002. Saharan dust transport and high-latitude glacial climatic variability: The Alboran Sea record. Quaternary Res. 58, 318-328, doi:10.1006/qres.2002.2383.

Muiños, S.B., Frank, M., Maden, C., Hein, J.R., van de Flierdt, T., Lebreiro, S.M., Gaspar, L., Monteiro, J.H., Halliday, A.N., 2008. New constraints on the Pb and Nd isotopic evolution of NE Atlantic water masses. Geochem. Geophy. Geosy. 9(2), Q02007, doi:10.1029/2007GC001766.

Mulder, T., Migeon, S., Savoye, B., Faugères, J.-C., 2002. Reply to discussion by Shanmugam on Mulder et al. (2001, Geo-Marine Letters 21: 86-93) Inversely graded turbidite sequences in the deep Mediterranean. A record of deposits from flood-generated turbidity currents? Geo-Mar. Lett. 22, 112-120.

Mulder, T., Gonthier, E., Lecroart, P., Hanquiez, V., Marches, E., Voisset, M., 2009. Sediment failures and flows in the Gulf of Cadiz (eastern Atlantic). Mar. Petrol. Geol. 26, 660-672.

Pahnke, K., Goldstein, S.L., Hemming, S.R., 2008. Abrupt changes in Antarctic Intermediate Water circulation over the past 25 000 years. Nat. Geosci., AOP, doi: 10.1038/ngeo360.

Palmer, M.R., Edmond, J.M., 1989. The strontium isotope budget of the modern ocean. Earth Planet. Sc. Lett. 92, 11-26.

Petschick, R., 2001. MacDiff v4.2.5 (free geological software). Geologisch-Paläontologisches Institut, Universität Franfurt/Main. http://servermac. geologie.uni-frankfurt.de/Rainer.html.

Piepgras, D.J., Wasserburg, G.J., 1983. Influence of the Mediterranean Outflow on the isotopic composition of neodymium in waters of the North Atlantic. J. Geophys. Res. 88(10), 5997-6006.

Pinardi, N., Masetti, E., 2000. Variability of the large scale general circulation of the Mediterranean Sea from observations and modelling: a review. Palaeogeogr. Palaeocl. 158, 153-173.

Piotrowski, A.M., Goldstein, S.L., Hemming, S.R., Fairbanks, R.G., 2004. Intensification and variability of oceanic thermohaline circulation through the last deglaciation. Earth Planet. Sc. Lett. 225, 205-220.

Piotrowski, A.M., Goldstein, S.L., Hemming, S.R., Fairbanks, R.G., 2005. Temporal relationships of carbon cycle and ocean circulation at glacial boundaries. Science 307, 1933-1938.

Piotrowski, A.M., Banakar, V.K., Scrivner, A.E., Elderfield, H., Galy, A., Dennis, A., 2009. Indian Ocean circulation and productivity during the last glacial cycle. Earth Planet. Sc. Lett. 285, 179-189.

Pfannkuche, O., 2006. R/V Maria S. Merian cruise no. 1 leg 3 – Preliminary report. Institute of oceanography, University of Hamburg; http://www.ifm.zmaw.de /fileadmin/files/leitstelle/merian/MSM01/MSM01-3-SCR.pdf.

Rahmstorf, S., 1998. Influence of Mediterranean Outflow on climate. EOS, 79(24), 281-282.

Rahmstorf, S., 2002. Ocean circulation and climate during the past 120 000 years. Nature, 419, 207-214.

Reid, J.L., 1979. On the contribution of the Mediterranean Sea outflow to the Norwegian-Greenland Sea. Deep-Sea Res. 26A, 1199-1223.

Richter, T.O., de Stigter, H.C., Boer, W., Jesus, C.C., van Weering, T.C.E., 2009. Dispersal of natural and anthropogenic lead through submarine canyons at the Portuguese margin. Deep-Sea Res. 56, 267-282.

Rickli, J., Frank, M., Halliday, A.N., 2009. The hafnium-neodymium isotopic composition of Atlantic seawater. Earth Planet. Sc. Lett. 280, 118-127.

Roberts, N.L., Piotrowski, A.M., McManus, J.F., Keigwin, L.D., 2009. Synchronous deglacial overturning and Water Mass Source Changes. Science 327, 75-78.

Rogerson, M., Rohling, E.J., Weaver, P.P.E., Murray, J.W., 2005. Glacial to interglacial changes in the settling depth of the Mediterranean Outflow plume. Paleoceanography 20, PA3007, doi:10.1029/2004PA001106.

Rutberg, R.L., Hemming, S.R., Goldstein, S.L., 2000. Reduced North Atlantic Deep Water flux to the glacial Southern Ocean inferred from neodymium isotope ratios. Nature 405, 935-938.

Sánchez-Román, A., Sannino, G., García-Lafuente, J., Carillo, A., Criado-Aldeanueva, F., 2009. Transport estimates at the western section of the Strait of Gibraltar: A combined experimental and numerical study. J. Geophys. Res. 114, C06002, doi:10.1029/2008JC005023.

Schaule, B.K., Patterson, C.C., 1981. Lead concentrations in the northeast Pacific: evidence for global anthropogenic perturbations. Earth Planet. Sc. Lett. 54, 97-116.

Schönfeld, J., 1997. The impact of the Mediterranean Outflow Water (MOW) on benthic foraminiferal assemblages and surface sediments at the southern Portuguese continental margin. Mar. Micropaleontol. 29, 211-236.

Schönfeld, J., Zahn, R., 2000. Late Glacial to Holocene history of the Mediterranean Outflow. Evidence from benthic foraminiferal assemblages and stable isotopes at the Portuguese margin. Palaeogeogr. Palaeocl. 159, 85-111.

Schott, F., Koltermann, K.P., Stramma, L., Sy, A., Zahn, R., Zenk, W., 1999. North Atlantic 1997 cruise No. 39 18 April-14 September 1997. METEOR-Berichte 99, 1-197.

Sierro, F.J., Flores, J.A., Baraza, J., 1999. Late glacial to recent paleoenvironmental changes in the Gulf of Cadiz and formation of sandy contourite layers. Mar. Geol. 155(1-2), 157-172.

Sierro, F.J., Hodell, D.A., Curtis, J.H., Flores, J.A., Reguera, I., Colmenero-Hidalgo, E., Bárcena, M.A., Grimalt, J.O., Cacho, I., Frigola, J., Canals, M., 2005. Impact of iceberg melting on Mediterranean thermohaline circulation during Heinrich events. Paleoceanography 20, PA2019, doi:10.1029/2004PA001051.

Sparrow, M., Boebel, O., Zervakis, V., Zenk, W., Cantos-Figuerola, A., Gould, W.J., 2002. Two circulation regimes of the Mediterranean Outflow revealed by Lagrangian measurements. J. Phys. Oceanogr. 32, 1322-1330.

Spivack, A.J., Wasserburg, G.J., 1988. Neodymium isotopic composition of the Mediterranean outflow and the eastern North Atlantic. Geochim. Cosmochim. Ac. 52, 2767-2773.

Steiger, R.H., Jäger, E., 1977. Subcommission on geochronology: Convention on the use of decay constants in geo- and cosmochronology. Earth Planet. Sc. Lett. 36, 359-362.

Stumpf, R., Frank, M., Schönfeld, J., Haley, B.A., 2010. Late Quaternary variability of Mediterranean Outflow Water from radiogenic Nd and Pb isotopes. Quaternary Sci. Rev. 29 (19/20), 2462-2472, doi:10.1016/j.quascirev.2010.06.021.

Stuut, J.-B., Smalley, I., O'Hara-Dhand, K., 2009. Aeolian dust in Europe: African sources and European deposits. Quatern. Int. 198, 234-245.

Tachikawa, K., Jeandel, C., Roy-Barman, M., 1999. A new approach to the Nd residence time in the ocean: the role of atmospheric input. Earth Planet. Sc. Lett. 170, 433-446.

Tachikawa, K., Roy-Barman, M., Michard, A., Thouron, D., Yeghicheyan, D., Jeandel, C., 2004. Neodymium isotopes in the Mediterranean Sea: Comparison between seawater and sediment signals. Geochim. Cosmochim. Ac. 68(14), 3095-3106.

Tanaka, T., Togashi, S., Kamioka, H., Amakawa, H., Kagami, H., Hamamoto, T., Yuhara, M., Orihashi, Y., Yoneda, S., Shimizu, H., Kunimaru, T., Takahashi, K.,

Yanagi, T., Nakano, T., Fujimaki, H., Shinjo, R., Asahara, Y., Tanimizu, M., Dragusanu, C., 2000. JNdi-1: a neodymium isotopic reference in consistency with LaJolla neodymium. Chem. Geol. 168, 279-281.

Thorpe, S.A., 1976. Variability of Mediterranean undercurrent in Gulf of Cadiz. Deep-Sea Res. 23(8), 711-727.

Toucanne, S., Mulder, T., Schönfeld, J., Hanquiez, V., Gonthier, E., Duprat, J., Cremer, M., Zaragosi, S., 2007. Contourites of the Gulf of Cadiz: A high-resolution record of the paleocirculation of the Mediterranean outflow water during the last 50 000 years. Palaeogeogr. Palaeocl. 246(2-4), 354-366.

van de Flierdt, T., Robinson, L.F., Adkins, J.F., Hemming, S.R., Goldstein, S.L., 2006. Temporal stability of the neodymium isotope signature of the Holocene to glacial North Atlantic. Paleoceanography 21, PA4102, doi:10.1029 /2006PA001294.

Veizer, J., Ala, D., Azmy, K., Bruckschen, P., Buhl, D., Bruhn, F., Carden, G.A.F., Diener, A., Ebneth, S., Godderis, Y., Jasper, T., Korte, C., Pawellek, F., Podlaha, O.G., Strauss, H., 1999. $^{87}Sr/^{86}Sr$, $\delta^{13}C$ and $\delta^{18}O$ evolution of Phanerozoic seawater. Chem. Geol. 161(1-3), 59-88.

Voelker, A.H.L., Lebreiro, S.M., Schönfeld, J., Cacho, I., Erlenkeuser, H., Abrantes, F., 2006. Mediterranean outflow strengthening during northern hemisphere coolings: A salt source for the glacial Atlantic? Earth Planet. Sc. Lett. 245, 39-55.

Voelker, A.H.L., de Abreu, L., Schönfeld, J., Erlenkeuser, H., Abrantes, F., 2009. Hydrographic conditions along the western Iberian margin during marine isotope stage 2. Geochem. Geophy. Geosy. 10(12), Q12U08, doi:10.1029 /2009GC002605.

von Blanckenburg, F., Igel, H., 1999. Lateral mixing and advection of reactive isotope tracers in ocean basins: observations and mechanisms. Earth Planet. Sc. Lett. 169(1-2), 113-128.

Weiss, D., Boyle, E.A., Wu, J., Chavagnac, V., Michel, A., Reuer, M.K., 2003. Spatial and temporal evolution of lead isotope ratios in the North Atlantic Ocean between 1981 and 1989. J. Geophys. Res. 108(C10), 3306, doi:10.1029/2000JC000762.

Windom, H.L., 1976. Lithogenous material in marine sediments. In: Riley, J.P., Chester, R., Eds.. Chemical oceanography. Academic Press, New York, London, 5, 103-135.

Winkler, A., 1999. The climate history of the high northern latitudes since the Middle Miocene: indications from sedimentological and clay mineralogical analyses (ODP Leg 151, central Fram Strait. Ber. Polarforsch. 344, ISSN 0176-5027.

Zenk, W., 1975. On the origin of the intermediate double-maxima in T/S profiles from the North Atlantic. METEOR Forsch.-Ergebn. A 16, 35-43.

Appendix

Tab. 2.1. Elution scheme for the chromatographic purification of Pb on 50 µl Biorad® AG1-X8 resin (anion exchanger, mesh size 100-200 µm).

Volume	Reagent	Stage
1 x total reservoir	1M HNO_3	clean column
2 x total reservoir	MilliQ-water	clean column
50 µl	resin	load resin
3 x 1 ml	0.25M HNO_3	clean resin
2 x 100 µl	solution A*	condition resin
1 x 300 µl	sample in solution A	load sample
2 x 100 µl	solution A	collect matrix (Nd+Sr)
1 x 150 µl	solution A	collect matrix (Nd+Sr)
1 x 200 µl	solution B#	collect matrix (Nd+Sr)
1 x 300 µl	solution B	collect Pb
backwash	MilliQ-water	waste resin

*solution A = 10 ml 1M HNO_3 + 1 ml 2M HBr + 4 ml MilliQ-water
#solution B = 5 ml 1M HNO_3 + 0.15 ml 2M HBr + 4.85 ml MilliQ-water

Tab. 2.2. Chromatographic procedure for the separation of the REEs (incl. Nd) from the alkaline earth metals (incl. Sr) on 0.8 ml Biorad® AG50W-X12 resin (cation exchanger, mesh size 200-400 µm).

Volume	Reagent	Stage
1 x 8 ml	6M HCl	clean resin
1 x 0.5 ml	1M HCl	condition resin
1 x 1 ml	1M HCl	condition resin
1 x 0.5 ml	sample in 1M HCl	load sample
3 x 0.6 ml	1M HCl	wash-in sample
1 x 5 ml	3M HCl	elute matrix
1 x 5 ml	3M HCl	collect matrix (Sr)
2 x 1 ml	MilliQ-water	change acid
1 x 8 ml	2.5 ml HNO_3	elute matrix
1 x 6 ml	6M HNO_3	collect matrix (Nd)

continued on next page

Volume	Reagent	Stage
1 x 6 ml	6M HNO_3	clean resin
2 x 1 ml	MilliQ-water	change acid
1 x 1 ml	1M HCl	store column

Tab. 2.3. Recipe for the chromatographic purification of Sr on 50 µl Eichrom® Sr-Spec resin (cation exchanger, mesh size 50-100 µm).

Volume	Reagent	Stage
1 x total reservoir	0.1M H_2SO_4	clean column
2 x total reservoir	MilliQ-water	clean column
50 µl	resin	load resin
1 x 1 ml	0.1M H_2SO_4	clean resin
2 x total reservoir	MilliQ-water	clean resin
2 x 50 µl	3M HNO_3	condition resin
2 x 75 µl	3M HNO_3	condition resin
1 x 50 µl	sample in 3M HNO_3	load sample
2 x 50 µl	3M HNO_3	elute matrix
1 x 300 µl	3M HNO_3	elute matrix
1 x 500 µl	MilliQ-water	collect Sr
backwash	MilliQ-water	waste resin

Tab. 2.4. Elution procedure for the chromatographic purification of Nd on 2 ml Eichrom® Ln-Spec resin (cation exchanger, mesh size 50-100 µm).

Volume	Reagent	Stage
1 x 8 ml	6M HCl	clean resin
1 x 0.5 ml	0.1M HCl	condition resin
1 x 1 ml	0.1M HCl	condition resin
1 x 0.5 ml	sample in 0.1M HCl	load sample
1 x 0.5 ml	0.1M HCl	wash-in sample
1 x 7.5 ml	0.25M HCl	elute matrix
1 x 5 ml	0.25M HCl	collect Nd
1 x 8 ml	6M HCl	clean resin
2 x 1 ml	0.3M HCl	store column

Tab. 3.1. Core locations with coretop εNd , $^{87}Sr/^{86}Sr$ values and 2σ errors of the leachates. Ratios in parantheses refer to the detrital fraction of the respective samples.

Core/Station	Lat. (°N)	Long. (°W)	Depth (m)	εNd (±0.35)	$^{87}Sr/^{86}Sr$ (±0.000033)
a) coretops, with downcore records available					
M39008	36.38	7.07	577	-9.3 [-10.6]	0.70859 [0.71889]
M39036	37.81	9.68	1 745	-9.2 [-10.5]	0.70880 [0.72327]
M39058	39.04	10.68	1 974	-9.1 [-9.7]	0.70905 [0.72579]
b) coretops only					
PO287-8	41.29	9.01	88	-9.3	-
PO287-14	39.74	9.23	94	-8.6	-
PO287-26	38.56	9.36	96	-7.7	-
LV044-316	36.87	8.17	84	-8.3	-
MSM01/3-139	35.46	9.00	3 054	-9.2	0.70838
MSM01/3-161	35.56	9.51	3 864	-9.2	0.70845
MSM01/3-168	35.79	8.42	2 200	-9.3	0.70842
MSM01/3-183	35.77	8.26	2 094	-9.1	0.70894
MSM01/3-190	35.66	7.33	1 320	-9.3	0.70882
MSM01/3-237	35.30	6.64	353	-8.9	0.70897
MSM01/3-240	35.29	6.62	401	-8.5	0.70855
MSM01/3-331	35.50	7.07	1 076	-9.1	0.70878

Tab. 3.2. Core locations with coretop $^{208}Pb/^{206}Pb$ and $^{206}Pb/^{207}Pb$ ratios (reported errors are 2σ from the mean). Ratios in parantheses refer to the detrital fraction of the respective samples.

Core/Station	Lat. (°N)	Long. (°W)	Depth (m)	$^{208}Pb/^{206}Pb$ (±0.0003)	$^{206}Pb/^{207}Pb$ (±0.0001)
M39008	36.38	7.07	577	2.0845 [2.0793]	1.1793 [1.1886]
M39036	37.81	9.68	1 745	2.0825 [2.0759]	1.1824 [1.1916]
M39058	39.04	10.68	1 974	2.0800 [2.0697]	1.1821 [1.1932]
PO287-8	41.29	9.01	88	2.0751	1.1842
PO287-14	39.74	9.23	94	2.0685	1.1891
PO287-26	38.56	9.36	96	2.0949	1.1678
LV044-316	36.87	8.17	84	2.0933	1.1721

Tab. 3.3. Downcore Nd and Pb isotope records (reported errors are 2σ from the mean).

Depth (cm)	Age (cal a B.P.)	$^{208}Pb/^{204}Pb$ (±0.0100)	$^{207}Pb/^{204}Pb$ (±0.0034)	$^{206}Pb/^{204}Pb$ (±0.0027)	εNd (± 0.35)
a) core M39008					
8	2 773	-	-	-	-9.2
13	3 760	-	-	-	-9.4
25.5	5 403	38.8785	15.6800	18.7809	-
43	6 901	38.9316	15.6997	18.7855	-
53	7 240	-	-	-	-9.1
107	8 684	38.8330	15.6700	18.7425	-9.0
303	9 972	-	-	-	-9.2
307	10 028	38.8449	15.6751	18.7475	-
367	11 556	38.8913	15.6806	18.8226	-
382	12 022	38.8364	15.6783	18.8435	-
397	12 488	38.7968	15.6773	18.9252	-
403	12 675	-	-	-	-9.2
408	12 921	38.8376	15.6814	18.8278	-
428	14 355	38.8762	15.6775	18.8356	-

continued on next page

Depth (cm)	Age (cal a B.P.)	$^{208}Pb/^{204}Pb$ (±0.0100)	$^{207}Pb/^{204}Pb$ (±0.0034)	$^{206}Pb/^{204}Pb$ (±0.0027)	εNd (± 0.35)
438	14 608	38.8371	15.6779	18.7958	-
448	15 178	38.8663	15.6746	18.7998	-
463	16 511	-	-	-	-9.2
473	16 809	38.8085	15.6724	18.7945	-
503	17 703	-	-	-	-8.9
512	17 971	38.7833	15.6656	18.7514	-9.3
522	18 269	38.7964	15.6718	18.7809	-
532	18 781	38.8720	15.6824	18.8786	-
537	19 287	-	-	-	-9.0
542	19 792	38.8330	15.6791	18.8229	-
547	20 298	38.8133	15.6755	18.8012	-
562	21 815	38.8772	15.6811	18.8594	-
567	22 320	38.8445	15.6794	18.8698	-8.9
b) core M39036					
10	690	-	-	-	-9.2
20	1 380	-	-	-	-9.3
35	2 416	38.8389	15.6713	18.7419	-
55	3 796	-	-	-	-9.3
80	5 540	38.8134	15.6664	18.7551	-
106	7 828	38.7800	15.6576	18.7253	-
111	8 019	-	-	-	-9.4
151	10 250	-	-	-	-9.0
156	10 364	38.7655	15.6704	18.7270	-
171	11 080	38.8414	15.6766	18.7901	-
186	12 273	38.8099	15.6743	18.8127	
200	12 883	38.8069	15.6673	18.7885	-8.9
210	13 817	38.8509	15.6771	18.7783	-
230	14 310	38.8008	15.6699	18.7522	-
245	14 605	38.8055	15.6710	18.7547	-
250	14 655	-	-	-	-8.9
260	14 753	38.8216	15.6742	18.7959	-
270	16 530	38.9189	15.6823	18.8872	-
280	17 003	38.8208	15.6754	18.8237	-

continued on next page

Depth (cm)	Age (cal a B.P.)	$^{208}Pb/^{204}Pb$ (±0.0100)	$^{207}Pb/^{204}Pb$ (±0.0034)	$^{206}Pb/^{204}Pb$ (±0.0027)	εNd (± 0.35)
290	17 475	38.8171	15.6741	18.8194	-
300	17 529	-	-	-	-9.4
314	17 861	38.8091	15.6743	18.8054	-
334	19 063	38.8434	15.6810	18.8256	-
339	19 107	-	-	-	-9.0
364	19 841	38.8629	15.6749	18.8222	-
399	21 384	-	-	-	-9.0
423	22 384	38.8247	15.6712	18.8069	-9.1
c) core M39058					
13	1 895	38.8664	15.6767	18.8170	-
16.5	2 406	38.8325	15.6654	18.8177	-
20	2 916	-	-	-	-8.7
25	3 645	38.8372	15.6659	18.8245	-9.0
34	4 957	38.8922	15.6801	18.8475	-
45	10 247	38.8127	15.6735	18.8642	-
50	12 324	38.8008	15.6690	18.8508	-8.9
60	13 878	38.8248	15.6774	18.8726	-
74.5	15 165	38.8330	15.6745	18.8999	-8.9
84	16 008	38.7881	15.6765	18.8570	-
90	16 541	38.8309	15.6781	18.8665	-
95	16 818	-	-	-	-9.1
103	17 261	38.9571	15.6891	18.9947	-
108	17 538	38.8324	15.6843	18.8752	-
113	17 910	38.7986	15.6760	18.8483	-
118	18 283	38.7883	15.6705	18.8470	-8.4
138	21 729	38.8209	15.6766	18.8454	-8.7

Tab 4.1. Core locations and downcore εNd, $^{87}Sr/^{86}Sr$ and $^{208}Pb/^{204}Pb$, $^{207}Pb/^{204}Pb$, $^{206}Pb/^{204}Pb$ isotope records with 2σ errors in parentheses.

Depth (cm)	Age (cal a B.P.)	$^{208}Pb/^{204}Pb$ (±0.015)	$^{207}Pb/^{204}Pb$ (±0.005)	$^{206}Pb/^{204}Pb$ (±0.005)	$^{87}Sr/^{86}Sr$ (±0.00004)	εNd (± 0.35)
a) core M39008 (577 m) 36.38°N, 7.07°W						
1	coretop	38.6343	15.6587	18.5618	0.720167	-10.2
13	3760	38.8812	15.6761	18.7405	0.719451	-10.9
	repeat	38.8804	15.6753	18.7385	0.719459	-
25.5	5403	38.9503	15.6890	18.7857	0.720771	-10.2
43	6901	38.9582	15.6867	18.7956	0.718522	-10.6
	repeat	38.9566	15.6868	18.7956	-	-
107	8684	38.9937	15.6948	18.8089	0.719942	-10.9
	repeat	-	-	-	-	-10.6
307	10028	38.9290	15.6814	18.7760	0.718652	-10.2
367	11556	38.9748	15.6841	18.8141	0.720522	-10.6
	repeat	-	-	-	0.720538	-10.3
397	12488	38.9277	15.6817	18.8459	0.721343	-10.7
	repeat	38.9454	15.6868	18.8486	-	-
428	14355	38.9991	15.6912	18.8231	0.720785	-10.7
448	15178	38.9516	15.6871	18.7892	0.719733	-10.1
463	16511	38.9938	15.6902	18.8496	0.723689	-10.9
	repeat	-	-	-	0.723687	-10.7
512	17971	38.9105	15.6801	18.8127	0.720753	-10.4
	repeat	38.9082	15.6803	18.8133	-	-
537	19287	39.0363	15.7030	18.8445	0.723425	-10.7
	repeat	-	-	-	-	-10.4
547	20298	38.9061	15.6807	18.7982	0.724112	-9.2
567	22320	39.0254	15.7063	18.8468	0.722127	-10.8
b) core M39036 (1745 m) 37.81°N, 9.68°W						
1	coretop	38.6751	15.6569	18.6139	0.723865	-9.9
55	3796	38.9550	15.6876	18.8234	0.721538	-10.2
	repeat	38.9413	15.6838	18.8205	-	-
80	5540	38.9008	15.6835	18.7858	0.720267	-9.7
106	7828	38.9381	15.6828	18.8294	0.724067	-10.3
	repeat	38.9390	15.6835	18.8313	0.724073	-
156	10364	38.8932	15.6773	18.7971	0.720018	-9.6
171	11080	38.9998	15.6981	18.8612	0.722594	-10.9
	repeat	-	-	-	-	-11.0

continued on next page

Depth (cm)	Age (cal a B.P.)	$^{208}Pb/^{204}Pb$ (±0.015)	$^{207}Pb/^{204}Pb$ (±0.005)	$^{206}Pb/^{204}Pb$ (±0.005)	$^{87}Sr/^{86}Sr$ (±0.00004)	εNd (± 0.35)
186	12273	38.9581	15.6871	18.8574	0.722578	-10.4
	repeat	-	-	-	0.722608	-10.6
210	13817	38.9722	15.6877	18.8286	0.722695	-10.7
	repeat	-	-	-	-	-10.7
230	14310	38.8876	15.6783	18.7859	0.722202	-10.4
	repeat	38.8799	15.6749	18.7820	0.722194	-
260	14753	38.9123	15.6874	18.8275	0.720556	-10.2
270	16530	38.9454	15.6838	18.8759	0.724770	-11.0
	repeat	-	-	-	-	-10.9
314	17816	38.9144	15.6859	18.8641	0.722562	-10.4
	repeat	38.8904	15.6767	18.8557	-	-
364	19811	38.9116	15.6807	18.8324	0.722456	-10.0
423	22384	38.9298	15.6836	18.8528	0.721897	-10.9
	repeat	-	-	-	-	-10.6
c) core M39058 (1974 m) 39.04°N, 10.68°W						
1	coretop	38.6080	15.6569	18.6519	0.724899	-9.5
25	3645	38.9034	15.6851	18.9103	0.723957	-10.1
34	4957	38.8407	15.6758	18.8803	0.724457	-9.1
45	10247	38.8190	15.6755	18.9234	0.721238	-9.2
50	12324	38.8738	15.6833	18.9522	0.723719	-9.7
	repeat	38.8672	15.6809	18.9489	0.723733	-9.7
60	13878	38.8823	15.6887	18.9629	0.724485	-10.0
	repeat	38.8559	15.6797	18.9568	0.724506	-9.7
74.5	15165	38.8941	15.6936	18.9423	0.726090	-9.9
84	16008	38.8582	15.6818	18.9456	0.726321	-11.2
	repeat	-	-	-	0.726332	-
90	16541	38.9024	15.6902	18.9651	0.725395	-11.0
	repeat	-	-	-	0.725402	-
103	17261	38.9216	15.6877	18.9568	0.726905	-11.5
113	17910	38.8859	15.6891	18.9570	0.724684	-10.0
	repeat	38.8930	15.6906	18.9571	-	-
138	21729	38.8585	15.6834	18.9395	0.724929	-9.1

Tab. 4.2. Core locations and downcore clay mineral abundances in weighted peak area percentage. Accuracy of the semi-quantitative clay mineral analysis is about ±2%.

Depth (cm)	Age (cal a B.P.)	Kaolinite (%)	Chlorite (%)	Illite (%)	Smectite (%)
a) core M39008 (577 m) 36.38°N, 7.07°W					
1	coretop	23	14	28	35
13	3760	21	11	27	40
25.5	5403	23	13	26	38
43	6901	24	13	25	38
107	8684	23	14	30	34
307	10028	22	17	30	31
367	11556	20	18	30	32
397	12488	13	12	23	52
428	14355	18	18	28	36
448	15178	22	19	27	32
463	16511	15	12	29	44
512	17971	17	8	28	47
537	19287	16	13	32	40
547	20298	14	10	28	48
567	22320	14	12	31	43
b) core M39036 (1745 m) 37.81°N, 9.68°W					
1	coretop	21	14	33	32
55	3796	24	14	35	27
80	5540	23	13	35	30
106	7828	27	14	34	26
156	10364	19	16	31	34
171	11080	20	14	33	33
186	12273	17	12	34	36
210	13817	22	17	36	25
230	14310	19	15	34	31
260	14753	17	12	29	42
270	16530	20	15	33	32
314	17816	21	10	31	37
364	19841	19	13	34	34
423	22384	17	11	40	31
c) core M39058 (1974 m) 39.04°N, 10.68°W					
1	coretop	26	12	29	33

continued on next page

Depth (cm)	Age (cal a B.P.)	Kaolinite (%)	Chlorite (%)	Illite (%)	Smectite (%)
25	3645	25	12	30	33
34	4957	27	13	33	27
45	10247	20	12	29	39
50	12324	21	12	29	37
60	13878	23	13	31	34
74.5	15165	19	7	27	48
84	16008	21	7	32	40
90	16541	22	12	33	33
103	17261	22	10	33	35
113	17910	24	9	32	35
138	21729	21	12	32	34